Master Thesis

within the framework of
the postgraduate studies “Geographical Information Science & Systems
(UNIGIS Msc) at the Center for Geoinformatics (Z_GIS)
at the Paris Lodron University of Salzburg

Spatial distribution of leaf area index and leaf chlorophyll in cotton fields of Khorezm, Uzbekistan estimated at leaf, plant and regional scale by spectroscopy, remote sensing and GIS modeling

by

Dipl.-Geogr. Jörg Grillenberger
U1245, UNIGIS Msc 2005

to obtain the academic title
“Master of Science (Geographical Information Science & Systems) – Msc (GIS)”

Reviewer:
Ao. Univ. Prof. Dr. Josef Strobl

München, April 2007

Declaration / Erklärung:

I assure that the present master thesis was carried out without external help and without using further than the stated sources. I also confirm that this thesis was not submitted to another examination board. All quotations are marked adequately.

Ich versichere, diese Master Thesis ohne fremde Hilfe und ohne Verwendung anderer als der angeführten Quellen angefertigt zu haben, und dass die Arbeit in gleicher oder ähnlicher Form noch keiner anderen Prüfungsbehörde vorgelegen hat. Alle Ausführungen der Arbeit, die wörtlich oder sinngemäß übernommen wurden sind entsprechend gekennzeichnet.

München, 23.04.2007

Jörg Grillenberger

Acknowledgements

This study was carried out within the ZEF/UNESCO Khorezm Project on “Economic and Ecological Restructuring of Land- and Water Use in the Region Khorezm (Uzbekistan)”. The field work was performed in the Khorezm region in Uzbekistan, while the data analyses were done at the German Remote Sensing Data Center (DFD) of the German Aerospace Center (DLR) in Oberpfaffenhofen, Germany. The project was funded by the German Federal Ministry for Economic Cooperation and Development (BMBF: project number 03399070C) and was supported by the European Space Agency (ESA).

My very special thanks go to Dr. Gerd Rücker (DLR-DFD) for the always patient and sound assistance during data collection and processing of all the different datasets, his always helpful advises and ideas and the productive discussions. I would also like to thank Dr. cand. Wouter Dorigo (DLR_DFD) for his very kind support while using ASTools, the provision of other very useful ENVI / IDL – Tools just at the right time, his technically sound advises and profitable discussions concerning the use and interpretation of reflection data. Furthermore I would like to thank Dr. Rudolf Richter (DLR-DFD) for the introduction in functionality and correct use of ATCOR for ENVI and his kind support regarding the atmospheric correction. I'd also like to thank Dr. Günter Strunz (DLR-DFD) for the possibility of the field campaign in Uzbekistan, to work at DLR-DFD and the allocation of the technical equipment and a workspace. Last but not least, I thank Prof. Strobl at UNIGIS for the supervision of this thesis and his deep interest on the research topic as well as his hints for the compilation of this thesis. I would like to thank Mrs. Kristin Wouters for proofreading and the exchange of experiences regarding vegetation indices.

Furthermore, I would like to thank Dr. John Lamers (ZEF–Project Leader) for his many constructive statements regarding the field measurements and for his comprehensive and essential backstopping and support for this research. I am very grateful to Prof. Nazar Ibragimov for the possibility to perform measurements on plants of his cotton fertilizer trial plots and for aharing his wide knowledge about cotton and the agricultural system of Uzbekistan in many productive meetings. I highly appreciated the support of Dr. cand. Kirsten Kienzler who established the contacts to the farmers on the study sites, supported me in essential issues regarding the field survey and gave me indispensable and valuable insights into the local farming system. Many thanks also to Mrs. Liliana Sin for her very helpful assistance during the field campaign. Without her the huge workload of this study would never have been possible to conduct, because she was able to arrange everything: cars, students for fieldwork, money exchange, plane-tickets and office workspace. Special thanks go to “my” Uzbek students Mrs. Nasiba Sultanova and Mr. Bunyod Allaberganov for being almost always in time and working really hard and carefully.

Last but not least, my very special thanks go to my beloved wife Corinna who had to suffer a lot due to her husband´s idea of writing his Master Thesis far away. Nevertheless, she gave me all her support which was also indispensable for me. Thank you, Corinna!

Abstract

In the irrigation-based agriculture of the Khorezm region in the Uzbek part of the Aral Sea Basin, cotton is the most common crop. In many areas of Khorezm the actual cotton yield is far below the potential. Within a large portion of the region cotton production is not economic and yields are very poor. Using time-series of satellite-based Proba-1/CHRIS images, spectrometer and biophysical data from 2006, this study compared the predictive capability of VIs for estimating cotton growth parameterized by leaf area index (LAI) and cotton nutrient content parameterized by leaf chlorophyll content (C_{ab}), and examined the spatial variation of cotton LAI and C_{ab}. The study was carried out at leaf, plant and regional scale and considered at plant and regional scale four growth stages of cotton.

The results in this thesis indicate moderate relationships between cotton LAI and VIs and C_{ab} and VIs at regional scale with the absolute best R^2 values reaching 0,55 and 0,62 for LAI and C_{ab} predictions, respectively. The performance of the normalized difference vegetation index (NDVI) was most stable for predicting cotton LAI, and modified chlorophyll absorption ratio index 1 (MCARI1) was most stable for predicting cotton leaf chlorophyll content at a regional scale over the different temporal stages. By performing regressions of VIs with chlorophyll values of leaves from different plant layers, the plant layers with the highest correlation were identified for each stage. It came out that neither only the top-leaves nor the whole cotton plant, but leaves from the upper two to three plant layers achieved the highest regression results for respective stages.

The found relationships between VIs and LAI for the whole season and VIs and C_{ab} for specific stages and plant layers, may be integrated into further agronomic studies to support decision makers on adjusting the fertilizer application norms to the seasonal and site-specific requirements, thus to help improving yields in a sustainable and economical way in Khorezm.

Table of contents

List of Figures

List of Tables

List of Abbreviations

ArcGIS	ArcGIS 9.1 software package by ESRI
ASD	ASD
ASTool	Add-on software package for ENVI / IDL by Dorigo et al. 2006
ATCOR	Software add-on for ENVI / IDL for atmospheric correction by Richter 2006
C_{ab}	Leaf chlorophyll a + b content
DLR	German Aerospace Center (Deutsches Zenrtum für Luft- und Raumfahrt)
ENVI	ENVI 4.1 / IDL 6.1 software package
ESA	European Space Agency
GCP	Ground Control Point
GIS	Geographic Information System
GPS	Global Positioning System
LAI	Leaf Area Index (dimensionless value), description: chapter 2.2
LED	Light Emitting Diode
Slb	Spectral Library, format used by ENVI to group and save spectral information
SPAD	Dimensionless value collected with Minolta SPAD-502 used to estimate C_{ab}
VI / VIs	Vegetation Index (VI); Vegetation Indices (VIs)

1 Introduction

In Soviet times, wide desert areas in the Aral Sea basin, especially along the two main rivers Amu Darya and Syr Darya, wide areas were transformed into irrigation based arable land. Huge water withdrawal from these rivers has lead to a dramatical loss of more than two-thirds of the volume of the Aral Sea during the last 50 years. With the current rate of decline continuing it is estimated that the Aral Sea will disappear completely by 2020 with the current rate of decline (Pidwirny 1999). One area with irrigation based agriculture is the Khorezm region in Uzbekistan. In this area unsustainable land and water use has led to a variety of ecological problems with impact on the farmers' economy. The rural population has suffered from high salinisation, groundwater pollution by fertilizer entry, high groundwater table, erosion and desertification, hence decreasing agricultural production. In addition, up to 70% of the water is lost in the extensive, old fashioned and holey irrigation system. Thus, since similar serious problems occur in a wider region, the Aral Sea region was declared as a world ecological disaster area by UNESCO in 1992 (Martius et al. 2004).

Within this regional problem framework, this work is embedded in the pilot research project „Economic and Ecological Restructuring of Land- and Water Use in the Region Khorezm (Uzbekistan)" initiated by the Centre for Development Research (ZEF) in Bonn in cooperation with the UNESCO, the University of Urgench and the German Aerospace Center - German Remote Sensing Data Center (DLR-DFD) among others. The project is "an interdisciplinary, application-oriented research project with the aim to provide appropriate regional development concepts based on sustainable and efficient land and water use" (Vlek et al. 2003 p.1). This research project started in 2001 and tries to develop recommendations that help to improve the ecological and economical situation of the Khorezm region.

1.1 Problem description

In the Khorezm region of Uzbekistan, cotton (*Gossypium hirsutum* L.) production plays a dominant role. However, fertilizer application rates are outdated and often not adapted to the prevailing, site-specific environmental conditions and recent varieties, leading to over-fertilization, soil and water pollution, unnecessary expenses and lower income. Such agricultural problems have been observed within the long-term and interdisciplinary ZEF/UNESCO project on "Economic and Ecological Restructuring of Land and Water Use in Khorezm, Uzbekistan". Because Nitrogen (N) is the most limiting nutrient in Khorezm soils as found by fertilizer trials (Kienzler 2007) the sufficient amount of Nitrogen application has to be identified carefully.

In order to support regional stakeholders to optimize N fertilizer application, maps showing the spatial distribution of leaf nitrogen status in their cotton fields could be an important information

source. Combined with information on soils, plant-nutrient uptake behaviour and farmers´ economic production conditions, leaf N status maps can be helpful for adjusting the fertilizer application according to the actual and site-specific N requirements and farmers´ individual crop production strategies. Fertilizer management approaches using field trials and crop simulation models have been mainly applied at a plot scale (Kienzler 2007). In contrast, satellite-based hyperspectral approaches have the potential to rapidly assess the crop nutrient status within fields over a larger region, and resulting maps could be helpful for regional decision makers and fertilizer producers supporting farmers. Such hyperspectral remote sensing approaches are based on the principle that N deficiencies in cotton leaves decrease the corresponding chlorophyll *a* and *b* content which in turn affects reflectance in the visible and near-infrared wavelengths. To determine the leaf area index (LAI), an index giving information about the plant coverage and crop growth, LAI-meter, e.g. LICOR 2000 is used on the ground. To estimate the leaf area index by remote sensing, the hyperspectral information of the satellite images is used to calculate vegetation indices (VIs) based on ratios of distinctive reflectance, e.g. at 641 nm and 864 nm. For determining the relative amount of leaf chlorophyll on the ground, the ratio of reflectance at 650 nm and 940 nm is used by the Minolta SPAD-502 Chlorophyll Meter. However, SPAD needs to be calibrated to the dominating cotton cultivar (Khorezm-127) before being functional in estimating the absolute cotton leaf chlorophyll content (Rücker 2006). To estimate the cotton leaf chlorophyll content by remote sensing different vegetation indices using distinctive ratios of reflectance are used, as for estimating LAI. Afterwards these VIs are transferred into real LAI or leaf chlorophyll content and the information is presented in form of maps showing the spatial LAI or leaf chlorophyll distribution pattern, the ambition of this thesis.

1.2 Objectives

The main research question of this thesis is to investigate the performance of hyperspectral vegetation indices for estimating the spatial distribution of cotton leaf area index and cotton leaf chlorophyll content over different temporal stages and at three different spatial scales. Each scale has a focus on a specific objective, and results from one scale were needed for the following scale.

- At leaf scale, the smallest, the calibration of SPAD to the cotton cultivar Khorezm-127 is the main objective. The equation derived at this scale is essential to transfer SPAD to C_{ab} values at the other scales.
- At plant scale LAI, SPAD and reflectance data will be combined for plants and plots with different fertilizer application rates to achieve a profound prediction of LAI and C_{ab} - content by reflectance based calculation of VIs.
- At regional scale the spatial within-field distribution of LAI and C_{ab} - content estimated by VIs based on the spectral information of hyperspectral and multiangular Proba-1/CHRIS images

will be presented in GIS-maps.

2.Literature review

2.1 Cotton

Uzbekistan is the world´s second largest exporter of cotton (according to FAOSTAT 2006a 0,45 mill. tons in 2004) after the United States (2,9 mill. tons). Countrywide raw-cotton production in 2005 was estimated up to 2,7 t/ha (FAOSTAT 2006a), that is higher than the world average with 1,9 t/ha, but less than the yield achieved under similar climatic conditions in Australia (4,2 t/ha, FAOSTAT 2006b). About 5% of the cotton in Uzbekistan is produced in Khorezm, an irrigated landscape (see chapter 3)

The cultivated cotton plant (Gossypium hirsutum L.) is the world´s most important fibre producing plant (Diepenbrock 1999). The white fibres, which are used to spin the textile fabric, are growing around the seeds in the bolls. The anatomy of cotton is more complex than of any other important annual crop. The growth phase lasts for 130 to 180 days, depending on temperature and water availability. The temperature has to be above 15°C for at least 160 days (Waddle 1984). The plant develops the vegetative (monopodial, for leaves only) and reproductive (sympodial, for flowers) branches more or less at the same time. Cotton has three different types of leaves. The first two are called cotyledon, the tiny prophyll – leaves at the top of each branch and the foliage leaves (Mauney 1984). The growing cycle can be divided into different stages:

1. 2 to 4 leaf stage
2. budding stage
3. flowering stage
4. fruiting stage
5. harvesting

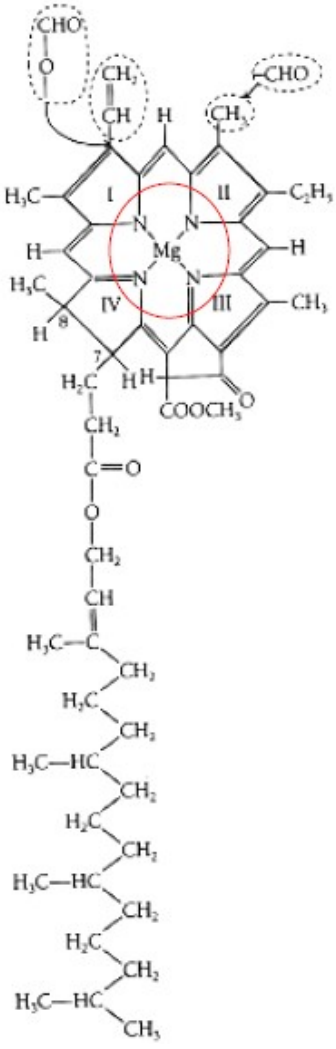

Figure 2.1: Chemical Structure of Chlorophyll

The structure of this thesis is based on observations at the stages 2 to 3 and partly 4 which are most important for adjusting fertilizer application (chapter 3.4). A fully developed cotton plant can be divided into different leaf layers which are separated by nodes (Grimes & El-Zik 1990). These nodes are characterized by a monopodial branch, separating sympodial ones. The number and distance of the nodes are influenced by environmental factors as water and fertilizer availability, temperature and type of soil (Waddle

1984). The first reproductive branch will be developed somewhere between the 5th and 9th node. The higher the location of a node, the longer the plant needs to grow the first bolls. This position is influenced by temperature, nitrogen availability and humidity during early growth (Grimes & El-Zik 1990). The flowering starts 60 to 80 days after seeding somewhere between mid June / mid August, the first bolls are opening 24 days after flowering (Grimes & El-Zik 1990).

2.2 Biophysical and biochemical parameters to characterize vegetation

To monitor the health status of crop it is important to find factors which can be detected without destroying the plants and which work fast.

One assessment to the physiological condition of plants is provided by the indication of their health or stress state. The stress can be caused by different factors such as heat, freezing, drought, flood, soil erosion, soil compaction, salinisation, diseases, insect action or nutrient loss.An indicator which is used for describing the general development state of a plant is the Leaf Area Index (LAI), while the only specific factor analysed is the nutrient stress due to limited Nitrogen.

LAI is a very important variable to estimate biomass, evapotranspiration, amount of photosynthesis, productivity and dynamic of plants (Xiao 2002). The variable was defined by Watson (1947) as the one side surface area of a photosynthetically active leaf accumulated per unit of ground surface area the leaves are growing on (Jonckheer 2004, Weiss 2004). The problem is, this definition is only true for plain leaves, if they are folded or rolled the one side is not defined anymore (Jonckheer 2004). A better and more common definition is the following:

Table 2.1: LAI-Values of different vegetation coverage
Source: Demircan 1995

Type of vegetation	*LAI*
tropical rainforest	>15.0
deciduous forest	< 12.0
maize	< 5.6
wheat	< 5.0

LAI is given as half of the whole Leaf Area in m² per m² ground as a simple figure without dimension (Chen & Black 1991). There are different methods to measure the LAI. The direct one is, to harvest all leaves, scan their leaf surface and calculate all together. This approach does not work if a monitoring of the same leaves or plants is planned. Therefore plants should stay alive at least as long as the monitoring lasts. On leaf scale SPAD and reflectance of some leaves was measured once and afterwards the plants were harvested. In this case it was possible to scan all leaves (see chapter 4.2.2). A less destructive method is the use of instruments like LICOR 2000 (described in chapter 4.1.4) or the indirect approach using vegetation indices calculated with help of the reflection data as described in the following chapters. To get an orientation for high or low LAI some mean values are given in table 2.1.

Considering the nutrient stress indicator Nitrogen, it is one of the basics the plants need to build up

chlorophyll, the green pigment for harvesting light energy. The chemical structure of chlorophyll in figure 2.1 shows this close relation.

Plant chlorophyll content is the most important biochemical compound as it is an indicator of photosynthetic potential (Baret & Foutry, 1997). It is closely related to the to nitrogen concentration in green vegetation and is therefore a sensitive indicator of crop response to nitrogen deficiency (Baret & Fourty, 1997). Chlorophyll is located in the chloroplast, where a cascade of photosystems works at different absorption maxima. Photosystem I (PS-I) with a central wavelength of maximum absorption at 700nm and Photosystem II (PS-II) also called carotenoids with 680nm, then chlorophyll a with 670nm and chlorophyll b with 650nm as the central wavelengths of their maximum absorption.

These characteristic wavelengths were used by different authors to estimate the content of the referring pigment by designing a Vegetation Index using this distinctive ratio. Some wavelengths are found to be disturbed by e.g. soil reflectance or less. This is pointed out for some indices found in literature in the referring chapters later on.

2.3 Remote Sensing

Remote sensing is the premier technology for giving an unbiased view of large areas, by providing spatially explicit information and the possibility of a repeated collection of this information, and it has thus been widely used to estimate crop yields at a regional scale (Quarmby et al. 1993; Baez-Gonzalez et al. 2002; Bastiaanssen & Ali 2003; Doraiswamy et al. 2003).

Therefore the launching of the first earth observation satellite, Landsat-1, in 1972 opened an excellent tool to monitor bio - geophysical processes that take place on planet earth from global to regional scales. (Goward & Williams 1997). Only a few years later the North-American Large Area Crop Inventory Experiment (LACIE) and AGRISTARS programs proved that Remote Sensing (RS) data could successfully assist in crop identification, estimation of some important crop canopy properties, and even help to forecast crop production (Moran et al. 1997). Since these early days many scientists have retrieved canopy state variables over large areas using all available sensors. Traditionally, aerial photography and digital broadband multispectral sensors have been used to obtain information in agriculture on crop yield and plant development based on the relationships between red and near-infrared (NIR) reflectance and crop yield and development. During the development of the Landsat sensors the spectral channels were adopted to maximize the collection of vegetation indicators (Zarco -Tejada et al. 2005b). Common methods to obtain spatial and temporal crop status based on these sensors rely on calculating vegetation indices as described in the following chapters.

Commonly applied methodologies are based on empirical relationships between the normalized

difference vegetation index (NDVI) and crop yield (Groten 1993; Dalezios et al. 2001; Conrad et al. 2004a). However, a simple empirical relationship is only of local and instantaneous significance. Furthermore, an empirical assessment requires excessive measurement programs to collect yield data in the field, which on a regional scale is time consuming and costly (Moulin et al., 1998).

2.4 Vegetation Indices

"Vegetation indices are models that use the characteristic reflectance properties of green vegetation in specific wavelengths to derive an index that represents biomass, vegetation cover and changes in vegetation cover pattern" (Bean 2000). In this part of the literature review some Vegetation Indices (VIs) used by other authors in a similar question as the topic of this thesis are introduced.

The spectral reflectance of a plant is always a combination of plant and soil reflectance components. These components are governed by the optical properties of these elements and photon exchanges within the canopy. As the vegetation grows the part of the soil signal decreases but may still be significant. This effect depends on plant density, row effects, canopy geometry, wind effects and more (Rondeaux 2006). Some VIs take a few of these effects into account, but not all.

The group of classical Broadband vegetation Indices can be subdivided into ratio and orthogonal indices (Broge & Mortensen 2002). The ratio indices are calculated more or less independently of soil reflectance properties, while orthogonal indices refer to a baseline specific to the local soil background. Hybrid indices can be considered as a combination of ratio and orthogonal indices. (Dorigo 2006).

Most of the ratio – based VIs use the reflectance in the red spectrum, which is related to the chlorophyll light absorption and the near – infrared spectrum, related to the green vegetation density. Together these two bands cover more than 90% of the information on a plant canopy. In red and near – infrared the contrast between vegetation and soil signal is maximal (Leblon 2006).

2.4.1 Broadband Vegetation Indices

RVI

The Ratio Vegetation Index (RVI) was developed by Pearson & Miller (1972).

$$RVI = \frac{R_{864}}{R_{671}}$$

with:

R_{XXX} = nadir reflection at the given wavelength

NDVI

The Normalized Difference Vegetation index (NDVI) was developed by Rouse et al 1974 to estimate the biomass content of a certain area and is now the most known VI. It is based on the contrast between the maximum absorption in the red spectrum, caused by chlorophyll pigments, and the near infrared reflection of the leaf cell structures (Giannico 2007). The NDVI is described by the following equation:

$$NDVI = \frac{R_{864} - R_{671}}{R_{864} + R_{671}}$$

with:

R_{XXX} = nadir reflection at the given wavelength

The values for NDVI are for selected targets within the following ranges (Witt 1998, Leblon 2006):

Soil: 0<=NDVI<=0.3

Vegetation: 0.2 <= NDVI<= 0.6

Water: -1<=NDVI<=1

The NDVI saturates in case of dense and multi-layered vegetation and shows a non-linear relationship with biophysical parameters as LAI (Haboudane 2004, Baret et al 1991, Lillesaeter 1982). This non-linearity becomes more prominent with darker soil background and with the presence of shadow. The NDVI may not be suitable to infer vegetation fraction because of its non – linearity and scale effects (Jiang et al 2006).

2.4.2 Orthogonal and Hybrid Vegetation Indices

Orthogonal indices were introduced in an attempt to reduce (soil) background effects. For orthogonal vegetation indices the LAI-isolines in the Red–NIR do not converge in the origin but remain parallel to the principal axis of soil spectral variation (Richardson and Wiegand, 1977). This soil line is expressed by the intercept and slope as determined by linear regression of the local soil reflectance in the Red–NIR feature space. The simple difference between NIR and red reflectance (Jordan, 1969) was the first index of this category. Other orthogonal VIs are the Perpendicular Vegetation Index (Richardson and Wiegand, 1977) and the Weighted Difference Vegetation Index (Clevers, 1989), but will not be used for this thesis.

RDVI

The Renormalized Difference Vegetation Index (RDVI) was developed by Roujean & Breon 1995 for a vegetation quantitative monitoring without the influence of different solar zenith angles. The given equation is useful for the optimal observation angle of 0° to the ground (nadir view). With observation angles between 90° and 45° complex factors for the correction are needed. These

factors are not needed for this thesis, though only the nadir scenes are used, but are given in the paper of Roujean 1995.

$$RDVI = \frac{R_{864} - R_{671}}{\sqrt{R_{864} + R_{671}}}$$

with:

R_{XXX} = nadir reflection at the given wavelength

SAVI

The SAVI (Soil – Adjusted Vegetation Index) was developed for low vegetation cover area by Huete (1988). "It´s intend is to minimize the effects of soil background an the vegetation signal by incorporating a constant soil adjustment factor L into the denominator of the NDVI equation. L varies with the reflectance characteristics for soil (colour and brightness). Huete (1988) provides a graph from which the values of L can be extracted. (...) The L-factor chosen depends on the density of the vegetation one wishes to analyse. For very low vegetation Huete (1988) suggest using an L factor of 1.0, for intermediate 0.5 and for high densities 0.25." (Thiam 2001 P. 95-96). For L = 0 the SAVI is equal to NDVI, for L = 100 the SAVI becomes similar to the PVI.

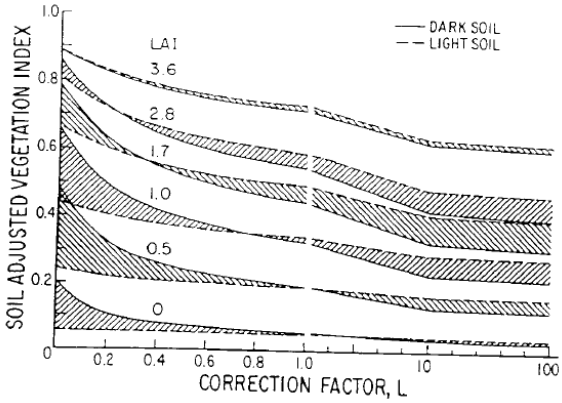

Figure 2.2: Influence of soil colour on SAVI for cotton
Source: Huete 1988 in Thiam 2001

$$SAVI = \frac{R_{864} - R_{671}}{(R_{864} + R_{671} + L) \cdot (1 + L)}$$

with:

L = 0.5 (default in ASTools by Dorigo 2006)

R_{XXX} = nadir reflection at the given wavelength

SAVI2

The second Soil Adjusted Vegetation Index (SAVI2) was created by Major, Baret and Guyot 1990. The SAVI2 is expressing canopy near infrared reflectance as a linear function of canopy red reflectance. Based on this finding a second version of SAVI (SAVI2) was developed, which models the vegetation isoline behaviour by using the b / a factor as a soil adjustment factor (Broge 2000).

$$SAVI2 = \frac{R_{864}}{R_{671} + \frac{b}{a}}$$

with:

a = 1.20, b= 0.04

R_{XXX} = nadir reflection at the given wavelength

MSAVI

The Modified Soil Adjusted Vegetation Index (MSAVI) was introduced by Qi et al 1994. They replaced the variable L by a developed function. The results were tested with ground and aircraft

based measurements of cotton plants. The MSAVI is shown to increase the dynamic range of vegetation sensitivity as defined by a “vegetation signal” to “soil noise” ratio (Qi et al 1993).

$$MSAVI = 0{,}5 * \{2 \cdot R_{800} + 1 - \sqrt{(2 \cdot R_{800} + 1)^2 - (R_{800} - a \cdot b)}\}$$

with:

R_{XXX} = nadir reflection at the given wavelength

TSAVI

The Transformed Soil Adjusted Vegetation Index created by Baret et al 1989 for crop canopies is 0 for bare soil and 1 for high LAI. According to Elvidge & Chen 1995 the TSAVI is higher influenced by background signals than SAVI for pinyon pine growing in shrublands and woodlands.

$$TSAVI = a \cdot \frac{R_{864} - a \cdot R_{671} - b}{R_{671} + a \cdot R_{864} - a \cdot b}$$

with:

a = 1.20, b= 0.04

R_{XXX} = nadir reflection at the given wavelength

ATSAVI

The Adjusted Transformed Soil Adjusted Vegetaton Index was developed by Baret & Guyot 1991 for a further minimizing the dependency on soil parameters. The factor X has been adjusted to 0.08 to minimize soil effects, variations in canopy structure and biochemistry . For a high canopy density the ATSAVI is close to 0.70 and for bare soil zero.

$$ATSAVI = a \cdot \frac{R_{864} - a \cdot R_{671} - b}{a \cdot R_{864} + R_{671} - a \cdot b + X \cdot (1 + a^2)}$$

with:

a = 1.20, b= 0.04, X= 0.08

R_{XXX} = nadir reflection at the given wavelength

OSAVI

The Optimized Soil Adjusted Vegetation Index (OSAVI) was created by Rondeaux et al in 1996 to pay further attention to the impact of the soil signals. Therefore they tested the different already described versions of the “SAVI – family”, especially for low vegetation coverage with a stronger soil signal, and adopted their own factors especially for agricultural applications (Rondeaux et al 1996).

$$OSAVI = \frac{(1 + 0{,}16) \cdot (R_{864} - R_{671})}{R_{864} + R_{671} + 0{,}16}$$

with:

R_{XXX} = nadir reflection at the given wavelength

2.4.3 Indices based on discrete narrow bands

With the recent development of imaging spectrometers, new indices have been explored using the information contained in narrow absorption features. In this way it is possible to improve estimations of leaf constituents like chlorophyll and water (Haboudane et al., 2004) or even to explore biochemicals with more subtle spectral absorption features such as protein, lignin and phosphorus (Fourty et al., 1996; Mutanga et al., 2004). Apart from new ratios based on a few discrete bands, novel approaches based on spectral shape and the depth of spectral absorption features have been developed. Although the majority of these new techniques were originally developed for identifying leaf constituents, many of them have been successfully applied in estimating other biophysical variables such as LAI (Broge and Leblanc, 2000; Haboudane et al., 2004).

TVI

The Triangular Vegetation Index (TVI) by Broge & Leblanc was developed in 2000 to describe the radiative energy absorbed by the pigments as a function of the relative difference between red and near infrared reflectance in conjunction with the magnitude of the green region reflectance, where the light absorption by chlorophyll is relatively lower (Hall & Rao 1987). The TVI is based on the fact that chlorophyll absorption causes a decrease of red reflectance and abundance of leaf tissue causes a increased near infrared reflectance (Broge & Leblanc 2000).

$$TVI = 60 \cdot (R_{750} - R_{550}) - 100 \cdot (R_{670} - R_{550})$$

with:

R_{XXX} = nadir reflection at the given wavelength

MTVI1 and MTVI2

The Modified Triangular Vegetation Index 1 and 2 were developed by Haboudane et al in 2004 to make the TVI suitable for LAI estimations. To achieve this the 750 nm was substituted by the 800 nm wavelength because this spectrum is more sensitive to changes in leaf and canopy structures and non – sensitive to changes in the pigment level (Haboudane 2004).

$$MTVI1 = 1{,}2 \cdot [1{,}2 \cdot (R_{800} - R_{550}) - 2{,}5 \cdot (R_{670} - R_{550})]$$

with:

R_{XXX} = nadir reflection at the given wavelength

The equation was still strongly influenced by soil reflection. Therefore the equation was optimised with the introduction of a soil adjustment factor as developed for SAVI (Huete 1988). The same adjustment was done for the MCARI as shown later.

$$MTVI2 = \frac{1{,}5 \cdot [(R_{800} - R_{550}) - 2{,}5 \cdot (R_{670} - R_{550})]}{\sqrt{(2 \cdot R_{800} + 1)^2 - 6 \cdot R_{800} - 5 \cdot \sqrt{R_{670}} - 0{,}5}}$$

with:

R_{XXX} = nadir reflection at the given wavelength

2.4.4 Narrow Band Chlorophyll Indices

New narrow band ratios have mainly been used for the retrieval of water and chlorophyll concentration. Absorption due to leaf water takes place at wavelengths greater than 1000 nm. This is why ratio indices attempting to explain water content always use one or more bands in this domain (Penuelas et al., 1997; Zarco-Tejada and Ustin, 2001). Most hyperspectral ratios used for estimating leaf chlorophyll content make use of the three discrete bands describing the typical reflectance pattern of green vegetation: the reflectance peak in the green and NIR and the region of maximum absorption in the red.

CARI

The Chlorophyll Absorption in Reflectance Index (CARI) was developed by Kim 1994 for minimizing the influence of the reflection of non – photosynthetic materials (Daughtry et al 2000) and is used as basis for different new developed indices.

$$CARI = \frac{\frac{R_{701}}{R_{671}} \cdot \left| (a \cdot 670 + R_{671} + b) \right|}{\sqrt{a^2 + 1}}$$

with:

$a = (R_{701} - R_{549}) / 150$; $b = R_{549} - 550 * a$;

R_{XXX} = nadir reflection at the given wavelength

MCARI

The Modified Chlorophyll Absorption in Reflectance Index was developed by Daughtry et al in 2000. This index was showed to be influenced by parameters as LAI, chlorophyll, LAI-chlorophyll interaction and background reflectance (Daughtry 2000). At low chlorophyll concentrations the MCARI is sensitive to non- photosynthetic elements (Haboudane 2002).

$$MCARI = [(R_{701} - R_{670}) - 0{,}2 \cdot (R_{701} - R_{550})] \cdot \frac{R_{701}}{R_{670}}$$

with:

R_{XXX} = nadir reflection at the given wavelength

TCARI

The Transformed Chlorophyll Absorption Ratio Index (TCARI) was created by Haboudane et al 2002 to make the MCARI less sensitive to soil influences.

$$TCARI = 3 \cdot [(R_{701} - R_{670}) - 0{,}2 \cdot (R_{701} - R_{550}) \cdot \frac{R_{701}}{R_{670}}]$$

with:

R_{XXX} = nadir reflection at the given wavelength

MCARI1 and MCARI2

The Modified Chlorophyll Absorption in Reflectance Index one and two were created by Haboudane et al 2004 in the same way with the MCARI they did for the TVI shown above.

$$MCARI1 = 1{,}2 \cdot [2{,}5 \cdot (R_{800} - R_{670}) - 1{,}3 \cdot (R_{800} - R_{550})]$$

with:

R_{XXX} = nadir reflection at the given wavelength

As for the MTVI1, a less soil reflectance influenced version was developed also for the MCARI1, the MCARI2.

$$MCARI2 = \frac{1{,}54 \cdot [2{,}5 \cdot (R_{800} - R_{670}) - 1{,}3 \cdot (R_{800} - R_{550})]}{\sqrt{(2 \cdot R_{800} + 1)^2 - (6 \cdot R_{800} - 5 \cdot \sqrt{R_{670}}) - 0{,}5}}$$

with:

R_{XXX} = nadir reflection at the given wavelength

SR705 and mND705

These indices where both developed by Sims & Gamon 2002 to predict the chlorophyll content from Satellite data. They selected the reflectance of 705 nm for the indices because this is said to be influenced only by higher or lower chlorophyll content. The result were the Simple Ratio Index (SR705) and the Normalized Difference Index (mND705)

$$SR705 = \frac{R_{750}}{R_{705}}$$

with:

R_{XXX} = nadir reflection at the given wavelength

$$mND705 = \frac{R_{750} - R_{705}}{R_{750} + R_{705} - 2 \cdot R_{440}}$$

with:

R_{XXX} = nadir reflection at the given wavelength

MTCI

The MERIS Terrestrial Chlorophyll Index was established by Dash & Curran 2004, to monitor the chlorophyll content of large regions by remote sensing. The used spectra are similar to the ones used for SR705 and mND705.

$$MTCI = \frac{R_{754} - R_{709}}{R_{709} - R_{681}}$$

with:

R_{XXX} = nadir reflection at the given wavelength

GI

The Greenness Index (GI) is mentioned by Zarco – Tejada et al 2005, but without any further comments.

$$GI = \frac{R_{554}}{R_{677}}$$

with:

R_{XXX} = nadir reflection at the given wavelength

Red edge parametrisation

The Red Edge Inflection Point (REIP) method is described by 4 different authors with 4 varying equations. Two are using the 1st and 2nd order Savitzky – Golay – Filter and the other two self - developed equations. The characteristic at the red edge infliction point (around 720nm) is a blue - or red – shift which is related to plant growth conditions. If a shift towards the shorter (blue) wavelength is observed, a decrease in vegetation density will be associated. If the shift is towards the higher (red) wavelength a increase in green material is the reason (Broge & Leblanc 2000).
Guyot et al 1988 introduced the following equation, called REIP1 in this thesis:

$$REIP1 = \frac{700 + \frac{740}{700} \cdot (R_i - R_{780})}{R_{740} + R_{701}}$$

with

$R_i = 0{,}5 * (R_{780}/R_{670})$

R_{XXX} = nadir reflection at the given wavelength

The Savitzky – Golay – Filter was developed to smooth a curve by a moving polynomial - fit using constant coefficients. Used in the VIs called REIP2 and REIP3 in this thesis. For further details look at http://www.statistics4u.info/fundstat_germ/cc_filter_savgol_math.html

Dawson & Curran 1998 developed an equation based on lagrangian interpolation, which allows the determination of REIP by only three data points. According to Broge & Leblanc 2001, Broge & Mortensen 2002, and Broge 2003 this method gives the most accurate estimation of REIP. In this thesis this index is called REIP4

2.4.5 Relations between vegetation index and biophysical / biochemical variables

To shorten the following equations only the acronyms for the VIs are given. The equations of the VIs available from literature are given in the corresponding chapters. To shorten the names of the LAI related VIs and to use distinct names they were numbered following their appearance in ASTools.

LAI – NDVI

Gardner & Blad 1986 developed for corn the following equation to estimate the LAI from NDVI:

$$LAI1 = -1{,}248 + 5{,}839 \cdot NDVI$$

Mohammed et al 2005 developed this version:

$$LAI2 = 0{,}45 \cdot e^{e^{NDVI}}$$

LAI - RVI

The combination of LAI and RVI is used by some authors.

Gardner and Blad 1986 developed for maize two equations:

$$LAI3 = 0{,}416 + 0{,}2553 \cdot RVI$$

$$LAI4 = 0{,}0305 + 1{,}9645 \cdot \log(RVI) - 0{,}1577 \cdot RVI$$

Liu et al 1996 developed also two different equations. One for deciduous forest and the other one for crops.

$$LAI5 = 0{,}475 \cdot (RVI - 2{,}781)$$

for deciduous forest

$$LAI6 = 0{,}325 \cdot (RVI - 1{,}5)$$

for crops

LAI – RDVI, LAI – MSAVI, LAI – MTVI2 and LAI - REIP

These combinations of indices were created by Broge & Leblanc 2000 and tested by Haboudane et al 2004 for corn, soybean and wheat:

$$LAI7: \qquad LAI - MTVI2 = 0{,}227^{3{,}6566 \cdot MTVI2}$$

$$LAI8: \qquad LAI - RDVI = 0{,}0918^{6.0002 \cdot RDVI}$$

$$LAI9: \qquad LAI - MSAVI = 0{,}1663^{4{,}2731 \cdot MSAVI}$$

The last of of the combination LAI – indices was created by Danson & Plummer in 1986 using the REIP1 method created by Guyot. (Dorigo et al 2006).

$$LAI10: \qquad LAI - REIP1 = e^{\log \cdot REIP - \frac{\log 710{,}1}{0{,}0084}}$$

Ca+b – REIP1 and Ca+b – TCARI/OSAVI

These two combinations for predicting the Cab – content were created by Curran & Hay 1986 and Haboudane et al 2004 (Dorigo 2006).

$$Cab1: \qquad Ca+b - REIP1 = -32{,}13 + 0{,}05 \cdot REIP1 \quad [\text{in: mg/g}]$$

$$Cab2: \qquad Ca+b - TCARI/OSAVI = -30{,}605 \cdot \log \frac{TCARI}{OSAVI} \quad [\text{in: } \mu\text{g cm}^{-2}]$$

3.Study Area

3.1 Broader setting

Measurements took place at four fields in Amir Temur Shirkat and on plots on the Urgench University campus, which are located in the irrigated area of the Khorezm oblast (region) in the Republic of Uzbekistan in Central Asia. Considering the broader setting, Uzbekistan is bordered to the west by the Ustjurt – Plateau and in the east and southeast by the partly snow covered Tien Shan mountain range with altitudes up to 4100m above sea level. The average altitude of Uzbekistan is between 113 and 138 m above sea level. The wells of Amu Darya, from which water is used to irrigate the fields in irrigation systems such as Khorezm, are located in Tadjikistan deep in the Tien Shan. Administratively, Uzbekistan is divided in 12 oblasts and the autonomous Republic Karakalpakstan. The total land area of Uzbekistan amounts to 44.9 million ha, of which 23.5 million ha are in pasture. A total of 4.3 million ha are irrigated of which 3.3 million ha are arable land and 1 million ha are pasture (FAO 2003). Approximately 98% of its water is used for the irrigated agriculture.

As shown in figure 3.1, Khorezm is a river oasis of the Amu Darya River near the border to Turkmenistan at the eastern edge of the Turan lowland between the deserts Kysylkum in the north and east and Karakum in the west and south, about 250 km south of the present shores of the Aral Sea. The capital of the region, Urgench, with about 150.000 inhabitants is surrounded by intensively used, irrigated agricultural land. The climate is extremely continental with large daily and seasonal temperature differences. The monthly averaged temperatures are 26 to 28°C in July and dominated by frost with temperatures down to -20°C in January. With average precipitation amounts of 92mm (varying between 40 and 160 mm) per year very arid area. The total daily potential evapotranspiration (ETo), calculated with the Penman-Monteith equation (Smith et al. 1991), amounted to 460 mm for 2002. Due to this climatic conditions a huge amount of water is needed to irrigate the fields. Agriculture accounts for 26% of the country´s GDP and employs more than a third of the population (FAO 2003). The sowjet style irrigation system, with open and often leaky canals and inappropriate irrigation of crops, leads to a high salinisation of water and soils, a problem often encountered in irrigation-based agriculture in arid and semiarid landscapes. Politically, the agricultural system is still affected by the former sowjet collective farm system. The agricultural land in Uzbekistan is divided in 1 389 collective farms (kolkhoz), 872 cooperative farms (shirkats), 21 675 family owned farms (dekhan) and 1 895 private farms. This division results in a patchwork of fields that vary in size from around 1 ha to 25 ha. Generally, the land is leased longterm to the farmers, because of the private landown ban. The small farmers of the dekhan and private farms do not possess their own machinery, therefore the shirkats, the successor

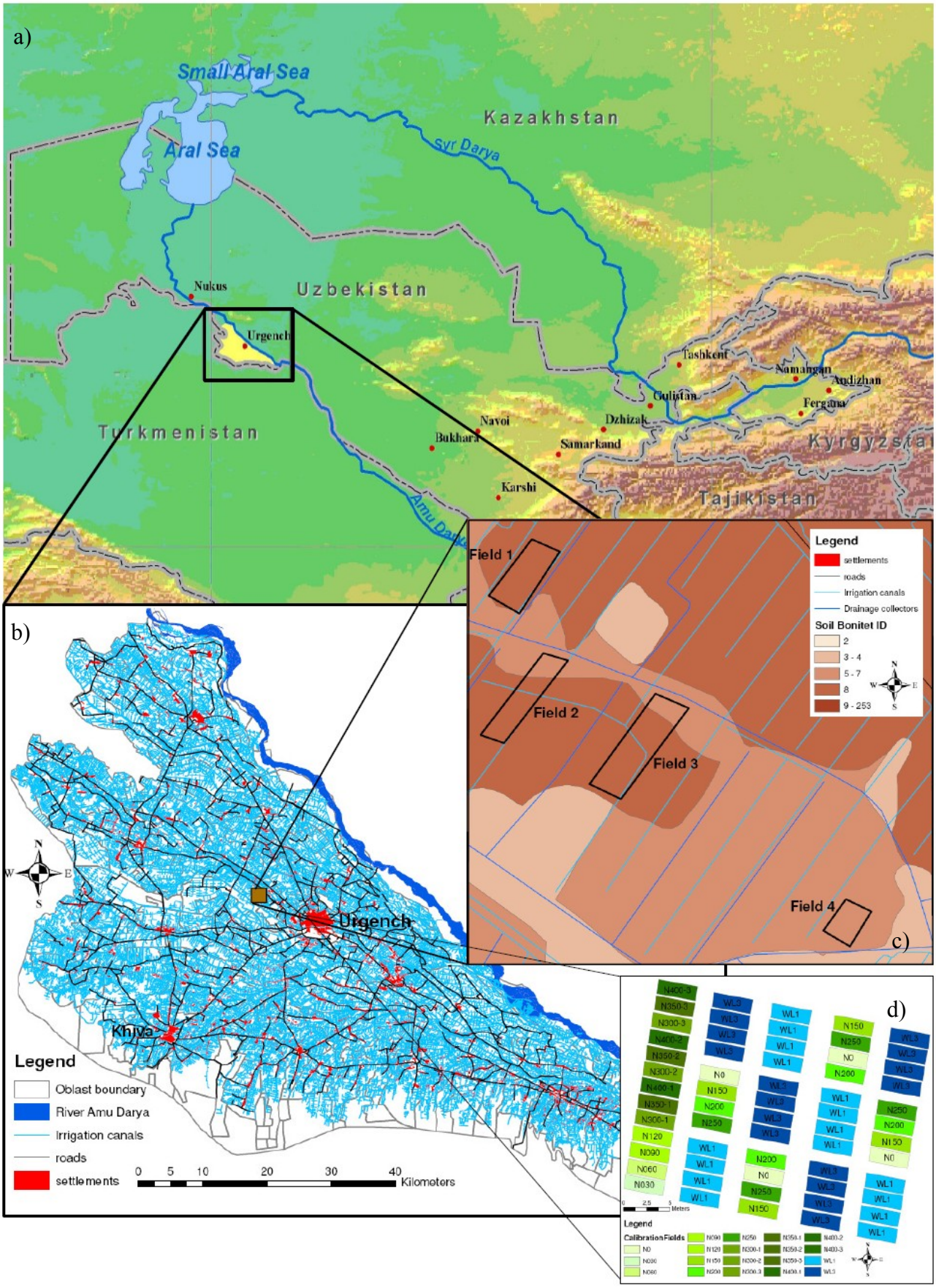

Figure 3.1: Wider setting of the study site within Uzbekistan, b) Khorezm oblast with irrigation canals and the location of the study fields and plots, c) location of the four study fields within Amir Temur Shirkat d) study plots on the campus of the Urgench University.

organisations of the former socialistic collective farms have tractor parks and provide the farmers with advice, fertilizer and access to the irrigation system.

3.2 Fields on Amir Temur Shirkat

The four study fields where the measurements of this study took place are part of the Amir Temur Shirkat located in Khorezm in the west of Urgench (compare with figure c).

The fields were selected based on certain criteria, such as to get the allowance from the Shirkat manager to perform the measurements, to select fields of the same cotton variety and the same fertilizer application and irrigation rate, but with variations of environmental conditions in order to capture different LAI and chlorophyll conditions among the fields. The different environmental conditions were parametrized by different soil bonitet levels.

Based on a joint field visit with the Shirkat manager of the Amir Temur Shirkat, four fields were selected on which the cotton variety “Khorezm 127” was planted at the end of April or the beginning of May 2006 after leaching of the fields. These fields were used to validate the satellite based estimations of LAI and chlorophyll. The main characteristics of the fields are shown in table 3.1.

Table 3.1: Fertilizer Application rates and modalities for regional scale

Field	*Planting Day*	*Fertilisation*	*Amount of Fertilizer*	*Irrigation*	*Amount of Water*
Field 1	11.04.06	04.05.06	400 Kg/ha	09.05.06	more than enough, nobody cared ...
		14.06.06	200 Kg/ha	16.06.06	
		18.07.06	200 Kg/ha	20.07.06	
Field 2	28.4./ 1.5.06	10.07.06	400 Kg/ha	15.07.06	
		-	-	20.07.06	
Field 3	14.04.06	10.05.06	200 Kg/ha	15.05.06	
		02.06.06	200 Kg/ha	04.06.06	
		05.07.06	200 Kg/ha	10.07.06	
		01.08.06	200 Kg/ha	04.08.06	
Field 4	20.04.06	09.05.06	400 Kg/ha	12.05.06	
		07.06.06	200 Kg/ha	08.06.06	
		07.07.06	200 Kg/ha	10.07.06	

3.3 Plots on fertilizer-trial

For leaf and canopy scale analysis, plots of a fertilizer trial with different fertilizer application rates were selected. The plots on the selected fertilizer trial for this study where located in front of the ZEF/UNESCO Khorezm project institute within the boundaries of the University of Urganch. The small plots were about 1.5 m wide and 3 m long.and were cultivated with the Khorezm 127 Cotton Variety with different fertilizer application rates (ranging from 0 to 400 kg nitrogen per ha) and water levels. Each plot consisted of four rows with a varying number of cotton plants because some plants died during the season. Within each plot of Water Level 2, the amount of water which is recommended as efficient for cotton (Kienzler 2007), five plants located in the two middle rows were randomly selected and labelled for an easier identification at each measurement. An overview on the fields is given in figure 3.2.

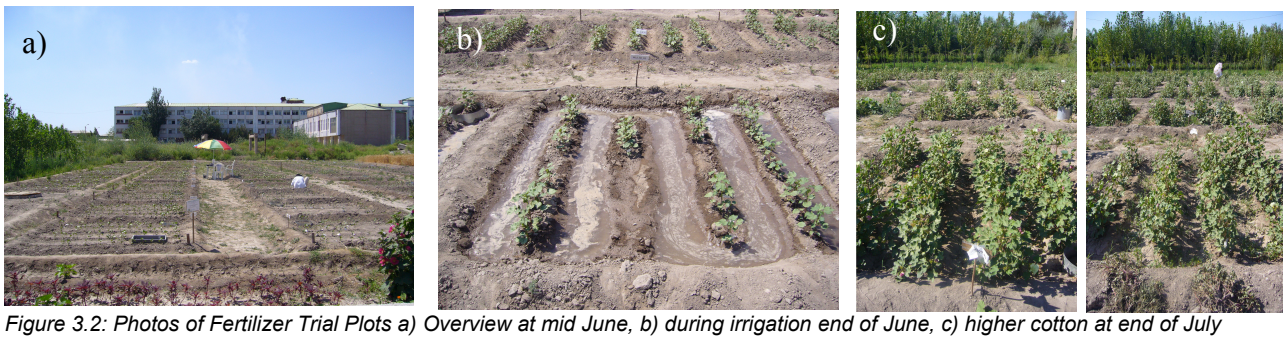

Figure 3.2: Photos of Fertilizer Trial Plots a) Overview at mid June, b) during irrigation end of June, c) higher cotton at end of July

Source: Own photos

4.Data and Methods

4.1 Conceptual framework

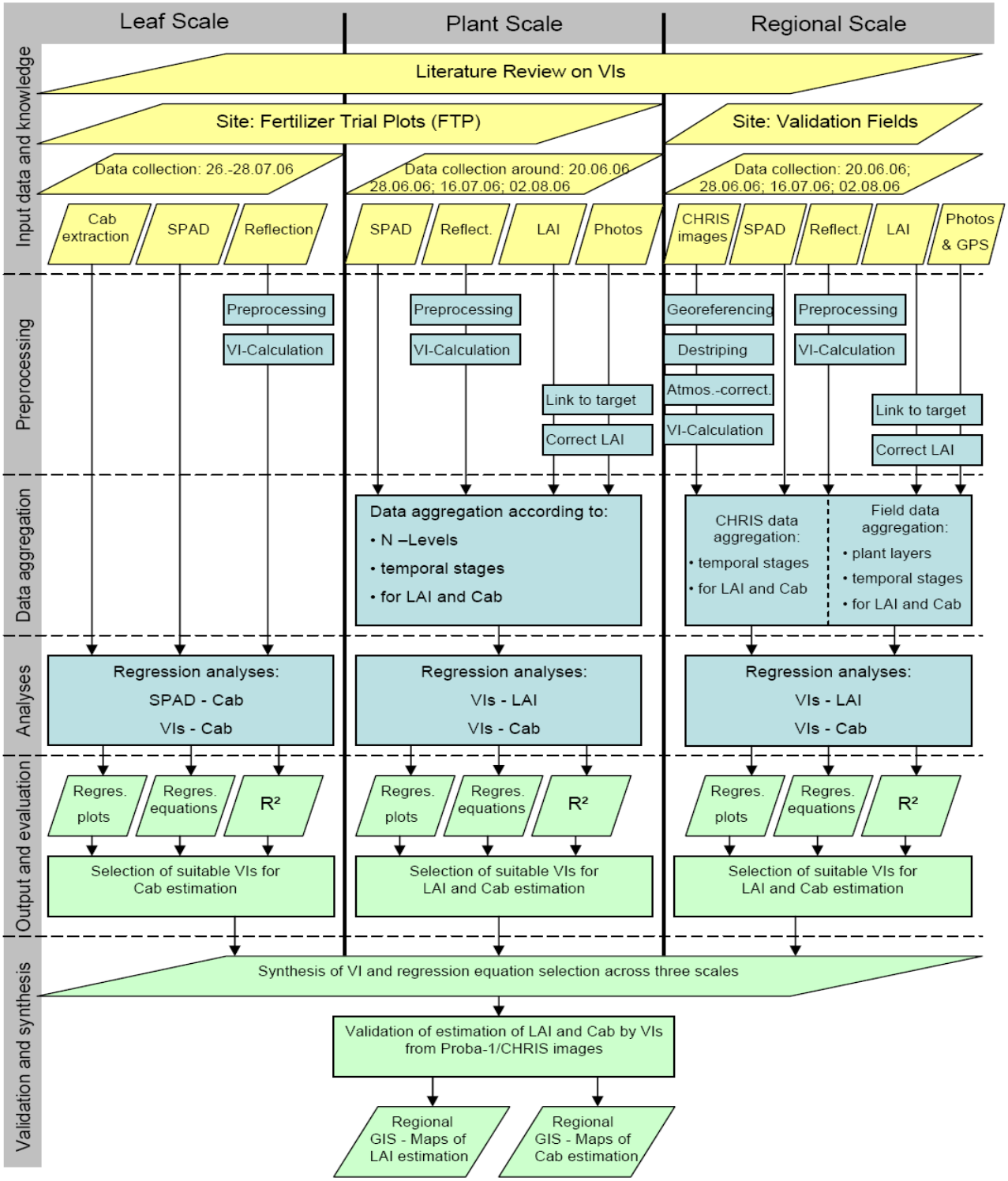

Figure 4.1: Diagram visualizing the conceptual framework of this thesis

The conceptual framework of this thesis is organized at three spatial scales (fig. 4.1) leaf, plant, and field scale.

At a leaf scale SPAD and reflectance measurements of cotton leaves collected at one date were combined with the laboratory analyses results to establish a relationship between SPAD and absolute C_{ab} content extracted in the laboratory. As a result of this scale the equation to transfer SPAD into C_{ab} content was achieved. Furthermore relationships between VIs based on spectral reflectance measurements, and Cab were analysed to determine the best VI for estimating the leaf C_{ab} content by spectral reflectance measured by ASD field spectrometer.

At a plant scale the measurements (LAI, SPAD, reflectance) were carried out based on cotton plants treated with different fertilizer application rates on fertilizer trial plots (FTPs) (map figure 3.1d, photos figure 3.2). At this scale LAI, SPAD and reflectance measured by ASD field spectrometer of 5 plants per trial plot and at four dates relating to fertilizer and irrigation events were measured. These dates were set approximately at the time of Proba-1/CHRIS satellite-sensor data takes. The referring dates are shown in figure 4.2. The results of these measurements were aggregated by date and nitrogen application level of the FTPs separated for LAI and C_{ab} respectively. The results of plant scale comprised the determination of the VI predicting LAI and C_{ab} best at the different temporal stages and N-levels.

At a regional scale VIs were calculated based on Proba-1/CHRIS images acquired during four dates at which main irrigation and fertilizer events for cotton occured. These VIs were used to predict LAI and SPAD measured from cotton plants that were located in four farmer-managed fields and covered by the satellite images. To correct and verify the satellite – images reflectance of different targets was measured using ASD field spectrometer during the satellite overpasses. The location where LAI and SPAD values were collected were identified by GPS measurements and photos that were in turn used for georeferencing the satellite images. As results of this spatial scale the VIs with the best prediction power for LAI and C_{ab} per temporal stage were determined, the relationship evaluated by cross-validation and the respective VIs and equations created to estimate LAI and C_{ab} at the last three dates identified. These results are presented in form of GIS maps to visualise the spatial distribution and the development over time for LAI and C_{ab}, respectively.

The dates when all measurements of this field campaign were fulfilled are given in figure 4.2. Additional measurements for LU-training areas collection are shown as part of the field campaign but were not described in the following chapters, because they were not part of this thesis.

Workplan for chlorophyll/nitrogen and land use research activities in 2006

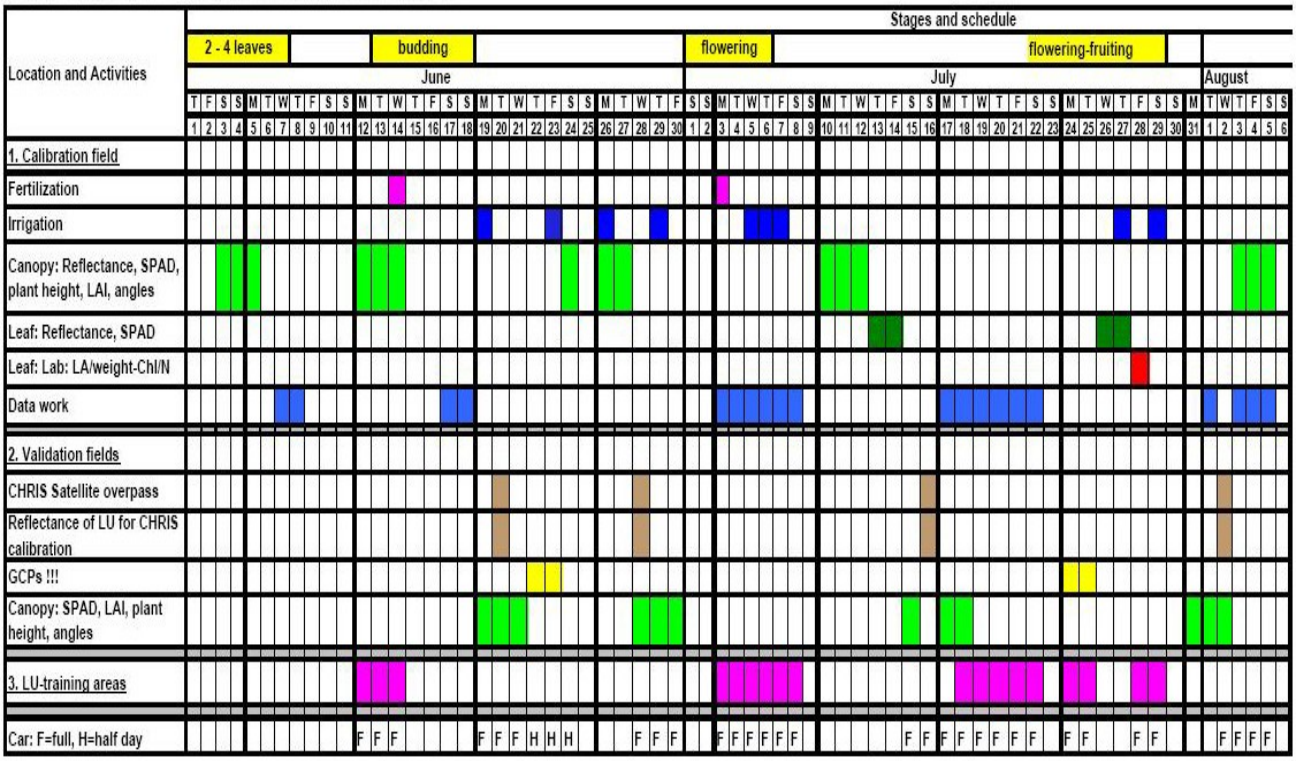

Figure 4.2: Time Table for Measurements during Field Campaign in Uzbekistan

Source: Own work with Excel

4.2 Used field instruments and measurements

4.2.1 Spectral reflectance measurements

Spectral reflectance was measured with the Analytical Spectral Devices (ASD) Field Spectrometer (figure 4.3), a instrument consisting of three photodiode arrays with a changing sensitivity and covers different wavelength bands to collect spectral reflectance information of a target via an optical pointing device. The VNIR spectrometer covers the 350 – 1000nm range with a sensitivity of 3nm. The SWIR1 spectrometer (1000 – 1800nm) and SWIR2 spectrometer (1800 – 2500nm) have a sensitivity of 10nm.

Figure 4.3: Author using ASD Field Spec on wheat field
Source: Own photo

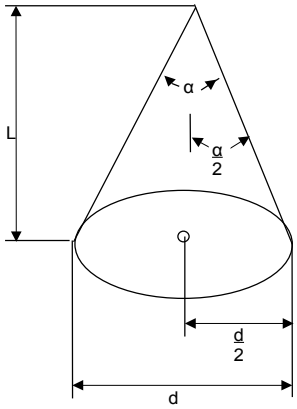

Figure 4.4: Scheme of cone of the ASD fibre opening angle
Source: ASD Technical Guide

Table 4.1 shows different heights with the corresponding spot size for both, bare fibre optic and foreoptic to adjust the measuring height according to the height and width of the target. Figure 4.4 shows the cone within which the reflection was collected.

All the collected spectra showed noisy spectral behaviour at around 1400 and 1800nm as shown in the figure 4.5. ASD Technical Guide (HATCHELL 1999) explained this phenomenon as the Water Band Noise and the ASTools (DORIGO et al. 2006) are providing a special tool to remove it, but this was not necessary because the Water Band Noise was out of the spectral area of interest.

Table 4.1: ASD fibre opening angles and corresponding spot sizes

ASD with bare fibre Angle 25° With α/2= 12,5°			**ASD with foreoptic Angle 8°** With α/2=4°	
L in m	**d/2 in m**	**d in m**	**d/2 in m**	**d in m**
0,10	0,02	0,044	0,01	0,014
0,15	0,03	0,066	0,01	0,021
0,20	0,04	0,089	0,01	0,028
0,25	0,06	0,111	0,02	0,035
0,30	0,07	0,133	0,02	0,042
0,35	0,08	0,155	0,02	0,049
0,40	0,09	0,177	0,03	0,056
0,45	0,10	0,199	0,03	0,063
0,50	**0,11**	**0,22**	**0,03**	**0,07**
0,55	0,12	0,244	0,04	0,077
0,60	0,13	0,266	0,04	0,084
0,65	0,14	0,288	0,05	0,091
0,70	0,16	0,310	0,05	0,098
0,75	0,17	0,332	0,05	0,105
0,80	0,18	0,355	0,06	0,112
0,85	0,19	0,377	0,06	0,119
0,90	0,20	0,399	0,06	0,126
0,95	0,21	0,421	0,07	0,133
1,00	**0,22**	**0,44**	**0,07**	**0,14**
1,05	0,23	0,465	0,07	0,147
1,10	0,24	0,487	0,08	0,154
1,15	0,25	0,510	0,08	0,161
1,20	0,27	0,532	0,08	0,168
1,25	0,28	0,554	0,09	0,175
1,30	0,29	0,576	0,09	0,182
1,35	0,30	0,598	0,09	0,189
1,40	0,31	0,620	0,10	0,196
1,45	0,32	0,643	0,10	0,203
1,50	**0,33**	**0,66**	**0,10**	**0,21**

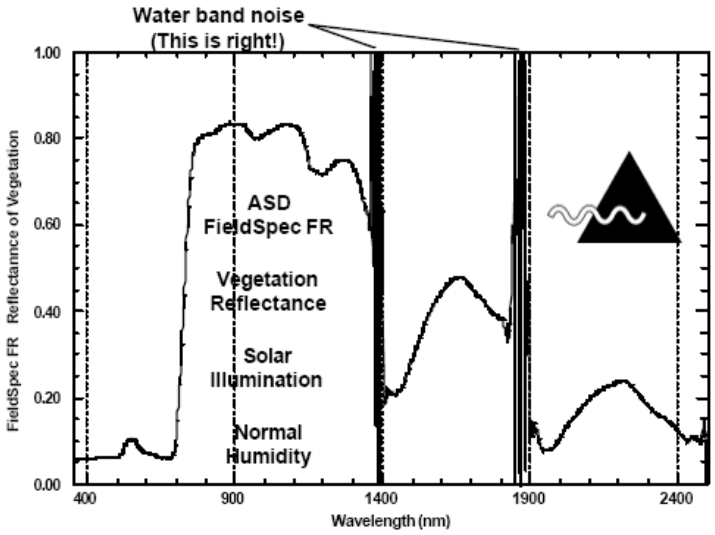

Figure 4.5: Graph with Water Band Noise
Source: HATCHELL 1999

The ten collected spectra per target were corrected following a standardized procedure to make the results comparable and to remove possible errors and outliers. After downloading the measured spectra from the ASD Field Spectrometer all spectral data collected of the same target on one day were stored in the same folder. Afterwards these spectra were imported to ENVI 4.1 and grouped in one Spectral Library for each day and sample collection. All intermediate processing results from the following steps were saved as new files to be able to reconstruct every processing step. Each file was named following a special naming convention. Each file name begins with the date of data collection, followed by the information on the location where the spectra were collected and the processing steps. The first step was to eliminate the small discrepancies between the reflection of the used spectralon and 100% white reflection, because the spectralon reflectance was used as reference, The plant reflectance was calculated from the differences to this reference. This correction, called “txt-correction”, was carried out using the program “ASTools” (DORIGO et al. 2006) and the ASD Spectralon correction file provided by the manufacturer. Secondly the spectral jump between the first spectrometer of the ASD was adjusted to the second spectrometer using the corresponding function in the ASTools. The third step included the corrections of deviations in spectral reflectance due to changes in atmospheric conditions during the target measurements. For this last correction, the spectralon measurement directly following the ASD calibration and the measurement of the spectralon and the measurements of the target within a time period of around five minutes were saved in different files and corrected using ASTools` ”spectralon correction” mode in order to adjust the gain and the curve of the spectra correspondingly. The changes in the spectral information during the process of correction is stepwise shown in figure 4.6.

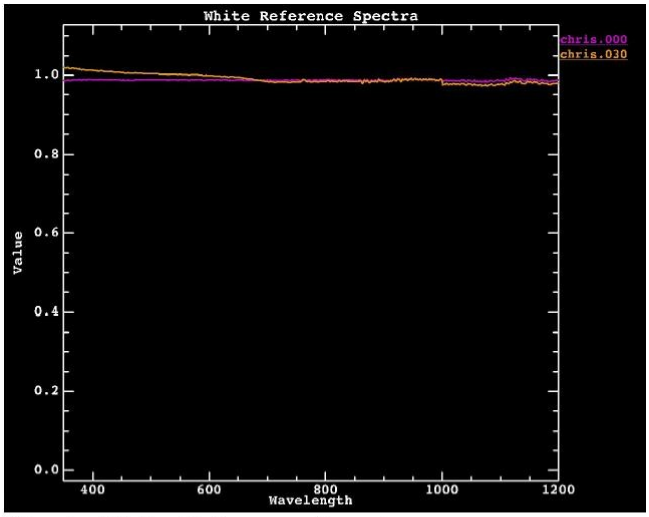

Step1: White Reference Spectra

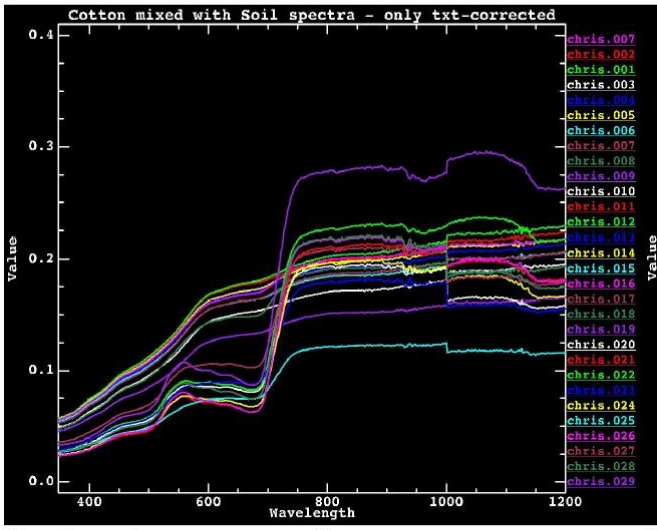

Step2: only txt-corrected

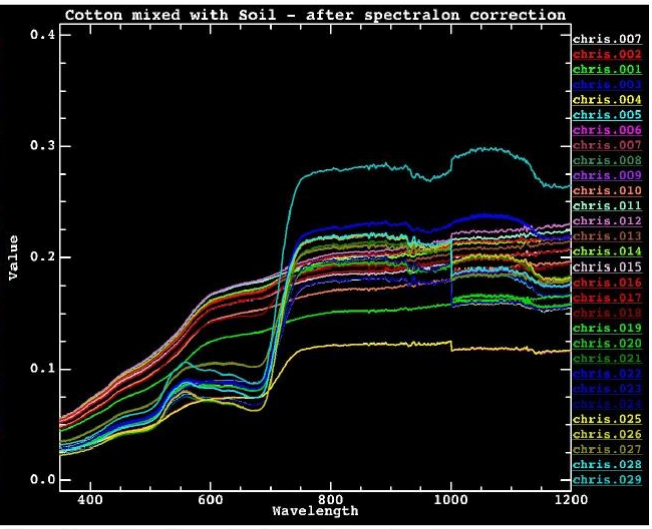

Step3: after Spectralon interploation

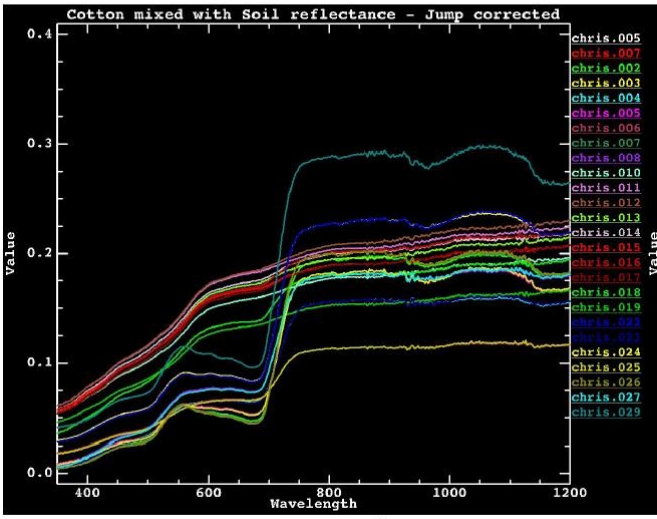

Step4: ASD - Jump corrected

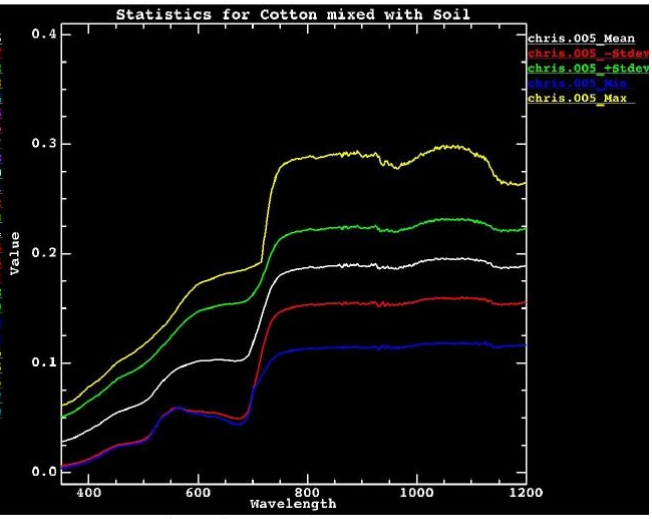

Step5: Result - the Statistics

Figure 4.6: Different steps of the Spectra preparation process

Source: Own work with ENVI 4.1

4.2.2 Measurements with Minolta SPAD Chlorophyll Meter

The chlorophyll meter SPAD-502 produced by Minolta (SPAD) was applied to determine the relative amount of chlorophyll present in cotton leaves at a certain growth stage. The instrument measures leaf absorption in two wavelength regions, comprising the red and the near infrared regions. The SPAD emits therefore light by two built in LED´s. The part of the light transmitted through the leaf sample is collected by a receiver and the corresponding SPAD value is computed. See figures 4.7 to 4.9.

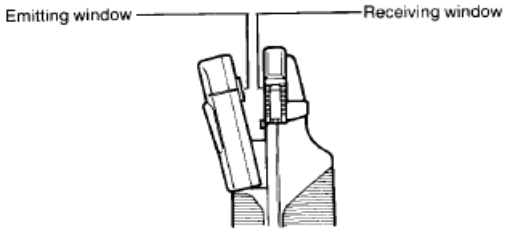

Figure 4.8: Function of the Minolta SPAD-502
Source: Konica 1989

Figure 4.9: Minolta´s SPAD-502
Source: BRONSON 2005

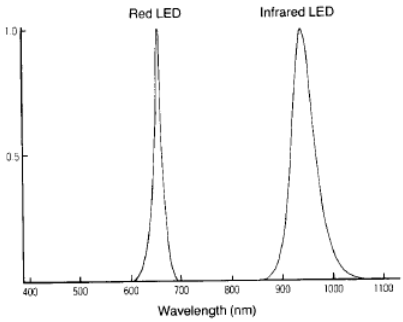

Figure 4.7: Wavelength emitted by the LED ´s built in the SPAD
SOURCE: Konica 1989

SPAD provides a rapid and nondestructive diagnosis of plant chlorophyll status and has been widely tested for crops like rice, corn, wheat and cotton (TURNER et al. 1991, PETERSON et al. 1993, VARVEL et al. 1997, FOLLET et al. 1992, BRONSON 2005). BRONSON et al. 2001 and RÜCKER 2005 found for different cotton varieties that in-season chlorophyll – meter measurements of cotton leaves had a strong correlation with leaf N.

4.2.3 LICOR – 2000 LAI-Meter

The LI-COR LAI-2000 Plant Canopy Analyzer was used to estimate the Leaf Area Index of cotton plants on fields in a non-destructive way. The optical sensor consists of a “fish-eye” lens with a hemispherical field of view and a zenith cutoff angle of 74°. This range is divided into five detector rings of different view angles. The photodiode detector is filtered to respond only to radiation below 490 nm to minimize the influence of leaf reflectance and transmittance (LI-COR Manual). This instrument cannot distinguish the gap fraction produced by the obstruction by stems, bolls, flowers, dead or active leaves. It takes all light resistant objects into account. Welles and Norman (1991) therefore called the LAI Foliage Area Index, to strengthen the difference of the plant material of the whole plant and only the leaf area. The measurement strategy was, that the first measurement was directly above the plant, followed by 4 measurements at ground level around the stem of the plant. For avoiding the influence of the measurement person on data capturing, a quarter circle view cap was applied. The measurement area was always shaded using a dark and thick umbrella that was covered by a glossy sheet to avoid measurements in direct sunlight, which

would be inaccurate due to transmittance and leaf reflectance effects.

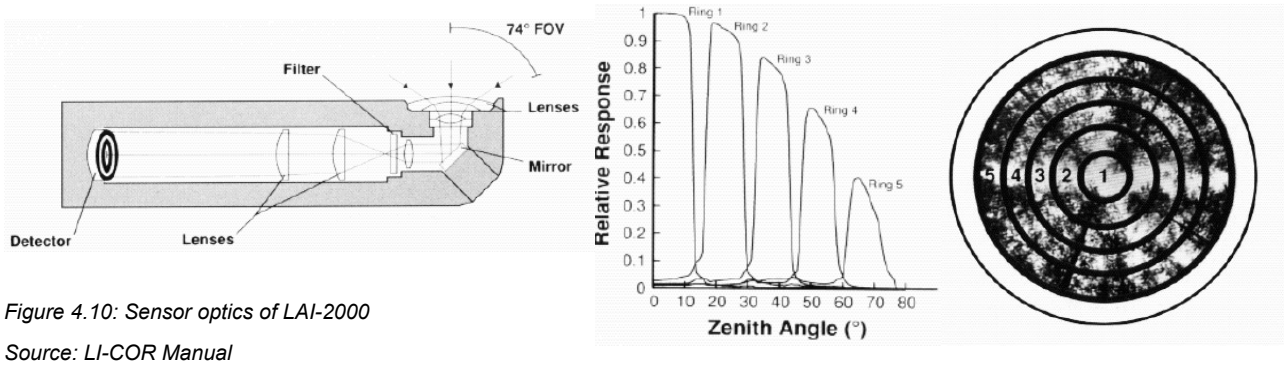

Figure 4.10: Sensor optics of LAI-2000

Source: LI-COR Manual

Blenk 2004 used a different measuring method for a similar topic. She also took the first measurement above the plants but spread the 4 ground measurements as shown in Figure 4.11 over approximately one square meter. This made it easier to interpolate the point-based LAI – values to cover a larger area.

Figure 4.11: Measuring Method for LAI by Blenk 2004

As in this study all 4 measurements were taken under one plant, a correction factor was introduced to reduce the overestimation of LAI for larger areas. The calculations of these correction factors are described in chapter 4.5.5.2. Table 4.6 (also chapter 4.5.5.2) shows the correction factors for the different stages.

4.3 Leaf scale measurements and analyses

The leaf scale measurements were carried out on the fertilizer trial plots. Therefore four plants of the rows 1 and 4 of the trial plots with leaves covering a range of SPAD values as wide as possible where selected. The measurements were necessary to establish a relationship between the SPAD values, the reflectance measurements and the actual leaf nitrogen content. 33 leaves of 4 plants were measured and harvested for the laboratory analysis. With the results of this analysis the calibration of the SPAD values can be performed and the results of the reflectance measurements can be validated. Each step of this process is described in the following chapters.

4.3.1 Leaf scale spectral reflectance measurements

The spectral reflectance measurement of the whole cotton plants was carried out by holding the fibre optic of the ASD field spectrometer in a certain height above the plant canopy. Small movements of the leaves due to slight wind and movements of the optic due to trembling were averaged by taking 10 measurements per target. For single leaf spectral reflectance measurements the leaf was fixed in a special construction, shown on the photos in figure 4.12.

Figure 4.12: Reflectance Measurement Procedure at Leaf Scale

Source: Own photos

This construction was modified after Adams (2005). In this study a hole with a diameter of around 34 mm diameter was drilled in a 3 mm thick metal plate. Afterwards the plate was covered by a black flock paper that exhibits almost no reflection. Heating up of the metal plate that may change the leaf pigment properties was avoided by cooling the metal between the measurements using a freezer box. The optic of the field spectrometer was fixed on an adjustable tripod and put in a position of 10 cm above the leaf. The amount of transmission of the leaf was taken into account by measuring the leaf once against an strongly absorbing and once against a strongly reflecting background. The reflectance of the different background materials as well as the reflectance of a leaf above white and black background is shown in the figure 4.13. The differences are small but easy to recognize.

The area from which the reflectance was taken, was marked with and thin waterproof pen, to ensure that the SPAD was collected within these areas and that the laboratory takes its samples out of the same area.

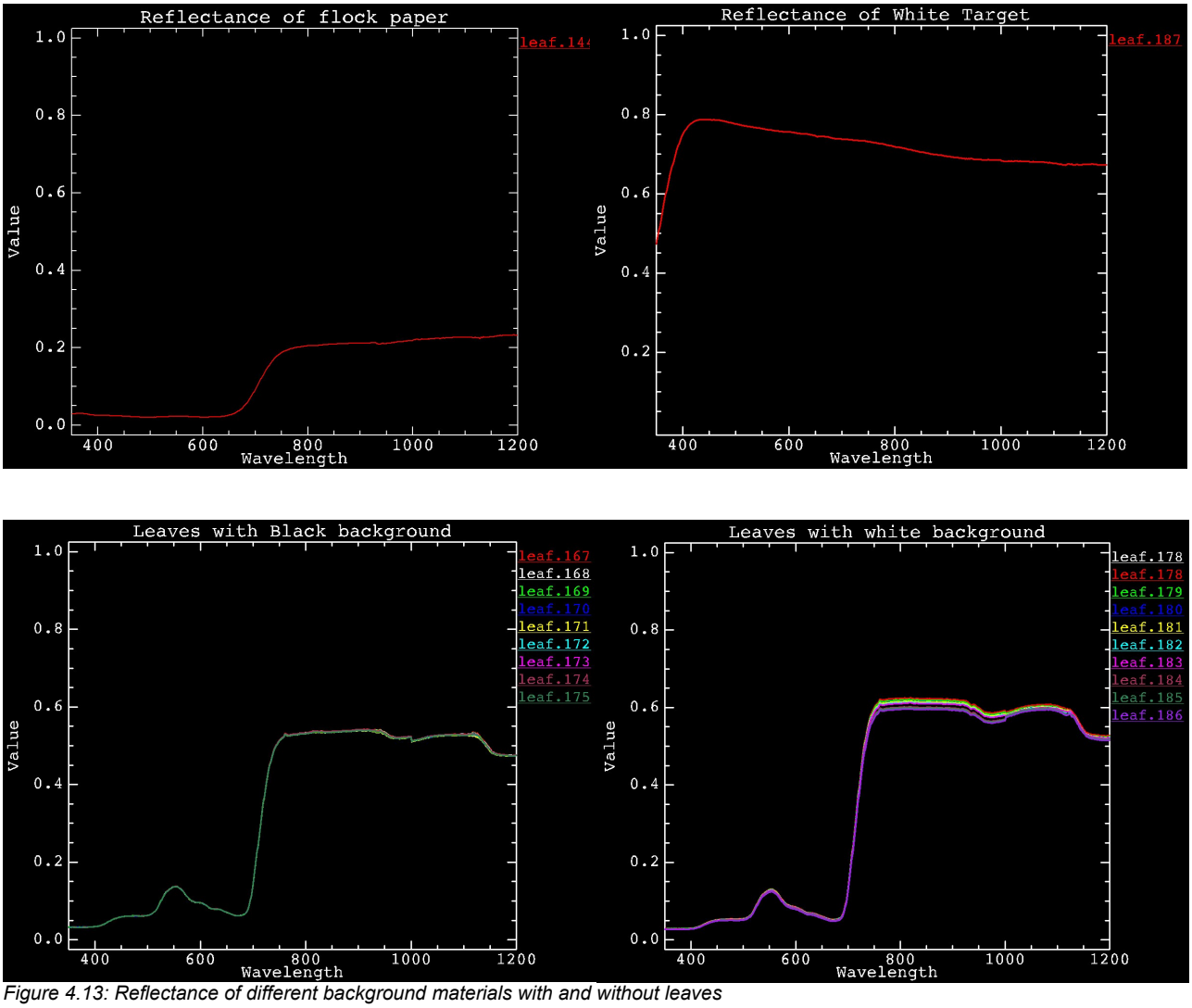

Figure 4.13: Reflectance of different background materials with and without leaves

Source: Own work with ENVI 4.1

4.3.2 Leaf scale chlorophyll determination by SPAD and in the laboratory

Using the SPAD tool, three readings were taken on each of the 33 leaves within the same area from where reflectance was measured. This sampling number was chosen to get an average SPAD-value for the leaf, thus averaging potential within-leaf variability of chlorophyll distribution. One day after the reflectance and SPAD measurements, the selected leaves were harvested early in the morning and fresh weight and leaf area of these leaves was measured by LI-3100 Leaf Area Meter subsequently. Afterwards the leaves were put in labelled plastic bags and kept fresh in a cooler bag that contained freezer elements. The cooled leaves were transported to Tashkent by plane and brought to the UzHydroLab for laboratory analysis. The institute analysed the 33 leaves for total nitrogen content, chlorophyll a, b content, amount of caratenoids, anthocyanins and water content. Afterwards these results were combined with the results of the SPAD measurements to

calibrate the SPAD – values for the Khorezm 127 cotton variety. The Vegetation Indices calculated with ASTools and the reflectance measurements were also combined with the laboratory results to identify possible empirical relationships.

4.4 Plant scale measurements and analysis

Plant scale measurements were performed on cotton plants of the fertilizer trial plots near Urgench University. Five plants of each plot were randomly selected and labelled. The SPAD, LAI and reflectance, as well as biometric parameters such as plant height and diameter, number of nodes, and leaf angles, of these plants were determined following the field survey time table (compare fig. 4.2). The results were entered into one Excel file per measurement date and joined with the respective points of each plot (fig. 3.2).

These measurements were accomplished within 3 days around the satellite overpasses to compare the data collected on plant scale with the regional data.

4.4.1 Spectral reflectance measurements

The reflectance measurements for whole cotton plants were taken using the ASD field spectrometer without the foreoptic thus achieving a measurement angle of 25°. Depending on the diameter of the plant, the optic was hold in a vertical orientation at a distance of 15 to 45 cm above the plant. Following this measurement strategy, reflectance data was mainly collected for the foliage, thus capturing reflectance data from soil was avoided. For each plot five plants were selected and measured with 10 repetitions to average influences such as moving the optic by trembling or plant movements due to wind. The height of each measurement as well as the average leaf angle was recorded and added to the corresponding data in the Excel sheet. All measurements were performed from 10am until 2pm to guarantee relative homogeneous illumination conditions.

4.4.2 Biometric data collection on canopy scale

At plant scale, biometric data such as plant height, plant diameter and number of nodes was collected for each plant. SPAD values were measured for all leaves within plant layers that were demarcated by nodes on the stem. The measured SPAD values were averaged per layer and afterwards per plant. In the afternoon the LAI measurements of the monitored plants were conducted by LICOR – 2000 LAI-meter. The plants were shaded using a big and thick umbrella and the LAI was collected according to the procedure described in chapter 4.1.5.

4.5 Regional scale satellite image acquisition, measurements and analyses

4.5.1 Proba-1/CHRIS satellite mission and image acquisition

4.5.1.1 Proba-1/CHRIS satellite mission

PROBA (Project for On Board Autonomy) is a micro-satellite developed by ESA's General Support Technology Programme (GSTP) The satellite was launched from India on 22nd October 2001 and operated from ESA's Redu Ground Station in Belgium. Its CHRIS (Compact High Resolution Imaging Spectrometer) instrument, is a multiangular imaging spectrometer. With just 60 x 60 x80 cm dimension and 14 kg weight, CHRIS is the smallest hyperspectral imager ever flown in space and can scan the earth surface at a maximum resolution of 17 m. The multiangular sensor is able to acquire up to five images of approximately the same target at five observation angles (around ± 55°, ± 36° and nadir viewing) during one overpass, with up to 62 spectral channels (ESA homepage). It now serves as a technology demonstration mission of ESA (Teston, 2004). Therefore the mission provides images of only a limited number of pilot-sites throughout the globe that are selected by a scientific board of ESA. (BEGIEBING 2004) Dr. Gerd Rücker at DLR became one of the principal scientific investigators and is now authorized by ESA to acquire Proba-1/CHRIS satellite images of the pilot-site in Uzbekistan free of charge.

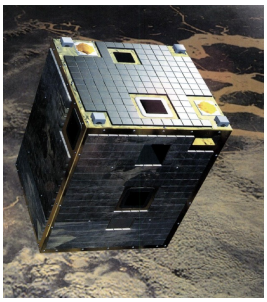

Figure 4.14: PROBA - Satellite in Space
Source: ESA homepage

The satellite images selected for this project are Proba-1/CHRIS Mode 5 data, because this mode has the highest spatial resolution (17 m pixel resolution at nadir sensor orientation) as well as hyperspectral information (37 bands) that is suitable for LAI and chlorophyll estimation. This mode is called the “half swath mode” because the images cover only one half of the nominal imaging area. The platform attitude system has only one pointing reference frame, which is coincident with the optical axis of the imaging system. Thus it is necessary to define a shifted longitude coordinate pointing to the eastern edge of the area to be imaged. This is approximately ¼ of the full swath width in normal imaging modes. The precise eastward shift depends on platform altitude and is given by:

$$Shift = \frac{altitude \cdot 0{,}0255 \cdot 748}{746 \cdot 4}\, km$$

In June 2006 the altitude varied between 552 and 685km, resulting in eastward imaging shifts between 3.1 and 3.9km (CHRIS data format). This image shift is represented in the coverage variation of the images acquired at different dates.

4.5.1.2 Proba-1/CHRIS image acquisition and time table

The multiangular Proba-1/CHRIS sensor images are acquired within a 55º cone, as defined by a vector connecting the centre of the earth to the spacecraft, as illustrated in figure 4.15. The cone creates a circular orbit with the distance to the spacecraft equal to the semi-major axis of the orbit, but this distance is not fixed. For orbits higher or lower than the semi-major axis the cone traced by the satellite during acquisition will be slightly different. The first acquisition is initiated at the leading edge of the cone at C1 and the final acquisition finishes at the finishing edge of the cone at C5. The centre time of the image acquisition therefore does not correspond to the edge of the cone. The red stripes (shown in figure 4.15) are indicating the area of image acquisition and the C1 to C5 the corresponding image acquisition times. (CHRIS data format)

Table 4.2: Order of CHRIS Image delivery

Source: Cutter 2005

Chronological Imaging Order	Tag No. order	Scan Direction	Nominal FZA
First	3	N-S	+55°
Second	1	S-N	+36°
Third	0	N-S	0°
Fourth	2	S-N	-36°
Last	4	N-S	-55°

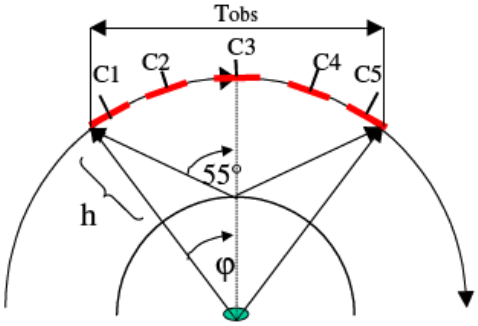

Figure 4.15: Angles of CHRIS Image acquisition
Source: Cutter 2005

Table 4.3: CHRIS Mode 5 Land Channels

Source: Cutter 2005

Band	Min λ (nm)	Max λ (nm)	Mid λ (nm)	Width (nm)	Corresponding to:
H1	438	447	442	9	L1,W2
H2	486	495	489	9	L2,W3
H3	526	534	530	9	L3,W5
H4	546	556	551	10	L4
H5	566	573	570	8	L5
H6	627	636	631	9	L6
H7	656	666	661	11	L7
H8	666	677	672	11	L8,W11
H9	677	689	683	11	W12+13
H10	694	700	697	6	L9
H11	700	706	703	6	L10
H12	706	712	709	6	L11
H13	712	719	716	6	
H14	719	725	722	6	
H15	725	732	728	7	
H16	732	738	735	7	
H17	738	745	742	7	L12
H18	745	752	748	7	L13
H19	752	759	755	7	W15
H20	759	766	762	7	
H21	766	773	770	7	
H22	773	788	777	15	L14,W16
H23	788	796	792	8	
H24	796	804	800	8	
H25	863	881	872	18	L15,W17
H26	881	891	886	10	
H27	891	900	895	10	L16
H28	900	910	905	10	L17
H29	910	920	915	10	
H30	920	930	925	10	
H31	930	950	940	20	
H32	950	960	955	10	
H33	960	971	965	11	
H34	971	981	976	11	
H35	981	992	987	11	
H36	992	1003	997	11	
H37	1003	1036	1019	33	L18,W18

The images are delivered following the order as specified in table 4.2. The wavelength covered by each channel is shown in the table 4.3. The CHRIS images for this project were acquired on the dates as shown in table 4.4. The table shows also if the study area is fully covered.

Used Symbols:

Table 4.4: Satellite Images covering validation fields

Source: internship - report Richard Fuchs (2006)

date	*-55*	*-36*	*0*	*36*	*55*
11.06.06	n/a	+	+	+	3 of 4
20.06.06	+	+	+	+	+
28.06.06	+	+	+	+	+
07.07.06	+	+	+	+	+
17.07.06	+	+	+	+	+
02.08.06	0 of 4	+	+	+	0 of 4

+ = ok (4 of 4 validation fields in the scene)
n/a = not available
x of 4 = number of validation fields in the scene

4.5.2 Bad line removement and noise reduction of the Proba-1 / CHRIS satellite images

Some of the acquired satellite images included several small stripes and bad lines. The stripes consisted of two different types of lines. Both line types are shown in figure 4.16 as indicated by the red arrows. Several stripes are shown as blue-green dotted lines crossing the image horizontally (white arrows in the image above). Other bad lines are shown in dark grey and white line running vertically across the image (black arrow in the image above). All stripes and bad lines were successfully removed using the ESA HDFclean V2 algorithm programmed by Jeff Settle (pers. Communication) (Cutter, 2006) provided by courtesy of Lisa Haskell from Surrey Satellite Technology Ltd. The result of the bad line removement and noise reduction can be seen easily by comparing the two images shown as an example in figure 4.16.

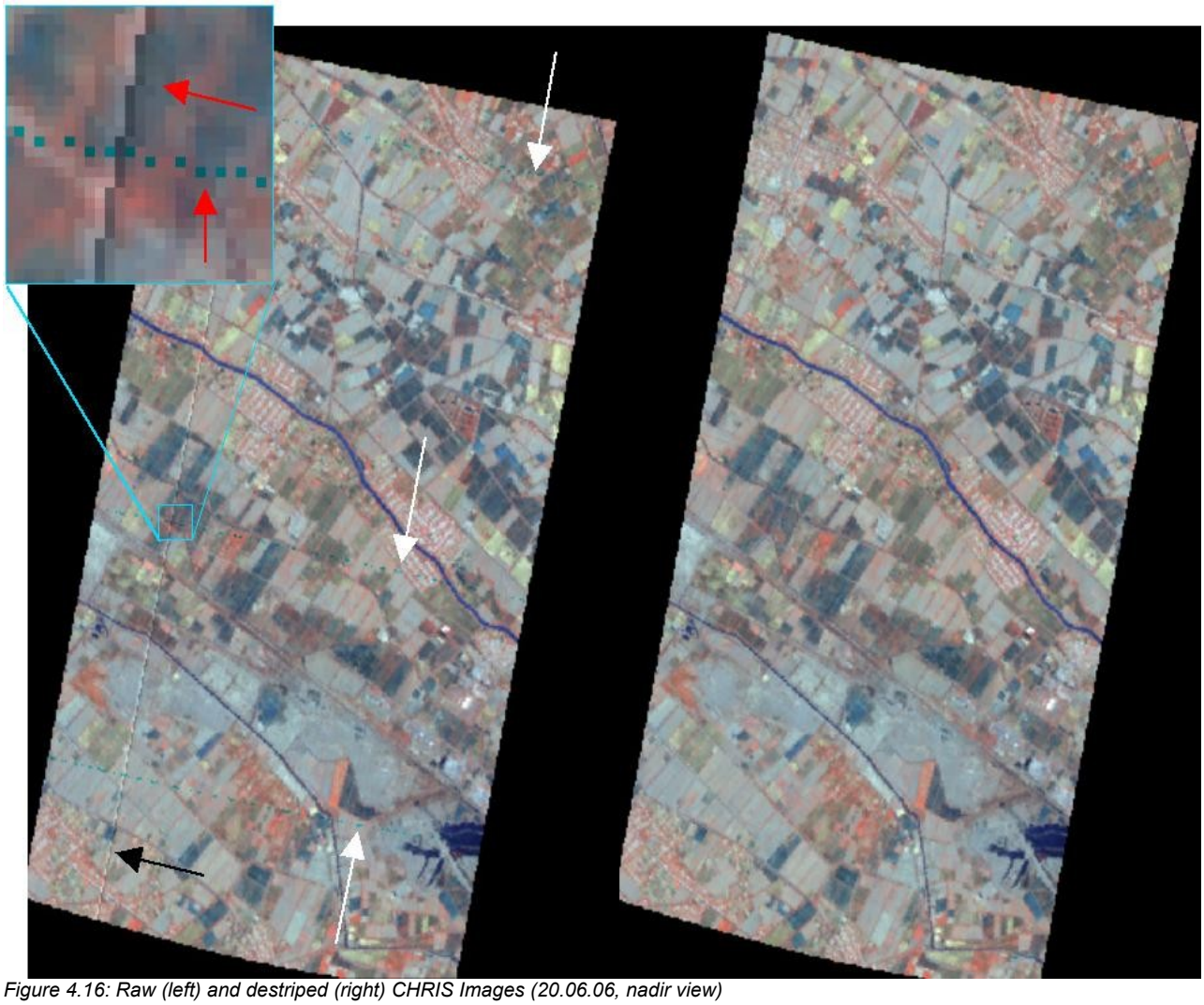

Figure 4.16: Raw (left) and destriped (right) CHRIS Images (20.06.06, nadir view)
Source: Own work / ESA

4.5.3 Georeferencing of Proba-1 / CHRIS Images

In order to validate the LAI and chlorophyll estimations with measurements in the field, all satellite images were georeferenced using ground control points (GCPs). These points were collected using a GARMIN GPS 12 handheld receiver. For higher precision of the determined coordinates the GPS was continuously kept switched on between the point collection and the average button was hit just before marking a GCP. Crossroads of bigger streets, bridges over wider irrigation or drainage channels or street / railway crossings were selected as GCPs. To identify the GCPs

Figure 4.17: Pictures of GCP´s on bridges, crossroads and rail road crossing
Source: Own photos

within the Images only structures bigger than the pixel size of the CHRIS-Images of 17 m were selected. A photo was taken of the location and the surrounding of each GCP and a sketch map was drawn. The red arrows in the photos in figure 4.17 show the exact point where the GCP was set. The arrows on the photos were created in the office in Urganch in the evening after the GCP-acquisition to incorporate the information of the quickly drawn sketch maps directly into higher quality information. The GPS points were downloaded using GPS TrackMaker software, saved as txt-file, imported to Excel and complemented with additional information such as photo number, number of GCP and point type. The result was imported as X,Y - Data to ArcGIS, reprojected to standardized projection used in the Khorezm project (Pulkovo 1942 using the Geographic transformation No. 7) and saved as shape-file. The result is shown in figure 4.18. Since the spatial extent of the multiangular images differed (see also figures 4.22 and 4.23), additional GCPs were collected in a wider surrounding area to allow proper georeferencing of all acquired satellite images. However, the focus of the GCP point collection was to capture suitable points in close vicinity of the field sites.

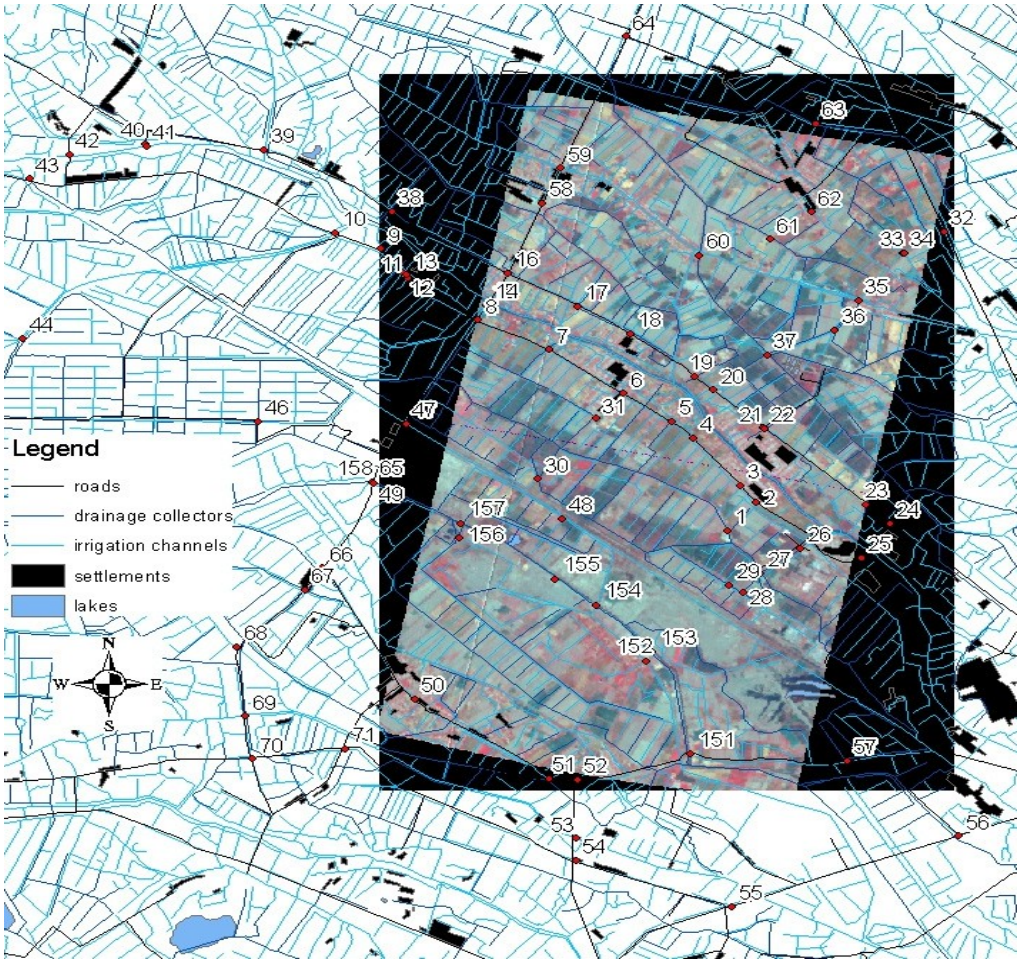

Figure 4.18: Map of the collected Ground Control Points with satellite image;
Source: Own map created with ArcGIS 9.1

The georeferencing of the Proba-1/CHRIS – Images was performed with kind support by Richard Fuchs, bachelor student from Jena University who did an internship at DLR. The results shown in this chapter were created in a co-production.

The georeferencing was carried out using ENVI 4.1 / IDL6.1. To identify the exact position of each GCP in the 17 x 17m resolution satellite image, different sources were taken simultaneously into account, including the GPS-Points in shapefile-Format in ArcGIS 9.1, the photos of the GCP´s of the GCP´s location and Google Earth.

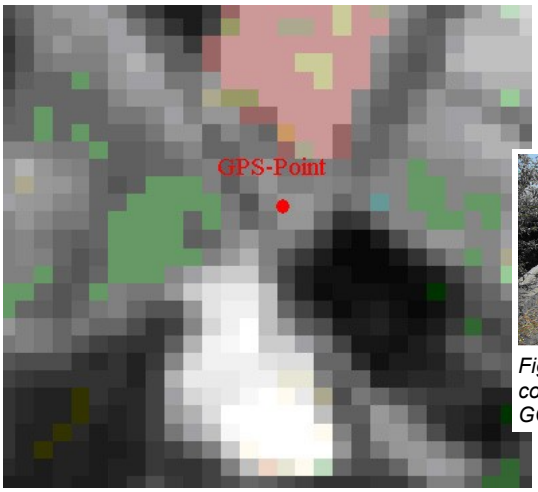

Figure 4.19: ENVI 4.1 Magnifier Window with 14x Zoom of GCP

Figure 4.21: Photo of corresponding location of GCP

Figure 4.20: Screenshot of Google Earth zoomed to GCP location

Following this procedure all GCP´s lying within the borders of the image where identified and adjusted until an optimum fit was achieved for all. Using a low Root Mean Square Error (RMSE) as guidance. The verification of the optimum fit with the validation fields and the GCP´s had the highest priority, afterwards the fitting with streets, settlements and the irrigation system was checked. Table 6 givs an overview of the results of the georeferencing of all images.

After verification of suitable GCP data collection, a second degree polynomial transformation using nearest neighbour analysis was applied. Due to the different angles, the 36° and 55° images had a varying resolution and needed a resampling to fit the 17x17m resolution of the nadir image to be comparable. The results were transferred to ArcGIS 9.1 as GeoTiff-Format.

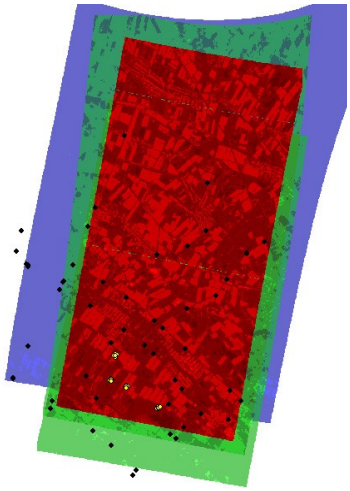

Figure 4.22: Images acquired at 11.06.06 (-55° is not available)

Table 4.5: Results of Georeferencing

Source: Own work /internship report Richard Fuchs

	-55		-36		0 (nadir)		36		55	
Date	RMSE	GCP´s	RMSE	GCP´s	RMSE	GCP´s	RMSE	GCP´s	RMSE	GCP´s
11.06.06	n/a	n/a	0,029717	20	0,237194	21	0,039764	21	0,036731	23
20.06.06	0,036795	22	0,047063	27	0,047681	23	0,028421	25	0,046306	24
28.06.06	0,055519	24	0,444662	25	0,437286	19	0,027268	23	0,036234	23
07.07.06	0,038230	26	0,019168	24	0,102996	21	0,045018	25	0,035177	27
17.07.06	0,048868	28	0,051576	20	0,084418	24	0,063859	24	0,043628	27
02.08.06	n/a	n/a	0,086166	20	0,056017	16	0,046227	19	0,043611	19

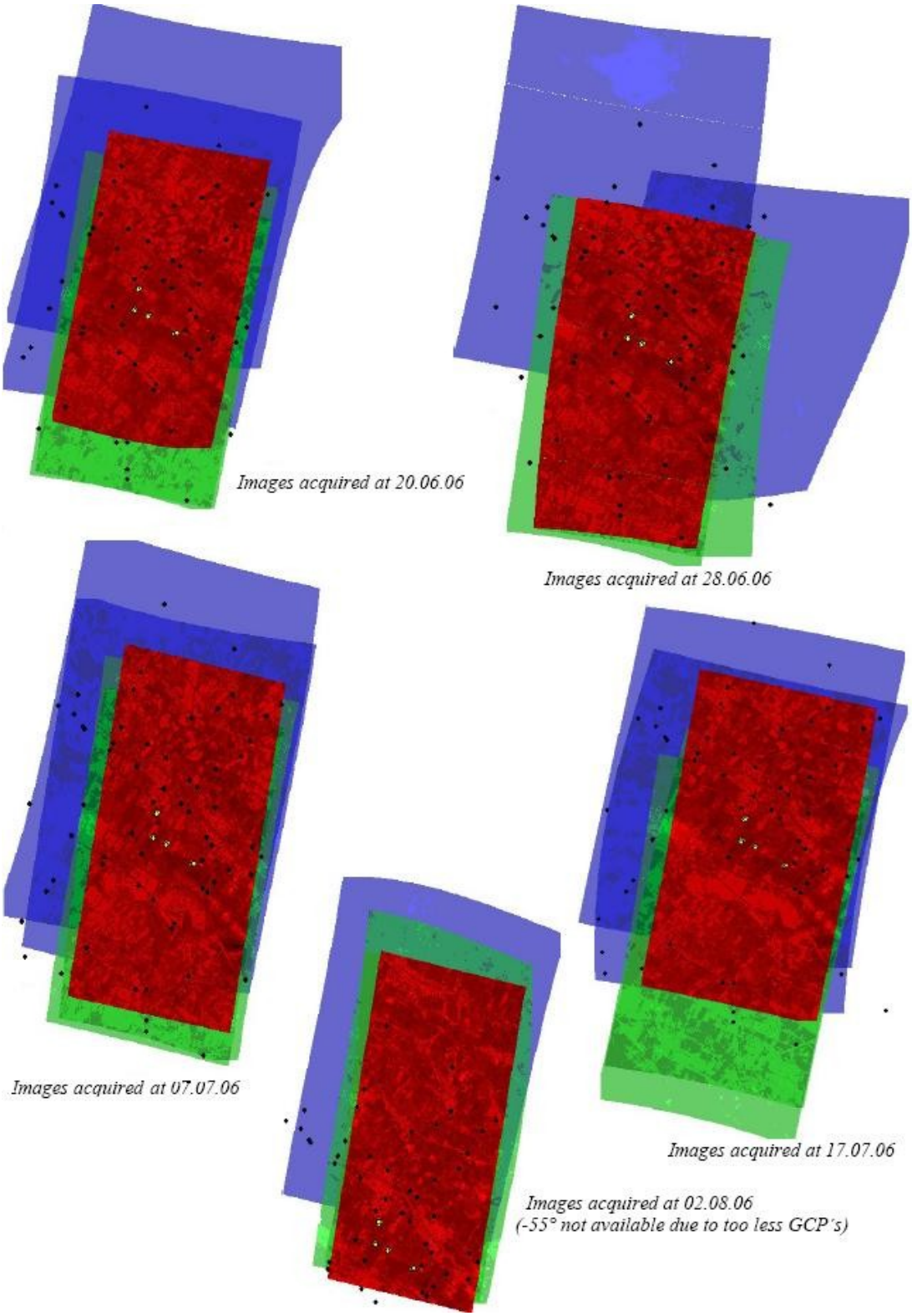

Figure 4.23: Proba-1/CHRIS images acquired at the specified dates and their spatial fitting
Source: Own work / internship report Richard Fuchs

In order to show the different spatial coverages of the satellite images, all images were imported into ArcGIS 9.1 and overlayed using different colours for each image (figure 4.26) The black dots symbolize the location of the GCPs and the four yellow ones represent the location of the validation fields. The blue areas represents the coverage of the +/- 55°, the green of the +/-36° and the red one shows the coverage of the nadir image. The differing shape of the images occurs mainly in the upper image parts which is due to few GCPs in this parts, thus,resulting in distortions. These image areas are out of the area of interest and did not effect the spatial congruence of the image with the fields where the validation measurements were taken.

4.5.4 Atmospheric Correction of Proba-1 / CHRIS images

4.5.4.1 Spectral reference targets

In order to correct atmospheric influences on the Proba-1/CHRIS-Satellite-Images the ground reflectance of one target was measured with the ASD field spectrometer (described in Chapter 4.1.2.1). An approximately 500 x 200 m big sandy field (fig. 4.25) with almost no vegetation was selected from which reflectance was measured on 14.06.06. This area was covered by almost every Proba-1/CHRIS Image, except the nadir, -36° and -55° images of the 02.08.06.

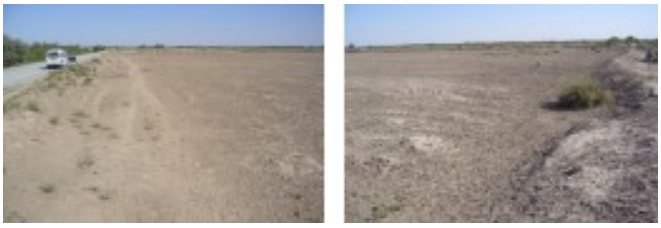

Figure 4.25: Sandy Bare Soil Field, Khorezm Uzbekistan
Source: Own Pictures

Figure 4.24: Pictures Top to Bottom: Rice, Cotton, Wheat, Alfalfa, fresh Rice and Bare Soil Fields in Uzbekistan
Source: Own Pictures

4.5.4.2 Targets for validation of atmospheric correction

To validate the outcome of the atmospheric correction the reflectance of different targets was measured during and shortly after the satellite overpasses. Fields with different land uses near the validation fields were selected, including a rice field (top), two cotton fields with different developed plants, a wheat field and one alfalfa field (fig. 4.24). Due to the harvest of the wheat field during the second overpass a change of the landuse took place. For the third and fourth image acquisition the wheat field was converted into a new rice field with very few tiny transplanted plants and next to the alfalfa field another former wheat field was transformed to a small bare soil field. The reflection of both was collected during last two satellite overpasses.

The reflectance measurements during the satellite overpasses (except 11.06.06 and 07.07.06) were always taken on the same fields (shown on the pictures in figure 4.24) and each time all measurement locations were photographed and marked by GPS. The additional data like landuse, density of vegetation and plant height was written in therefore prepared forms and afterwards transferred to Excel. These Excel files were linked with the GPS points and imported as attribute table to ArcGIS 9.1 (see maps below). Now all information available for each GPS point is easily accessible (see screenshot of attribute table, fig. 4.30, and figures 4.26 to 4.29). The pictures acquired on 11.06.06 and 07.07.06 were provided additionally by ESA that´s why no ground control reflectance measurements were collected on these days. These datasets were used for the validation of the atmospheric correction. But all these targets have one big problem in common: their surface exhibits different degree of heterogeneity which produces varying reflectance that would lead to inaccuracies in the comparison with the reflection of the atmospheric corrected satellite images. Therefore some preprocessing of the collected spectra was necessary.

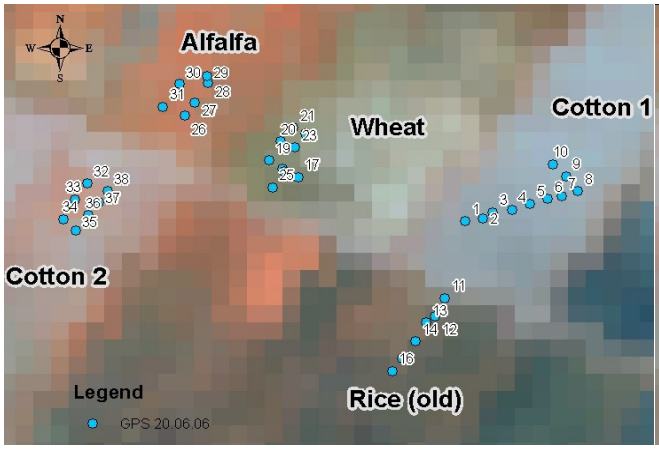

Figure 4.26: GPS - Reference - Points 20.06.06
Source: Map created with ArcGIS 9.1

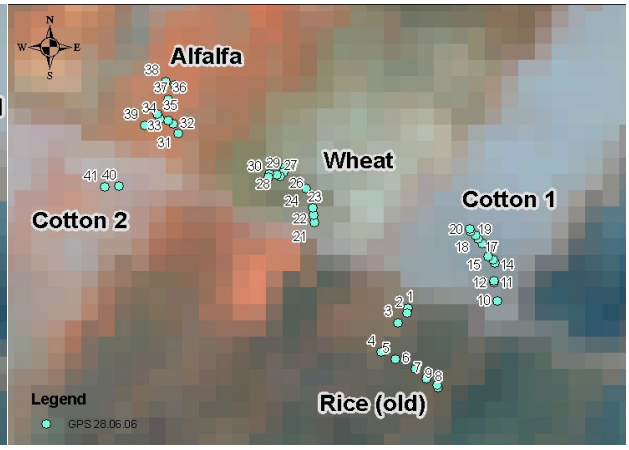

Figure 4.27: GPS - Reference - Points 28.06.06
Source: Map created with ArcGIS 9.1

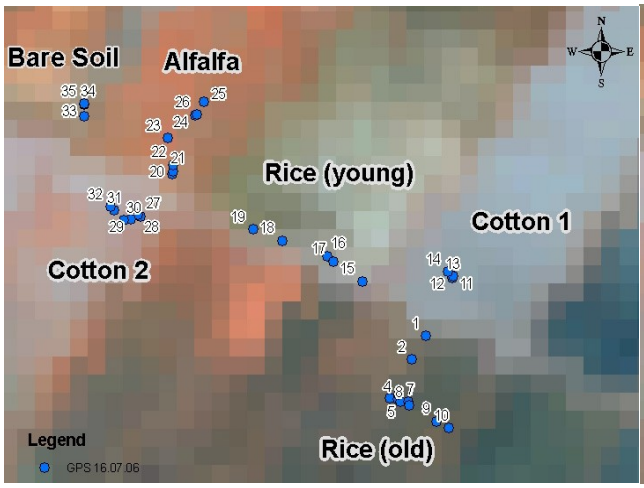

Figure 4.29: GPS - Reference - Points 17.07.06
Source: Map created with ArcGIS 9.1

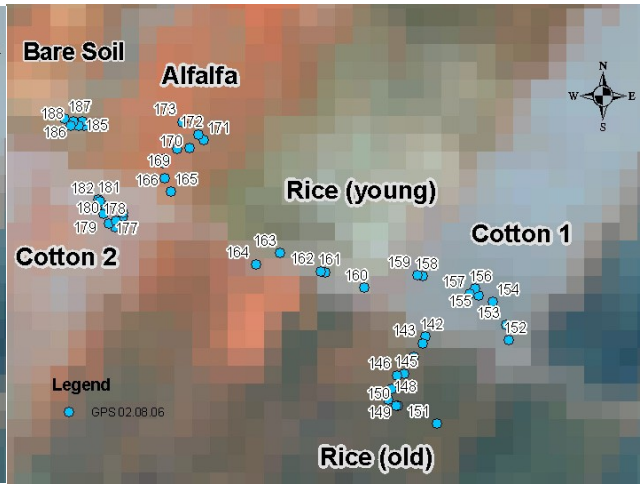

Figure 4.28: GPS - Reference - Points 02.08.06
Source: Map created with ArcGIS 9.1

Attributes of CHRIS-060802-Pulkovo

GPS	X	Y	Field	ASD	Reflect	FotoOVER	FotoNad	Remarks
142	41,588466	60,506151	Rice	1-10	5	0	245	High Rice
143	41,588407	60,506119	Rice	11-19	5	0	246	
144	41,588289	60,506027	Rice	20-30	5	0	247	
145	41,588139	60,505915	Rice	31-40	5	0	248	
146	41,588123	60,50584	Rice	41-50	5	0	249	rice with reed.
147	41,58801	60,505781	Rice	51-60	5	0	250	small rice with water.
148	41,587919	60,505743	Rice	62-71	5	0	251	
149	41,587865	60,505856	Rice	74-84	5	0	253	
150	41,587865	60,50584	Rice	85-94	5	0	255	
151	41,587721	60,506312	Rice	95-104	5	0	256	
152	41,588455	60,5071	Cotton	108-118	5	258	259	different cotton plants.
153	41,588584	60,507073	Cotton	119-128	5	0	260	different cotton plants.
154	41,588777	60,506907	Cotton	129-136	5	0	0	between two plants.
155	41,588826	60,506746	Cotton	137-146	6	0	262	bare soil with shadow and without.
156	41,58889	60,506698	Cotton	147-155	5	0	263	different cotton plants.
157	41,588842	60,506644	Cotton	158-166	5	0	264	
158	41,588981	60,506097	Cotton	167-180	6	0	267	with and without shadow.
159	41,588992	60,506038	Cotton	181-191	5	0	268	different cotton plants.
160	41,588868	60,505437	Rice	193-203	5	270	269	fresh rice with water
161	41,588992	60,504987	Rice	204-214	5	271	272	fresh rice with water
162	41,588997	60,504928	Rice	215-224	6	0	273	water with soil
163	41,589142	60,504456	Rice	225-234	5	0	274	fresh rice with water
164	41,58904	60,504187	Water	235-240	6	0	275	water with soil

Record: 0 Show: All Selected Records (0 out of 48 Selected.) Options

Figure 4.30: Attribute Table of the GPS-points collected on 02.08.06
Source: Own work with ArcGIS 9.1

4.5.4.3 Preprocessing of the collected spectra for validation

After all the steps described in chapter 4.1.2.2 were completed the spectra were grouped in one Spectral Library for each GPS point and averaged. The same process was repeated for the different landuse type to get one averaged signal for each date and landuse to be able to control the result of the atmospheric correction. Therefore the necessary graphs were exported as ASCII – .txt – Files to be used in ATCOR.

For verifying the result of the atmospheric image correction and for estimation of conversion factors for LAI, the area share of cotton plants relative to soil area was investigated in detail. In the study site the cotton plants were planted in a row distance of 60 cm. At an early growing stage (28.06.06) the spatial coverage of cotton leaves was relatively small (plants were less than around 25 cm in diameter and 20 cm in height), leading to higher reflectance information from the soil within the furrows compared to that of the sparse vegetation. In order to generate a vegetation signal for cotton fields covered by Proba-1/CHRIS pixels the following reflectance targets were measured

- Bare Soil
- Cotton plants
- Cotton plants mixed with grass
- Soil between two cotton plants

The spatial share of cotton and soil was estimated by the following method:

- mosaic all overview photos available per plot to one big image and import it to ArcMAP
- classify the photos in green / soil / shadow area shares and perform reclassification
- look at the new attribute table and look at the pixel count for each class

- set the pixel-count into ratio to get information on the spatial share of plants and soil.
- Simplify this ratio to one digit
- Search for Pixels of the Proba-1/CHRIS-Image containing more than one GPS – Point
- Load all collected spectra into ENVI
- Identify all GPS-Points within one Pixel
- Look for all relating spectra for each Pixel and put them together in one spectral library (slb)
- Average the new created slb and save the MEAN for each Pixel in a new slb
- Name the slb after the corresponding GPS-Points

The result should be a good estimation of the real reflection of the surface reflection within a Proba-1/CHRIS pixel. Zarco-Tejada 2005 (S.4) used a similar method to estimate the variability within vine yards. They used high resolution aerial photos, but as cotton is not as large as vine and only a small area is planned to be examined in this study, the overview photos were considered to be adequate for the estimation of the area shares.

Example for 28.06.06:

Figure 4.31: Pasted Pictures for 28.06.06
Source: Own pictures

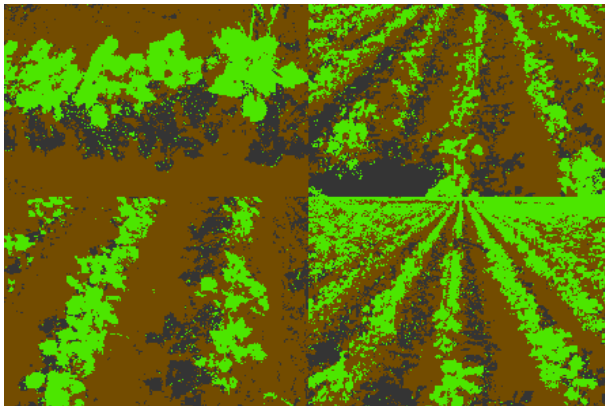

Figure 4.32: Classification with ArcMAP
Source: Own work with ArcMAP 9.1

At 5 spots 2 spectras collected and averaged as "between cotton plants"
Soil reflectance in the shade and bright sunlight each 10 times and averaged separately
Cotton plant reflection 10 spectra per plant averaged, sometimes mixed with grass

Result of this classification: 1:3:1 one part shaded soil, three parts sunny soil, one part plant cover

This classification process was repeated for all 4 days, but with 6 randomly selected nadir photos of the plants. The results are shown in table 4.6.

Table 4.6: Percentage of Plant / Soil Coverage and correction factors for LAI
Source: Own work with ArcGIS

	Stage1	***Stage2***	***Stage3***	***Stage4***
Plant	2,5	3,1	3,5	2,2
Soil	4,6	4	3,6	1,3
Resulting Factor	0,543	0,775	0,97	1,692

4.5.4.4 ATCOR Module and settings

To fulfil the atmospheric correction the ATCOR module for ENVI / IDL 4.1 created by Dr. Rudolf Richter at DLR was used. With the ATCOR option “inflight calibration” the first image from 11.06.06 was used to generate the calibration file for the 37 channels of CHRIS Mode 5 using the reflectance collected on the sandy bare soil field described in chapter 4.4.2.1. The settings for this are shown in figure 4.33.

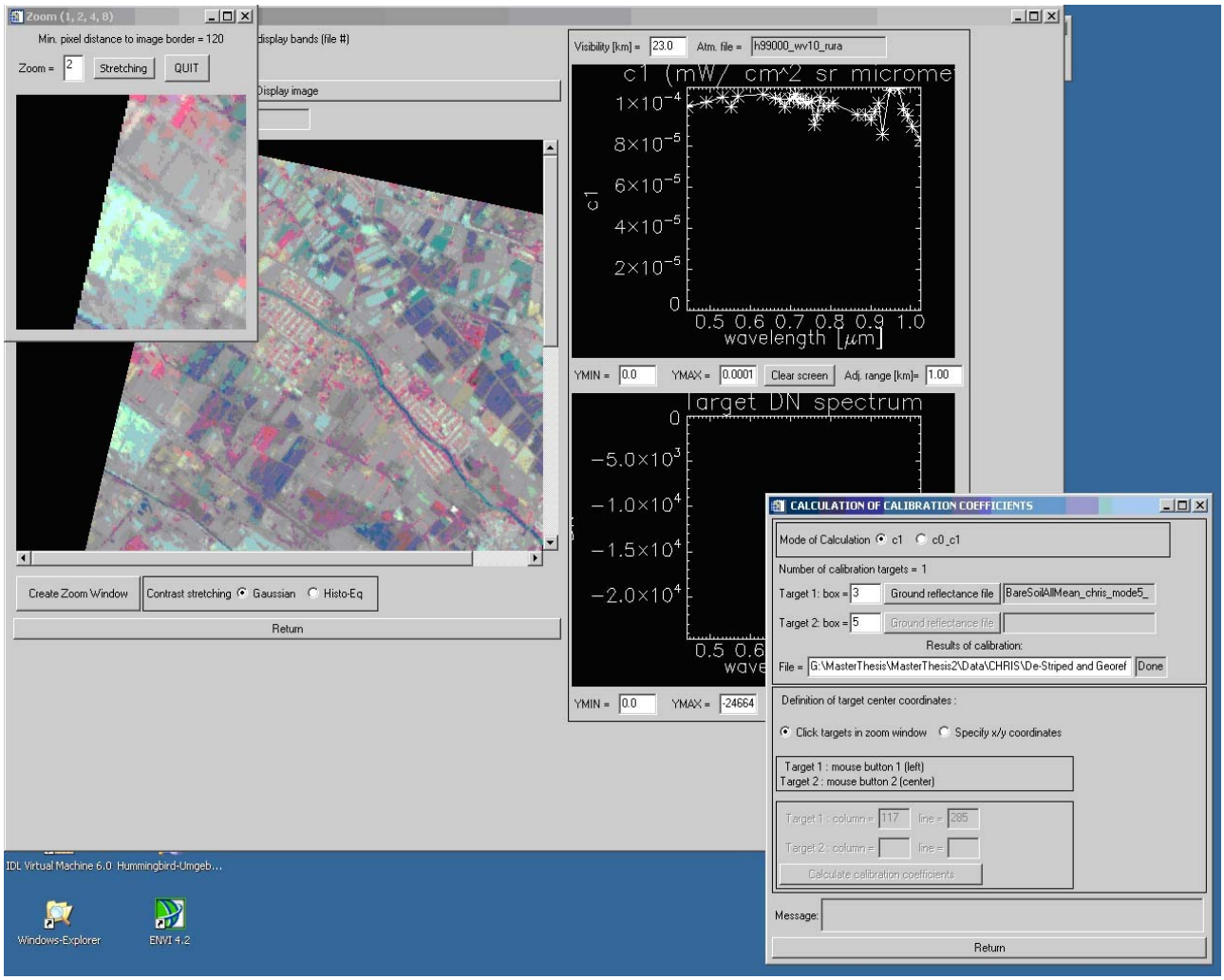

Figure 4.33: Inflight calibration for the nadir image of 20.06.06 with ATCOR Source: own work

The spectrum of the reference target (sandy field) was collected from the satellite image and the spectrum is set as a reference for the corresponding pixel in the image. The selected area is part of the cyan area in the Zoom window of Figure 4.33 shown above.

4.5.4.5 Atmospheric Correction – Processing

After creating a new calibration file the atmospheric correction for all 28 images started with the following settings:

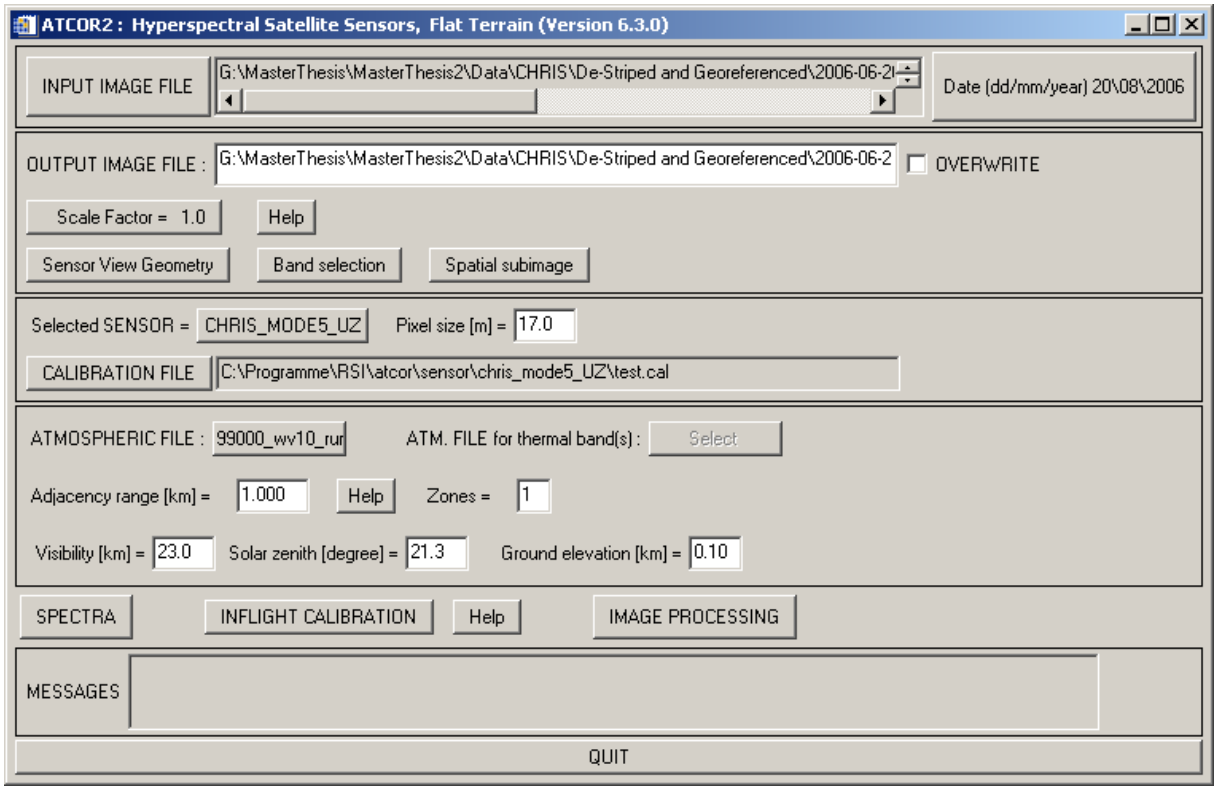

Figure 4.34: settings for the atmospheric correction with ATCOR
Source: Own work

The visibility was set per default to 23.0 Km and changed only for some of the 36° and 55° images. All the other values for all images can be taken from table 8.1 in the appendix.

4.5.4.6 Atmospheric Correction – Results and Validation

The results and the validation of the atmospheric correction was performed following two approaches. The first one is the visual comparison of the corrected image with the source. The second one is to test the corrected image using the spectra that were collected in the field at the same time as the image was acquired. Therefore the spectra were prepared as described in chapter 4.5.5. Using the “Display Spectra” option of ATCOR on one screen and the corresponding ArcGIS – map (fig. 4.18 shown in chapter 4.5.3) on the other screen, the pixel from which the

spectra were collected, were identified and the two graphs were compared. The fit of these two graphs can be used as a measure for the accuracy of the atmospheric correction. Sometimes the shape of the graphs is similar but not all wavebands showed a perfect fit. To measure the quality of the fit, the standard derivation of the collected spectra for validation was taken into account. If the discrepancy of the two compared spectra is lower than the minimum and maximum boundaries of the collected spectra, the fit was accepted. As an example demonstration the comparison of the images is shown for one image only. For the other images the resulting corrected images are presented only. The band combination of all images was set to Band 17, Band 12 and Band 4 for R,G,B for easier comparison.

The first image was acquired at 11.06.06 and provided as a additional image by ESA. Unfortunately no ground reflectance measurements took place at that day. The image is presented in figure 4.35.

Figure 4.35: Nadir Proba-1/CHRIS Image collected 11.06.06 atmospheric corrected

Figure 4.37: Nadir Proba-1/CHRIS Image collected 20.06.06 atmospheric corrected

Figure 4.36: Proba-1/CHRIS nadir Image aquired 28.06.06 after atmospheric correction

On the 20.06.06 the first reflectance measurements took place in the fields. The results of the atmospheric correction are shown in figure 4.37.

On 28.06.06 all measurements took place and the results of the atmospheric correction were tested as shown in figures 4.38 to 4.40 and the resulting image in figure 4.36. The white graphs in figure 4.39 represents the spectrum taken out of the satellite image for the specified landuse and the green graphs are the means of the referring ground spectra, which are presented in fig. 4.38 and 4.40. The fit of alfalfa is not considered as good match, because the white graph is higher than

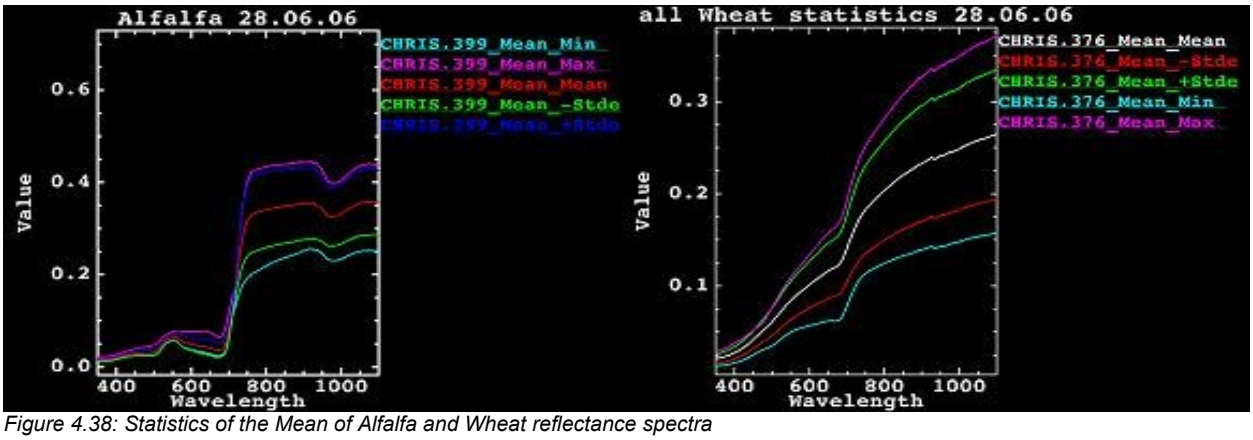

Figure 4.38: Statistics of the Mean of Alfalfa and Wheat reflectance spectra

Source: Own work with ENVI 4.1

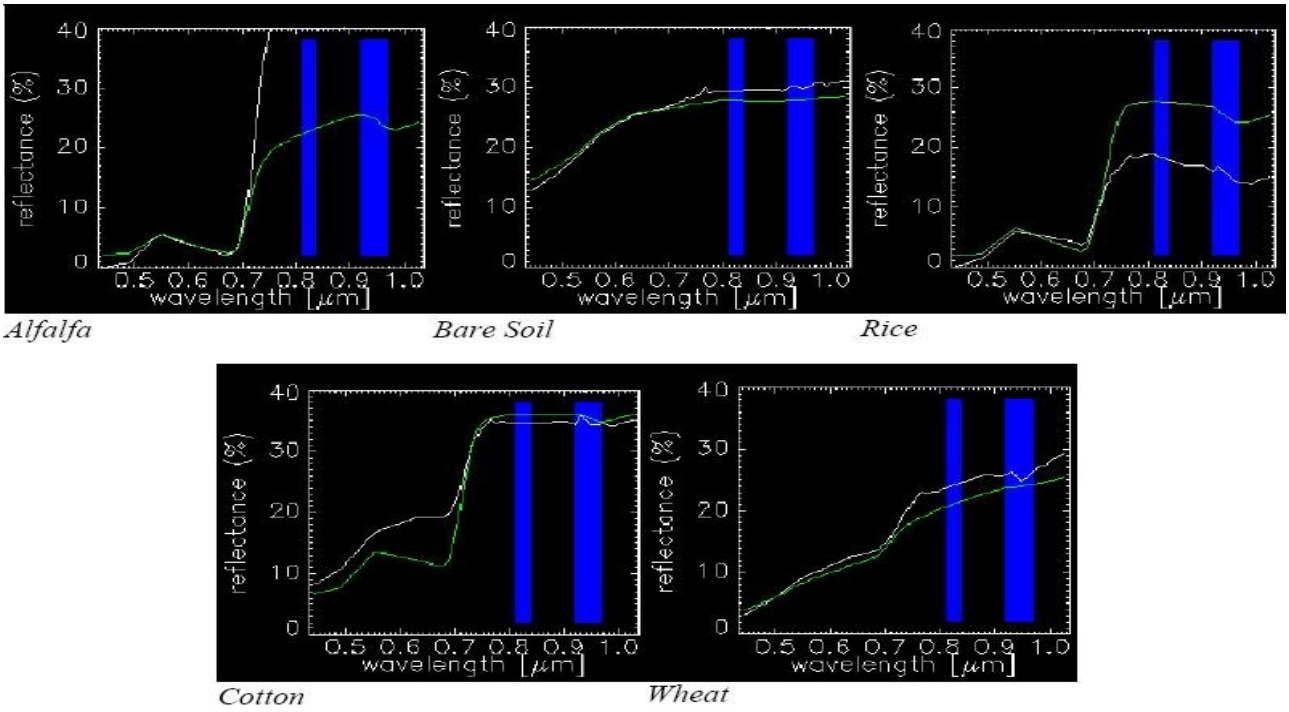

Figure 4.39: Graph out of Image (white) and reference spectra (green) for specified targets 28.06.06

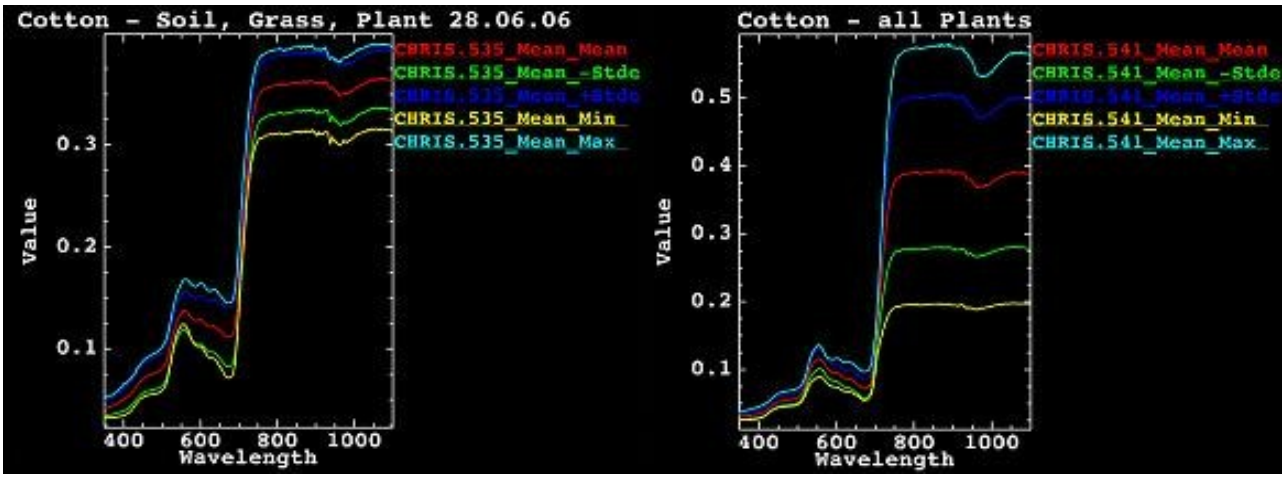

Figure 4.40: Two variants of spectral mixture for cotton 28.06.06

Source: Own work with ENVI

the maximum graph of the corresponding ASD measurements. The good fit of the bare soil and wheat graphs is obvious. As described in chapter 4.5.5.2 the row structure, the varying plant development and the high part of soil signal of the cotton fields made it difficult to mix a matching spectra. The differences between high disturbed and pure cotton signal are shown in figure 4.40. The spectrum extracted from the Proba-1/CHRIS satellite image shows a fit somewhere in between. Important is the very good fit in the area from 680 nm to 900 nm. The part of the graph between 400 and 600 nm is varying due to different spatial distributions of soil and plant signal.

The image from 07.07.06 was an additional images acquisition by ESA. Therefore no ground reflectance was measured, but the spectra collected on 28.06.06 were taken to control the results of the atmospheric correction shown in figure 4.41.

On the 16.07.06 all ground measurements took place and the verification of the corrections was done the same way as shown for 28.06.06. The nadir image is shown in figure 4.43 as an example.

All ground measurements were fulfilled on 02.08.06, but only the nadir image is presented in figure 4.42.

Figure 4.41: Proba-1/CHRIS nadir Image 07.07.06 after atmospheric correction

Source: Own work with ENVI 4.1

Figure 4.43: Proba-1//CHRIS nadir Image 16.07.06 after atmospheric correction

Source: Own work with ENVI 4.1

Figure 4.42: Proba-1/CHRIS nadir Image 02.08.06 after atmospheric correction

Source: Own work with ENVI 4.1

4.5.4.7 Example of different view angles of Proba-1/CHRIS - 16.07.06

In order to investigate the influence of different view angles on chlorophyll and LAI estimation, one complete scene (Fig. 4.45 to 4.47) with higher growth stage of the cotton plants was used out of the time-series to test the influence of the different CHRIS angles on VIs (Chapter 5.3.3).

Figure 4.45: Proba-1/CHRIS Satellite Image -55°, 16.07.06

Source: Own work with ENVI 4.1

Figure 4.44: Proba-1/CHRIS Satellite Image -36°, 16.07.06

Source: Own work with ENVI 4.1

Figure 4.46: Proba-1/CHRIS Satellite Image +36°, 16.07.06

Source: Own work with ENVI 4.1

Figure 4.47: Proba-1/CHRIS Satellite Image +55°, 16.07.06

Source: Own work with ENVI 4.1

4.5.5 Biophysical and biochemical measurements of cotton

4.5.5.1 LAI and chlorophyll determination in the field

In addition to the reflectance measurements, biophysical measurements as described for the fertilizer trial plots were carried out on the four fields in Amir Temur Shirkat (compare figure 3.1c). The measurements in the cotton fields were taken in a homogeneous area within each of the four selected fields. A distance of ca. 20 m to each side of the field was chosen to avoid mixed reflectance signals on the pixels of the Proba-1/CHRIS sensor due to adjacent cotton and other land uses. The measurements were taken following a more or less X-shaped sampling path with measurements ca. every 15 m. Each measurement point was marked by GPS. Plant height, crown width, number of buds, LAI, and SPAD values were collected, averaged in different height levels of the plant and entered in field data forms. This procedure was repeated on all four validation fields within two days before or after each satellite image acquisition. This was done for the fpur image acquisition dates. Back in the office LAI data was downloaded using LAICOR´s FV2000 Version 1.04 Software and saved as txt-File. The GPS data was also downloaded using GPS TrackMaker software, exported as txt-File, imported into Excel and all the collected descriptive information was added as attribute information to each corresponding point. Afterwards the whole file was saved as txt-File and imported as X,Y-Data to ArcMap. The point signature in the maps of figure 4.48 present the GPS-dataset where measurements took place at each time step. This information was then used to relate the measured LAI and chlorophyll data in the field with the calculated data of the satellite images.

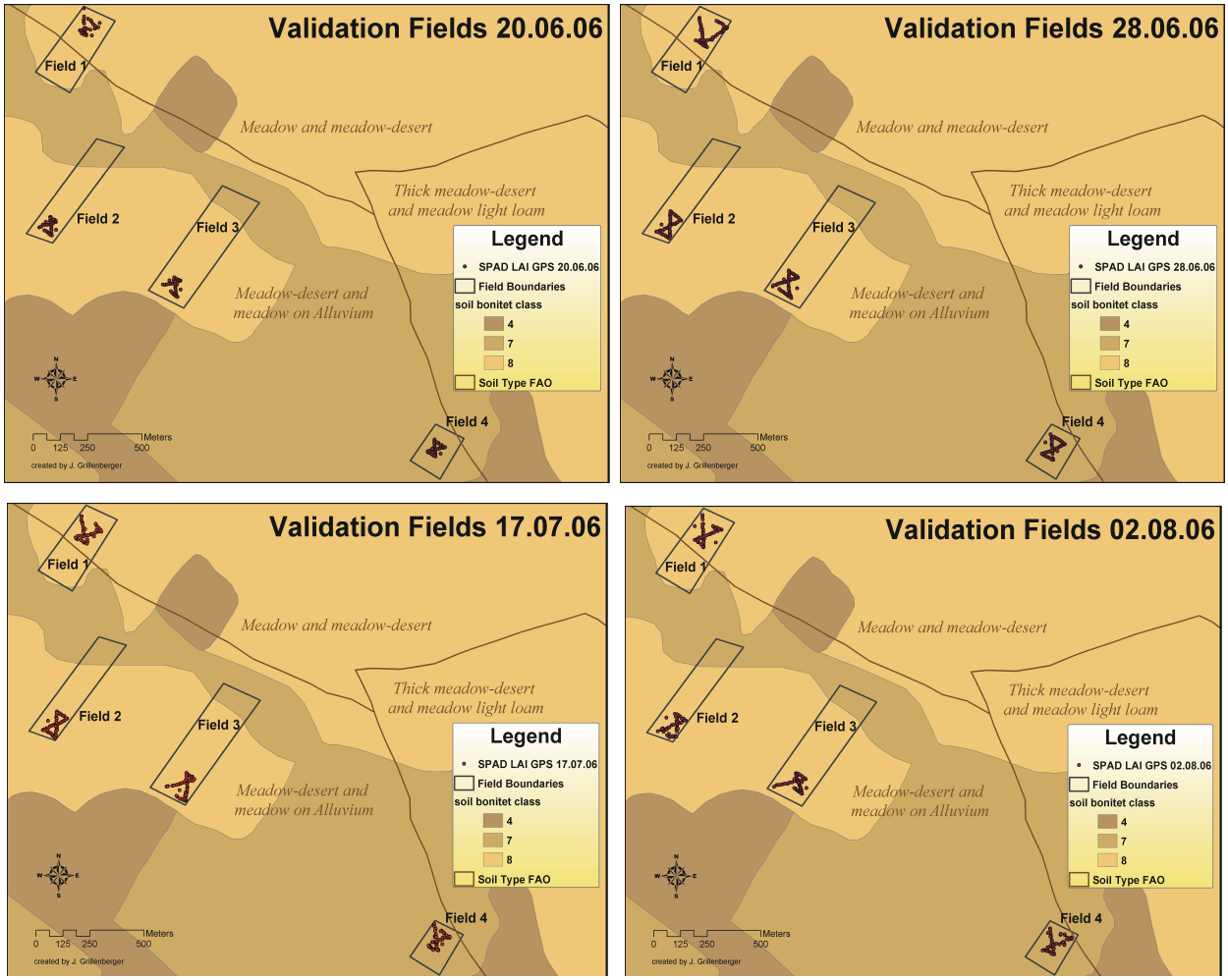

Figure 4.48: Overview GPS, SPAD and LAI collection Validation Fields

Source: Own work with ArcMap 9.1

4.5.5.2 Calculating Vegetation Indices based on Proba-1/CHRIS Images

The calculation of vegetation indices was carried out using the ASTools (Dorigo et al. 2006). This tool is able to calculate 60 different VIs from both spectral libraries and satellite images. The resulting VIs are stored in spectral libraries or as an output image with the VIs as separate channels, respectively. With the spectral information provided by the 36 channels of the Proba-1/CHRIS Mode 5 sensor it was possible to calculate 49 different VIs, of which 38 were chosen as probably suitable. They were calculated for every stage and data aggregation. The details on the most important VIs were described in chapter 2.2.

The newly created image with VI information was saved as GEOTIFF-File and imported to ArcGIS 9.1. Now the distribution of each VI can be shown as a graduate colours map. A map for each time step is shown in figures 5.33 and 5.34. For relating the VIs of the satellite image with the LAI and chlorophyll measured in the field, only the VI-information of these pixels that cover exactly the spatial dimension of the measurement area was taken into consideration. The information of every

pixel from all channels representing VIs was transformed into an attribute table using a zonal statistics tool that was created for application with ERDAS Imagine 8.7 by Michael Bock from DLR. As input into this tool a shapefile with rectangular polygons (vector grid) of the same geographic projection, a multiple of the spatial dimension as the raster pixels, and the same spatial extent as these raster pixels that cover the measurement area was prepared. The multiple dimension of the spatial pixel dimension was set in this study to 2x2 raster cells in order to reduce the influence of the spatial variability of LAI and chlorophyll within each pixel. These polygons were created using ArcGIS 9.1 and the Hawth´s Tool extension (Hawthorne 2006). Every new created polygon covered exactly 4 raster cells of the image that contained the VIs. Only those polygons containing GPS points indicating the field measurements were selected and saved in a new shapefile. The ERDAS zonal statistics tool calculated the mean and standard derivation for every channel of all raster cells that were within the boundaries of one polygon and attached the results to the attribute table of a newly created shape file. For establishing the relationship between the VIs from satellite imagery and the measured biochemical data, the mean of all measured LAI and chlorophyll values at those GPS-Points that were covered by a raster grid of the created polygon was computed. Therefore the attribute tables were exported as txt - Files and imported to Excel to perform this calculation. The results were added in ArcGIS 9.1 to each of the shape files as dbf – File. Finally, the relationship between VIs and LAI on one side and VIs and C_{ab} on the other side was determined by regression analysis following the statistical procedures described in chapter 4.6

4.6 Statistical and spatial analyses at leaf, plant and regional scale

All data measured on the field and extracted from satellite images were compiled in one standardized GIS database to generate a geographically referenced and complete dataset for statistical and spatial analyses, especially on the regional scale. Statistical analysis were used to determine the relationship between VIs and C_{ab}-content of the leaves or plants based on SPAD measurements. The statistics were calculated for each temporal stage at the three different spatial scales (leaf, plant, region) as well as for different data aggregations (e.g. according to nitrogen levels of plots of the fertilizer trial plots) at the plant scale. Afterwards the results of the different temporal stages, spatial scales and data aggregations were compared with each other to investigate whether certain VIs show stable prediction power over time, space or aggregation level. At the regional scale the spatial distribution of the VIs and the resulting C_{ab}-content was analysed using ArcGIS 9.1 and the results printed as maps.

4.6.1 Statistical analyses of LAI and C_{ab} prediction by VIs

The statistical basics, including minimum, maximum, mean and standard deviation were calculated for all the datasets described in the previous chapters using Excel. These values were used to calculate the range, coefficient of variation and total variability for each dataset and for different aggregations within one or between different datasets. The coefficient of variation was calculated as standard derivation / mean * 100 as a normalized variability indicator for comparison between different datasets. The results of these statistics were printed in Excel as scatter plots and used for a first screening of the data. Only some extraordinary high or low values were removed as outliers after a critical examination. For the examination, all available data were taken into account, including the handwritten field data forms. This screening was done for the data collected on the ground as well as for the Vegetation Indices calculated based on the Proba-1/CHRIS images or ASD reflectance data.

To link the SPAD to the $C_{ab,}$ all SPAD values measured on leaf scale were displayed in Excel scatter plots with the corresponding C_{ab} contents determined by the laboratory. Using Excel the coefficients of determination for different types of regressions were calculated and the best fits were identified. The corresponding equation was compared with the one calculated for the dataset collected by Rücker et al. in 2005. The results of this comparison are shown in chapter 5.1.

Using this resulting equation all SPAD values collected on plant and field scale were transferred into C_{ab} – values µg cm^{-2}. Scatter plots were printed for each VI - C_{ab} combination and the regression equation and the coefficient of determination were calculated. For each dataset the coefficients of determination were interpreted according to the strength of the relationship following the guidelines of Hamilton (1990). The interpretation scheme is shown in table 4.7. Using this method the best fitting VIs determining LAI and C_{ab} were identified for each dataset. The achieved fit was classified using the classes given in table 4.7.

Table 4.7: Rules of thumb for coefficient of determination estimation and interpretation
Source: Hamilton 1990, Table 14.5

Coefficient of determination (R^2)	Interpretation	Classification
1,0	Perfect positive (negative) relationship	Not applicable
1,0 > R^2 > 0,64	Strong positive (negative) relationship	Group 1
0,64 > R^2 > 0,25	Moderate positive (negative) relationship	Group 2
0,25 > R^2 > 0,04	Weak positive (negative) relationship	Group 3
0,04 > R2 > 0	No relationship	Group 4

4.6.2 Transferability of relationships

Based on the classification of R^2 values into groups reflecting the strength of the relationship between VI and LAI or Cab, the membership of VIs to specific groups was investigated in detail. Specifically it was investigated, whether certain VIs show higher relationships with with LAI or Cab over temporal stages, spatial scales and data aggregation. As a result of this classification the best fitting VIs are shown for each dataset and stage. In chapter 5.4 the results of all datasets were evaluated and the best fitting VIs selected. After that the LAI and leaf chlorophyll content at regional scale was calculated by applying the in the regression equations for the selected VIs on the satellite images.

4.6.3 Validation of the regional LAI and C_{ab} estimations

The validation of the resulting regression equations took place at regional scale. Therefore the regression equations for the best fitting coefficients of determination to estimate C_{ab} or LAI by VIs were used to predict the LAI or leaf chlorophyll content of the fields and compare the predicted values with the results of the ground measurements.

5.Results and Discussion

5.1 Leaf Scale SPAD calibration and leaf chlorophyll estimation by Vegetation Indices

5.1.1 SPAD Calibration

The investigations at leaf scale were performed to determine the relation between SPAD-value, VI calculation based on ASD reflectance data and corresponding C_{ab} -content of cotton leaves. After checking the results of the chlorophyll extraction from the laboratory, it was found that the standard deviation and coefficient of variation were relatively high for some leaves (table 4.7). Furthermore the data showed that the number of chlorophyll extractions per leaf varied considerably from one to six samples per leaf. Moreover, as the total number of leaf samples was only 33 the range of 33.8 – 58.9 SPAD values was relatively small. Due to the higher standard variations, irregularities in the laboratory and the relatively small data range, the suitability of this data set for calibrating the SPAD in order to transfer SPAD values during later measurement stages when both lower and higher chlorophyll content is expected, is not given. Instead, the calibration dataset collected by Rücker (2006) in late August 2005 had a population of 100 and a very high range of the SPAD values from 3,26 to 70,24. Thus, the established regression based on the latter dataset was used for transferring SPAD values to chlorophyll a+b content. The corresponding equation is

$$C_{ab} = 0{,}0008 \cdot SPAD$$

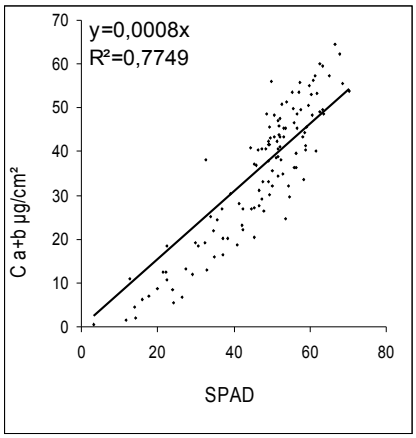

Figure 5.2: Scatter Plot for the combined 2005 and 2006 data

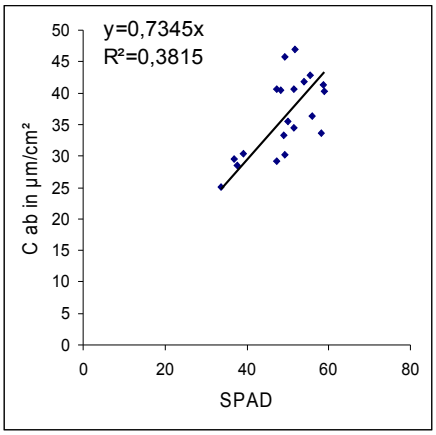

Figure 5.1: Scatter Plot for the remaining 21 leaves

Table 5.1: Results of Laboratory at Leave Scale with Mean, STDV and CV

Leaf ID	Lab. Result Cab in mg cm^{-2}	Mean Cab in mg cm^{-2}	Standard Derivation	Coefficient of Variation	Lab. Result C_{ab} in µg cm^{-2}	Mean C_{ab} in µg cm^{-2}
1,1	0,0260				25,95	
1,2	0,0242	0,0251	0,0145	57,8445	24,17	25,06
2,1	0,0398				39,82	
2,2	0,0415	0,0271	0,0235	86,6563	41,47	27,1
3,1	0,0362				36,18	
3,2	0,0302	0,0221	0,0194	114,1029	30,23	22,14
4,1	0,0330				32,97	
4,2	0,0359	0,0230	86,8359	0,0199	35,89	22,95
5,1	0,0340				33,96	
5,2	0,0389	0,0243	0,0212	87,1953	38,89	24,28
6,1	0,0290				29,04	
6,2	0,0294	0,0195	0,0169	86,6067	29,37	19,47
7,1	0,0330				33,02	
7,2	0,0264	0,0198	0,0175	88,1892	26,42	19,81
8,1	0,0338				33,78	
8,2	0,0427	0,0255	0,0225	88,3519	42,69	25,49
9,1	0,0542				54,24	
9,2	0,0638	0,0393	0,0344	87,4429	63,75	39,33
10,1	0,0742				74,16	
10,2	0,0849	0,0530	0,0462	87,1941	84,91	53,02
11	0,0405	n.a.	n.a.	n.a.	40,55	n.a.
12	0,0246	n.a.	n.a.	n.a.	24,64	n.a.
13	0,0507	n.a.	n.a.	n.a.	50,71	n.a.
14	0,0355	n.a.	n.a.	n.a.	35,5	n.a.
15	0,0336	n.a.	n.a.	n.a.	33,61	n.a.
16	0,0287	n.a.	n.a.	n.a.	28,73	n.a.
17	0,0426	n.a.	n.a.	n.a.	42,58	n.a.
18	0,0429	n.a.	n.a.	n.a.	42,86	n.a.
19	0,0406	n.a.	n.a.	n.a.	40,63	n.a.
20	0,0560	n.a.	n.a.	n.a.	55,99	n.a.
21	0,0413	n.a.	n.a.	n.a.	41,33	n.a.
22	0,0295	n.a.	n.a.	n.a.	29,52	n.a.
23,1	0,0306				30,56	
23,2	0,0303	0,0203	0,0176	86,6056	30,26	20,27
24,1	0,0348				34,82	
24,2	0,0283				28,35	
24,3	0,0274	0,0226	0,0154	68,2487	27,36	22,63
25,1	0,0199				19,9	
25,2	0,0343				34,26	
25,3	0,0283				28,28	
25,4	0,0237	0,0212	0,0130	61,3353	23,68	21,22
26,1	0,0286				28,56	
26,2	0,0276				27,56	
26,3	0,0281				28,12	
26,4	0,0295	0,0228	0,0127	55,9911	29,53	22,75
27,1	0,0384				38,45	
27,2	0,0423				42,28	
27,3	0,0348				34,77	
27,4	0,0407				40,69	
27,5	0,0419				41,94	
27,6	0,0437	0,0346	0,0155	0,0536	43,73	34,55
28,1	0,0409				40,92	
28,2	0,0449				44,86	
28,3	0,0464				46,41	
28,4	0,0478				47,78	
28,5	0,0466				46,57	
28,6	0,0475	0,0391	0,0174	0,0682	47,45	39,14
29	0,0513	n.a.	n.a.	n.a.	51,34	n.a.
30	0,0411	n.a.	n.a.	n.a.	41,07	n.a.
31,1	0,0337				33,71	
31,2	0,0308	0,0215	0,0187	86,8674	30,79	21,5
32	0,0470	n.a.	n.a.	n.a.	47	n.a.

5.1.2 Chlorophyll estimation by vegetation indices

The reflectance at leaf scale was collected with the ASD field spectrometer from leaves that were placed once on white (strongly reflecting) and then on black (strongly absorbing) background. For these measurements twenty additional leaf measurements of SPAD and reflectance with the ASD were taken two weeks after the first data collection, in order to overcome the problems that occurred with the 33 leaf dataset. The statistics for this dataset are shown in table 5.2 indicating a relatively small standard derivation and coefficient of variation.

Table 5.2: Statistics of the used leave reflection dataset

	n	Min	Max	Range	Mean	STD	CV
SPAD ( )	20	40,6	63,2	22,6	53,215	6,225	11,698
C_{ab} (µg cm^{-2})	20	32,48	51,00	18,52	43,00	4,90	11,698

Using a tool for ENVI / IDL that was written by Wouter Dorigo (2006) the reflectance excluding the transmittance was calculated for each leaf. The different spectral reflections of a leaf measured while positioned on a white or a black background as well as the results for the transmittance and adjusted reflectance is shown for one example leaf in figure 5.3. The graphs show the highest reflectance values for the leaf measured on white background (black signature), because the measured reflectance includes the reflectance of the leaf and the backscatter of the transmission. In contrast the reflectance of a leaf measured while positioned on a strongly absorbing black background (brown signature) is much lower. The actual leaf reflectance (dark green signature) has values between the reflectance based on black background and the transmittance.

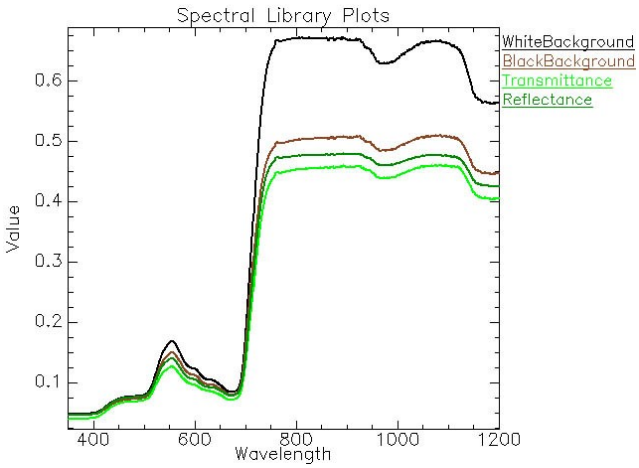

Figure 5.3: Comparison of white, black and adjusted reflectance and transmittance

Source: Own work with ENVI 4.1

Based on the adjusted reflectance data, the VIs were computed using the ASTools in ENVI. The statistics for this dataset are shown in table 8.2 in the Appendix. The coefficient of determination for each calculated VI is given in figure 5.4. Although the highest determined R^2 at leaf scale reaches almost 0.64, this estimation of C_{ab} is overall relatively low compared to sources cited in the literature amounting to ca. 0.8 (Blenk 2005). The major difference of this study is that all data were gathered under field conditions whereas the research found in the literature was conducted under laboratory conditions. The measurement in the field suffered from suboptimum illumination due to changing atmospheric conditions (clouds) that caused a reduction of the number of measurements per target. Since the measurement was non-destructive, the leaves were not cleaned and partly covered by dust and sand due to wind erosion, which alters the reflection properties. All these

constraints that could only partly be controlled during the measurements in the field together with the small sampling number of only 20 samples might have caused generally lower relationships between the VIs and the measured SPAD values.

Considering the relative performance, the coefficients of determinations range from 0,002 to 0,64. To ease the comparison the VIs were grouped into three classes representing different levels of fits according to Hamilton (1990). The first group, the one with the relative best fit (moderate relationship), includes the R^2-values of following VIs: LWVI1, GI, LWVI2, MSI, CAI, MCARI2 and MTVI2. The second group contains the R^2 of the VIs with a lower fit range (weak correlation). These are NDVI, RVI, the whole SAVI family, RDVI, TCARI, MCARI, MTCI, REIP1, Cab1 and all LAI´s. The last group are the ones with almost no correlation. These are CARI, LCI, SR705, mND705, DGVI2, NDNI, NDLI, CSI2, DWSI5, SWRLI and Cab2. The ones not mentioned are somewhere in between group two and three.

The classification of VIs into groups shows that often cited VIs such as MCARI2, MTVI2 were also in this study among these VIs showing the relatively best performance to predict C_{ab}. Relatively lower relationships were given mainly by the broadband vegetation indices such as NDVI, RVI and the SAVI family, and at a lower relationship with the other chlorophyll related VIs such as TCARI, MCARI.

To partly overcome the constraints of the field study, future research should focus on increasing the number of leaf samples. An increase of the number of SPAD-measurements, a more spatially distributed sampling within each leaf as well as conduction of the research under absolutely cloud-free conditions may also provide better results. This can only be managed if the plants are harvested after each measurement day and the leaves put into a suitable freezer, to guarantee a

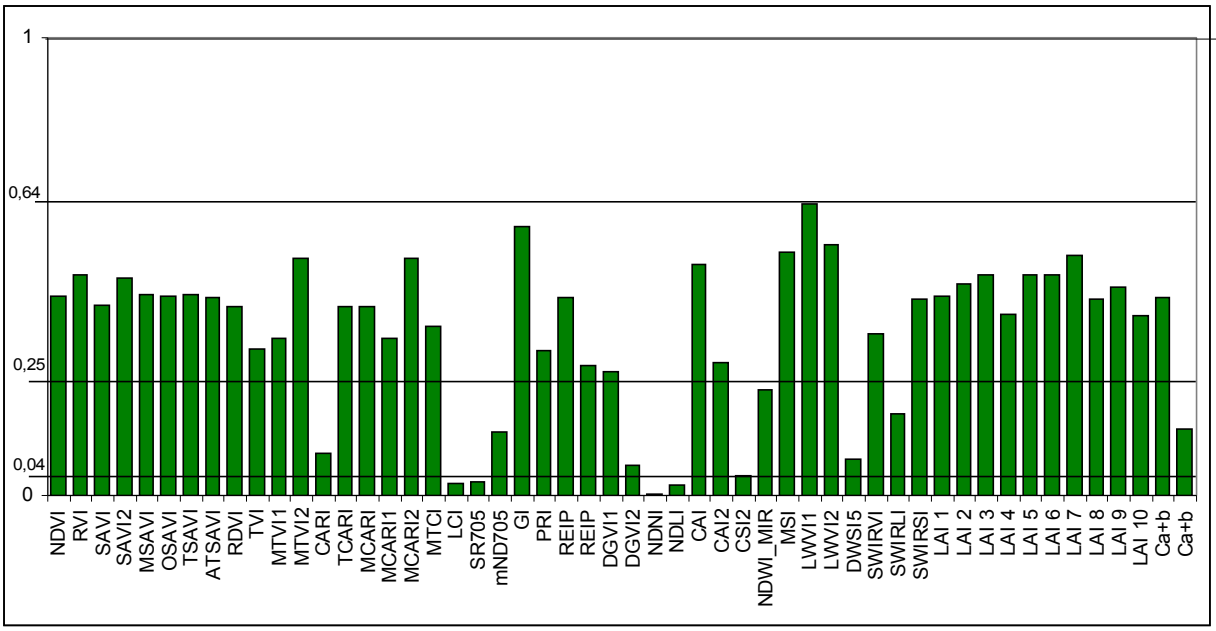

Figure 5.4: Coefficients of Determination for determining C_{ab} by VIs at Leaf Scale

longer measurement period of about one week. Or an easier procedure to conduct the reflectance measurements will be developed to avoid the time consuming adjustments and changes of the background materials. The best solution would be to use a laboratory meeting international standardized criteria.

5.2 Plant scale multi – temporal LAI and leaf chlorophyll estimation on fertilizer plots

5.2.1 Plant scale LAI and leaf chlorophyll estimation overview

At plant scale, reflectance, LAI, and chlorophyll data were measured taking all leaves grouped at different layers of cotton plants that were cultivated in plots with different fertilizer rates in a field trial at four growing stages. The descriptive statistics of measured LAI and C_{ab} for each stage are shown in table 5.3. The LAI values of the fertilizer trial capture a wide range from 0,09 in stage 1 to 6,08 in stage 4. The chlorophyll values capture also a wide range from 20 µg cm^{-2} to 50 µg cm^{-2}, whereas the SPAD values range from 22 to 63,3. This high range indicate both the increase of biochemical and biophysical parameters with time, but also the response of the different N application rates.

Table 5.3: Statistics for LAI and C_{ab} for Fertilizer Trial Plots on plant scale

	Stage	Min	Max	Range	Mean	STD	CV
LAI ( )	1	0,09	1	0,91	0,49	0,21	42,34
C_{ab} (µg cm^{-2})	1	25,2	50,64	25,44	41,78	4,04	9,66
SPAD( )	1	31,5	63,3	31,8	52,23	5,05	9,66
LAI ( )	2	0,13	1,9	1,77	0,79	0,32	41,11
C_{ab} (µg cm^{-2})	2	13,92	36,88	22,96	31,57	3,38	10,71
SPAD ( )	2	17,4	46,1	28,7	39,46	4,22	10,71
LAI ( )	3	0,35	4,91	4,56	1,48	0,94	63,24
C_{ab} (µg cm^{-2})	3	17,6	40,38	22,78	31,46	3,34	10,61
SPAD ( )	3	22	50,48	28,48	39,33	4,17	10,61
LAI ( )	4	0,45	6,08	5,63	3,61	1,44	39,84
C_{ab} (µg cm^{-2})	4	31,07	48,96	17,89	42,4	3,11	7,33
SPAD	4	38,84	61,2	22,36	53	3,88	7,33

For each stage the descriptive statistics of the VIs are presented in tables 8.3 to 8.6 in the Appendix.

5.2.2 Plant scale LAI and leaf chlorophyll estimation at stage level

The coefficients of determination resulting from the regressions of VIs against LAI or C_{ab} are shown in table 5.4 and 5.5, respectively.

Table 5.4: Statistics of Coefficients of Determination for determining LAI by VIs at Plant Scale

R^2	Min	Max	Mean	STD	Range
Stage 1	0,0000003	0,0772	0,0353	0,0243	0,0772
Stage2	0,0065	0,3189	0,1640	0,0932	0,3124
Stage3	0,0002	0,2554	0,1333	0,0696	0,2552
Stage4	0,0002	0,1795	0,0509	0,0485	0,1793
Stage 1-4	0,0000003	0,3189	0,0959	0,0589	0,3189

Averaged over all stages and plants measured in the fertilizer plots the mean R^2 – value for LAI estimation by VIs is with 0,096 low, the range with 0,32 high, the minimum with $3*10^{-7}$ very low, the maximum with 0,32 at a medium level within the moderate correlation group (after Hamilton 1990).

Table 5.5: Statistics of Coefficients of Determination for determining C_{ab} by VIs at Plant Scale

R^2	Min	Max	Mean	STD	Range
Stage 1	0,000001	0,4097	0,0652	0,1216	0,4097
Stage2	0,0007	0,0788	0,0264	0,0174	0,0781
Stage3	0,0069	0,2652	0,0910	0,0780	0,2583
Stage4	0,00002	0,1668	0,0284	0,0475	0,1668
Stage 1-4	0,000001	0,4097	0,0528	0,0661	0,4097

The R^2 - values for the C_{ab} / VIs regressions are within a range from $1*10^{-6}$ to 0,41 with an average of 0,053 and a standard derivation of 0,07. These values are, compared to the results at leaf scale, smaller. They are a sign for the low vegetation coverage combined with a high diversity of plant development.

The causes of such relatively lower correlation between VIs and LAI or C_{ab} may be due to the very small sized fertilizer trial plots, in which border effects affected almost every measurement with the ASD field spectrometer. Partly the captured reflectance was from plants and soil of the neighbouring plots. In addition, with five plants per plot, 20 plants per nitrogen level, the statistic population per fertilizer level was relatively low, but the maximum possible within the tight schedule of the field campaign. The photos in figures 5.5 to 5.8 provide an impression of the FTP´s for each stage. The coefficients of determination for the regression of the VIs with LAI and C_{ab} are shown for all stages as bar charts in figure 5.9 and 5.10, respectively. The performance of the VIs for predicting LAI and C_{ab} was assessed for each stage based on the classification of Hamilton (1990) given in table 4.7.

Figure 5.5: Close Photo of a fertilizer trial plot at stage 1 (20.06.06)

Figure 5.6: Close Photo of a fertilizer trial plot at stage 2 (28.06.06)

Figure 5.7: Close Photo of a fertilizer trial plot at stage 3 (16.07.06)

Figure 5.8: Close Photo of a fertilizer trial plot at stage 4 (02.08.06)

Performance assessment of VIs predicting LAI at plant scale at stage 1 (20.06.06):

Overall, the relationship between VIs and LAI at stage 1 was weak. The best LAI prediction was achieved by TCARI (R^2 =0,077). In a relative performance assessment, the VIs of the CARI family show the best correlation, followed by the VIs of the SAVI family with SAVI and MSAVI (R^2= 0,06) together with DGVI1 & 2, MTVI1 & 2 and LAI7 to 10. PRI, mND705 and REIP4 showed no relationship having R^2 values of around 10^{-6}. The R^2 of not mentioned VI´s are somewhere in between group two and three.

Performance assessment of VIs for predicting LAI at plant scale at stage 2 (28.06.06):

Moderate correlation between VIs and LAI at plant scale during stage 2 was achieved by the VIs including LCI (R^2=0,319), DWSI5 (0,311) and many others (RVI, NDWI, SAVI2, OSAVI, TSAVI, SR705, MND705, CSI2, MSI, LWVI1 & 2, LAI7, LAI9 within a range of R^2 from 0,20 to 0,29). The following VIs had weak correlations (R^2 ranging from 0,19 to 0,13): SAVI, MSAVI, RDVI, MCARI2, MTCI, GI, REIP1, NDWI_MIR, LAI8 and Cab. The VI´s MCARI, TCARI and SWIRVI showed almost no correlation with R^2 ranging between 0,0171 and 0,0065.

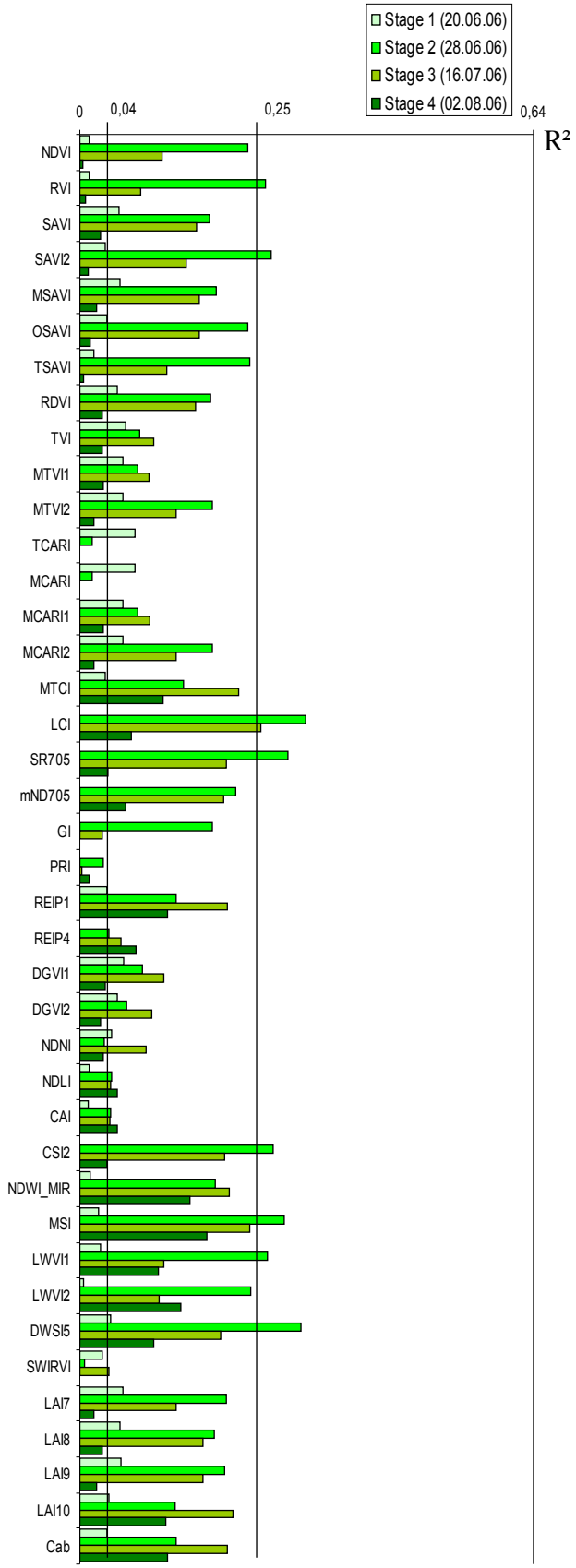

Figure 5.9: Coefficients of Determination for determining LAI by VIs at Plant Scale

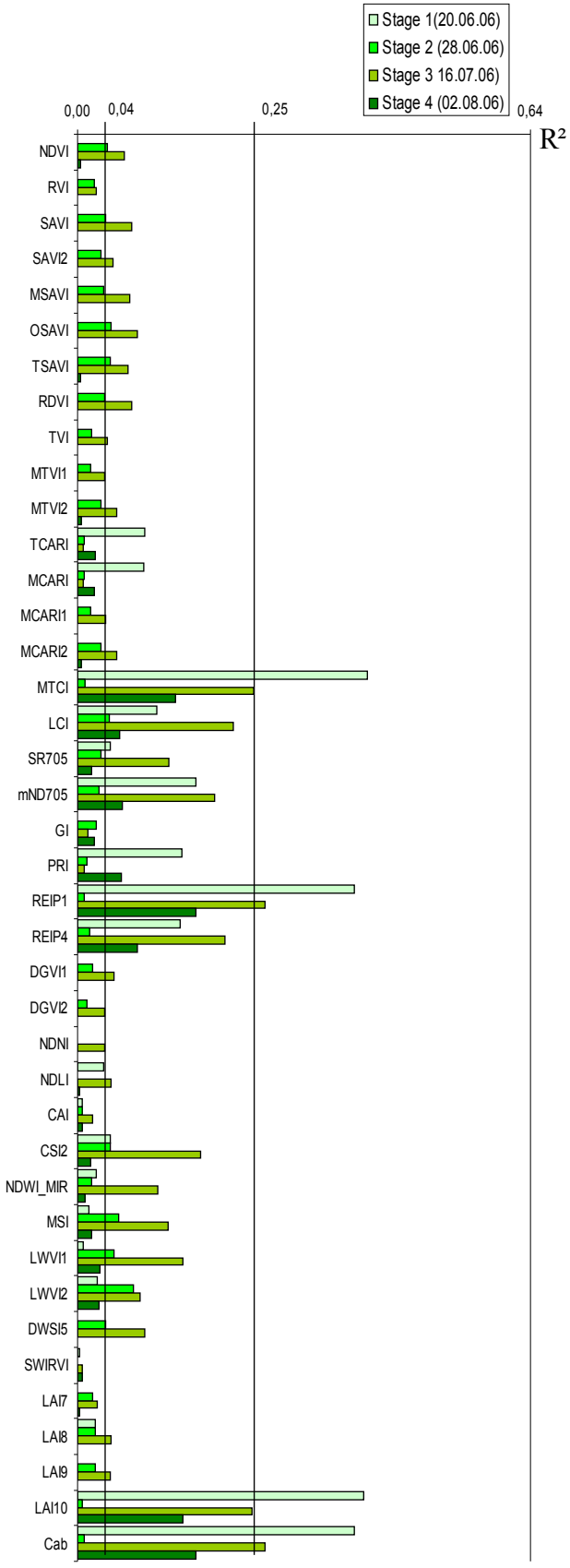

Figure 5.10: Coefficients of Determination for determining C_{ab} by VIs at Plant Scale

Performance assessment of VIs for predicting LAI at plant scale at stage 3 (16.07.06):

A moderate relationship between VIs and LAI at stage 3 was only indicated by one VI comprising LCI. However, with an R^2 of 0.25 the assignment of this VI is just at the lower boundary of the performance assessment group. Within the weak correlation level, but just at a slightly lower R^2 level (0,25 to 0,20) than LCI was ranked, a large group of VIs included the VIs LCI, MTCI, SR705, mND705, REIP1, CSI2, NDWI_MIR, MSI, DWSI5, LAI10 and Cab. Within the same group, but at a R^2 range between 0,17 and 0,11 were the SAVI-family, NDVI, MTVI2, DGVI1 and LWVI1 & 2. Almost no correlation showed TCARI and MCARI (R^2 = 0,0002).

Performance assessment of VIs for predicting LAI at plant scale at stage 4 (02.08.06):

Weak correlation between LAI and VIs was for the VIs comprising MSI (0,18), NDWI_MIR (0,16) and LWVI2 (0,14) followed by VIs with R^2 values ranging from 0,12 to 0,10 including MTCI, REIP1, LWVI1, DWSI5, LAI10 and Cab. The VIs TCARI, MCARI and GI showed almost no fit (R^2 around 0,001).

Performance assessment of VIs for predicting C_{ab} at plant scale at stage 1 (20.06.06):

The prediction of C_{ab} by VIs at stage 1 was moderate with MTCI, REIP1, LAI10, Cab reaching highest R^2 values around 0,4. Weak correlation with R^2 – values around 0,14 was for VIs such as nMD705, PRI and LCI . The VIs DGVI1, TSAVI, SAVI2 and NDVI show almost no correlation (R^2 around 10^{-5}).

Performance assessment of VIs for predicting C_{ab} at plant scale at stage 2 (28.06.06):

Overall, the relationship between VIs and C_{ab} at stage 2 was weak. The maximum R^2 was given by LWVI2 with R^2 = 0,0788. Within the same weak correlation group, further VIs such as MSI, CSI2, LCI, OSAVI and NDVI ranged from 0,0575 to 0,0426. The SWIRVI and NDNI showed no correlation with R^2 = 0,0008.

Performance assessment of VIs for predicting C_{ab} at plant scale at stage 3 (16.07.06):

A moderate relationship between VIs and C_{ab} at stage 3 was shown by MTCI, LCI, REIP1 & 4, LAI10 and Cab with R^2-values ranging from 0,27 to 0,21. Weak correlation between C_{ab} and VIs was found for SR705, mND705, CSI2, NDWI_MIR, MSI and LWVI1 with R^2 values ranging from 0,19 to 0,11. No correlation showed the VIs SWIRVI, MCARI, TCARI (R^2 – values ranging from 0,0069 to 0,0076).

Performance assessment of VIs for predicting C_{ab} at plant scale at stage 4 (02.08.06):

Weak correlation between C_{ab} and VIs was indicated with the best VIs including Cab and REIP1 having R^2 values around 0,17 followed by LAI10 and MTCI with similar R^2. Almost no fit showed MCARI1, MTVI1, TVI and RDVI with R^2 around 10^{-5}.

5.2.3 Plant Scale LAI and leaf chlorophyll estimation on nitrogen levels

As shown in chapter 5.2.2 the variability of the cotton plant development, LAI and chlorophyll values within and among the fertilizer plots is relatively high. To reduce this variability and to check if there is a dependence on the different nitrogen application levels, the measured LAI and C_{ab} data were aggregated according to the nitrogen application levels and for temporal stage. The statistics for these aggregated datasets are shown as an overview in table 5.6. The LAI data, partitioned according to N-levels and stage, showed a smaller range, STD and CV than datasets partitioned according to stage only (compare table 5.3). A similar behaviour was recognized for the C_{ab} data. This indicates the impact of different N application rates on development of plant growth resulting in specific LAI and C_{ab} development.

To compare the performance of the relationship between VIs and LAI and VIS and C_{ab} over different stages and N-levels the respective R^2 values are compared in vertical-bar charts. For an easier comparison the charts were sorted by stages and the charts for the different nitrogen levels for LAI / VIs and C_{ab} / VIs are presented on the same page in figures 5.11 to 5.18.

Overall, the performance of the relationship between LAI and VIs considering the datasets aggregated according to nitrogen levels and stages is with a mean R^2 of 0,26 and a maximum R^2 of 0,77 much better than considering the values for the whole stages stages only with 0.096

Table 5.6: Statistics for LAI and C_{ab} for Fertilizer Trial Plots on Plant Scale

LAI ( ) C_{ab} (µg cm-²)	Stage	N-Level	Sample Number[1)]	Min	Max	Range	Mean	STD	CV
C_{ab}	1	0	20	36,8	49,1	12,3	43,5	4,1	9,32
		150	19	36,5	50,1	13,6	44,1	3	6,82
		200	20	40,2	50,6	10,5	43,6	2,6	5,99
		250	15	33,5	49,7	16,2	42,7	4	9,27
	2	0	19	28,9	35,1	6,2	32,5	1,6	4,98
		150	20	29,1	36,9	7,8	33,4	2,1	6,34
		200	20	30	35,1	5,1	32,4	1,6	4,88
		250	20	29,1	34,5	5,4	32,6	1,5	4,67
	3	0	19	25,8	33,8	8	30,7	2,5	7,99
		150	10	31,3	36,8	5,6	33,6	1,5	4,51
		200	20	29,8	40,4	10,5	32,9	2,4	7,17
		250	15	27,5	37	9,4	31,9	2,5	7,71
	4	0	20	32,8	48,7	15,9	41,2	3,7	9,05
		150	20	38,2	46,2	8	42,5	2,2	5,24
		200	20	37,1	47	9,9	42,6	2,7	6,27
		250	20	37,8	47,9	10,2	43	2,6	6,13
LAI	1	0	14	0,23	0,97	0,74	0,42	0,19	45,85
		150	10	0,13	0,78	0,65	0,51	0,22	43,44
		200	15	0,09	0,93	0,84	0,46	0,26	56,43
		250	9	0,16	0,88	0,72	0,45	0,24	52,85
	2	0	19	0,36	0,96	0,6	0,69	0,16	23,93
		150	20	0,53	1,06	0,53	0,76	0,15	20,43
		200	20	0,51	1,5	0,99	0,86	0,36	41,97
		250	20	0,39	1,7	1,31	0,87	0,34	38,72
	3	0	19	0,86	1,64	0,78	1,21	0,19	15,3
		150	10	0,82	1,86	1,04	1,37	0,32	23,18
		200	20	0,89	4,44	3,55	1,6	0,88	54,81
		250	15	0,55	3,55	3	1,83	0,83	45,59
	4	0	20	1,31	5,52	4,21	3,76	1,05	27,82
		150	20	1,3	5,37	4,07	4,06	1,22	30,09
		200	20	0,73	5,65	4,92	4,01	1,51	37,74
		250	20	1,81	6,08	4,27	3,89	1,47	37,84

1) the sample number decreased for some datasets, due to zero LAI values, caused by LICOR2000 errors (stage 1) and SPAD measurements (stage 3 N250, N150) acquired using a dirty Minolta SPAD-502 with wrong values as a result.

and 0.32 for mean and maximum R^2, respectively (compare table 5.3). Similar improvements were noticed for the relationships between VIs and C_{ab}, when data were aggregated to nitrogen and stage levels with a mean R^2 of 0,19 and a maximum R^2 of 0,66. Therefore compare table 5.5 where mean R^2 is 0.053 and a maximum R^2 is 0.41 for relationships between VIs and C_{ab} for data aggregation according to stages only. These findings further support the theory that the different nitrogen applications had a significant influence on the development of cotton plants, LAI and C_{ab} distribution.

The performance of each VI to predict LAI and C_{ab} in the different N application rates and stages is described in the following sub-chapters. The corresponding R^2 values for the VIs that showed the best relationships are given in brackets after respective VIs in the later text.

5.2.3.1 Plant scale LAI and C_{ab} estimation at nitrogen levels at stage 1

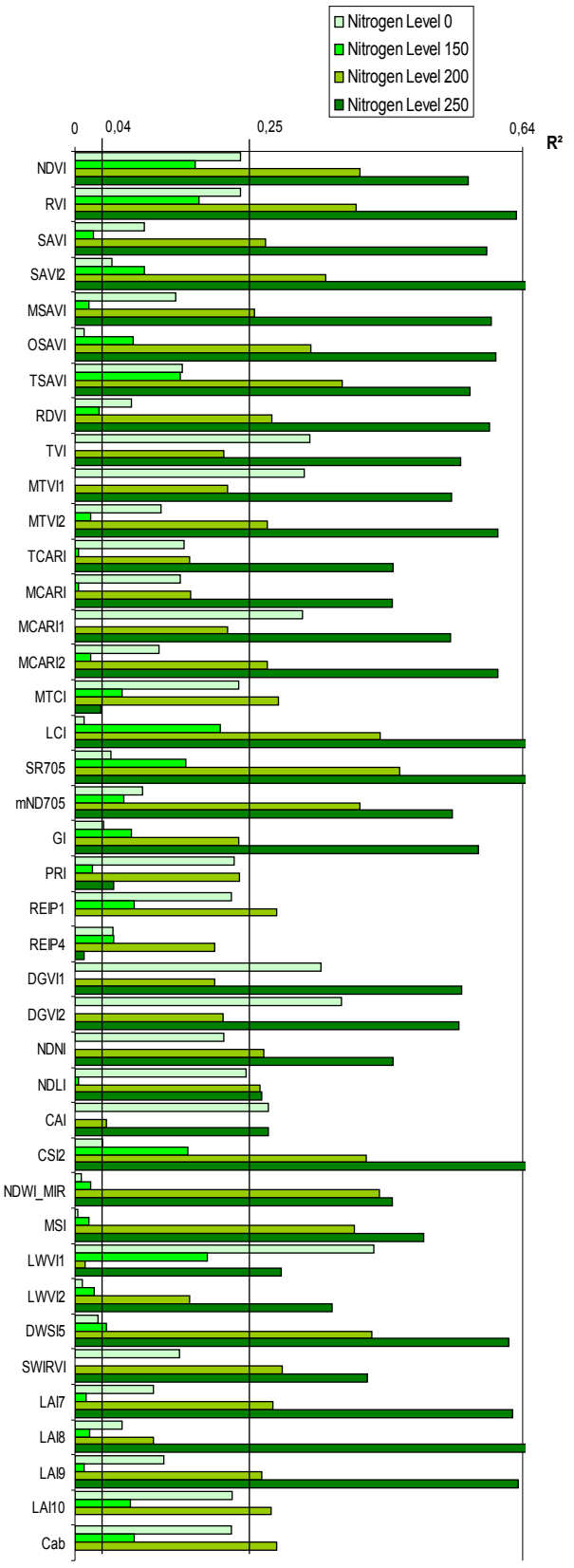

Figure 5.11: Coefficients of Determination for determining LAI by VIs at Plant Scale, Stage 1

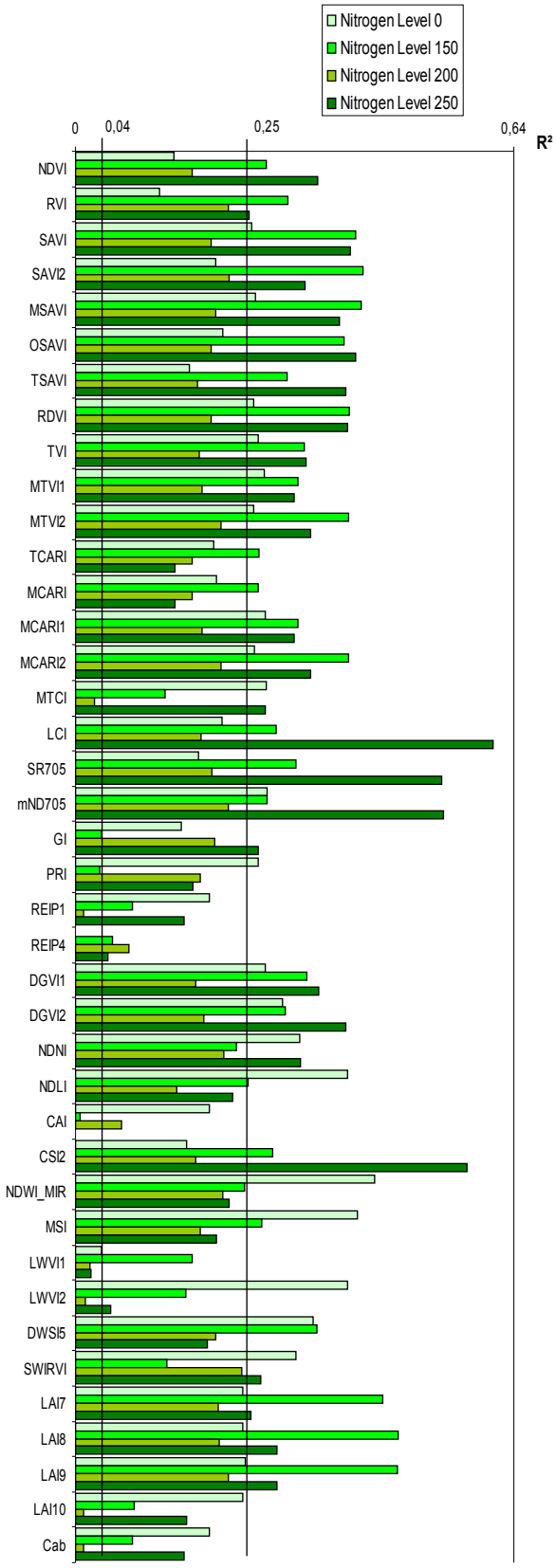

Figure 5.12: Coefficients of Determination for determining C_{ab} by VIs at Plant Scale, Stage 1

Performance assessment of VIs for predicting LAI at different N - levels at stage 1

At the first stage (20.06.06) the prediction power of VIs to estimate LAI of cotton plant canopies in different fertilizer application rates was strong ($R^2 > 0.64$) with the highest prediction power for plants growing on plots with Nitrogen Level 250. At this N-level, strong correlations were found for five VIs including SR705 (0,75), LCI (0,70), CSI2 (0,68), SAVI2 (0,67) and LAI8 (0,65). Most of the VIs showed moderate correlation from which six VIs (LAI9, LAI7, DWSI5, MTVI2, MCARI2 and OSAVI) with R^2 values higher than 0,6, whereas the majority had R^2- values higher than 0,5. Weak correlation was found for one VI (PRI with R^2 of 0,056), whereas Cab, LAI10, the REIP´s and MTCI had no correlation with LAI at this stage.

The second best relationships between VIs and LAI with moderate correlations were found for plants from nitrogen level 200 plots. The corresponding VIs included SR705 (0,46), LCI (0,44), NDWI_MIR (0,44), DWSI5 (0,42) and CSI2 (0,42) and 25 other VIs with lower R^2 values but higher than $R^2 = 0.25$. Weak correlations were found for 14 VIs, and no correlation was only shown by LWVI1 (0,014).

Moderate correlations, but at a lower range than at N-level 200 was indicated for Nitrogen Level 0 with the VIs LWVI1 (0,43), DGVI5 (0,35), TVI (0,34), MTVI1 (0,33), MCARI1 (0,33) and CAI (0,28). At this N-level 29 VIs had weak correlations, while 5 VIs (LCI, GI, NDWI_MIR, LWVI2, DWSI5) showed no correlation to LAI.

At Nitrogen Level 150 only weak correlations were reached with maximum R^2-Values of 0,21 (LCI), 0,19 (LWVI1 and 0,17 (NDVI) while 16 other VIs had even weaker correlations. No correlation was indicated for 24 VIs.

Performance assessment of VIs for predicting C_{ab} at different N-levels at stage 1

Similar as for LAI the best correlations of VIs with C_{ab} were found for plants on Nitrogen Level 250. However, the best correlations were only moderate with LCI (0,61), CSI2 (0,57), mND705 (0,54), SR705 (0,53) and OSAVI (0,41) having highest values among 20 other VIs that had R^2 values above 0.25. Weak correlation was indicated by 13 VIs while no correlation was shown for only 2 (LWVI1 and CAI) VIs.

LAI predictions for plants from Nitrogen Level 150 showed for the VIs LAI8, LAI9 (both 0,47), LAI7 (0,45) SAVI2, MSAVI (both 0,42) the second best performance besides 23 other VIs with R^2 values higher than 0.25. Weak correlation had nine VIs (MTCI, REIP´s, NDWI_MIR, LWVIs, LAI10, Cab and SWIRVI) and no correlation only by three VIs (GI, PRI, CAI).

Considering Nitrogen Level 0 had moderate correlation between the VIs NDWI_MIR (0,44), MSI (0,41) and C_{ab} besides further 16 VIs with R^2 values of > 0.25. Weak correlation was achieved by 20 VIs, while no correlation was indicated for two VIs (LWVI1 and REIP4).

Plants grown on Nitrogen Level 200 had the overall lowest (weak) correlation between VIs and C_{ab}

over the different N-levels in stage 2 with SWIRVI (0,24), mND705, LAI9, SAVI2, RVI (all 0,22) and MTVI2, MCARI2, NDWI_MIR, LAI8 (all 0,21) besides 15 other VIs. MTCI, REIP1, LWVIs LAI10 and Cab showed almost no correlation

5.2.3.2 Plant Scale LAI and C_{ab} estimation on Nitrogen Levels at stage 2

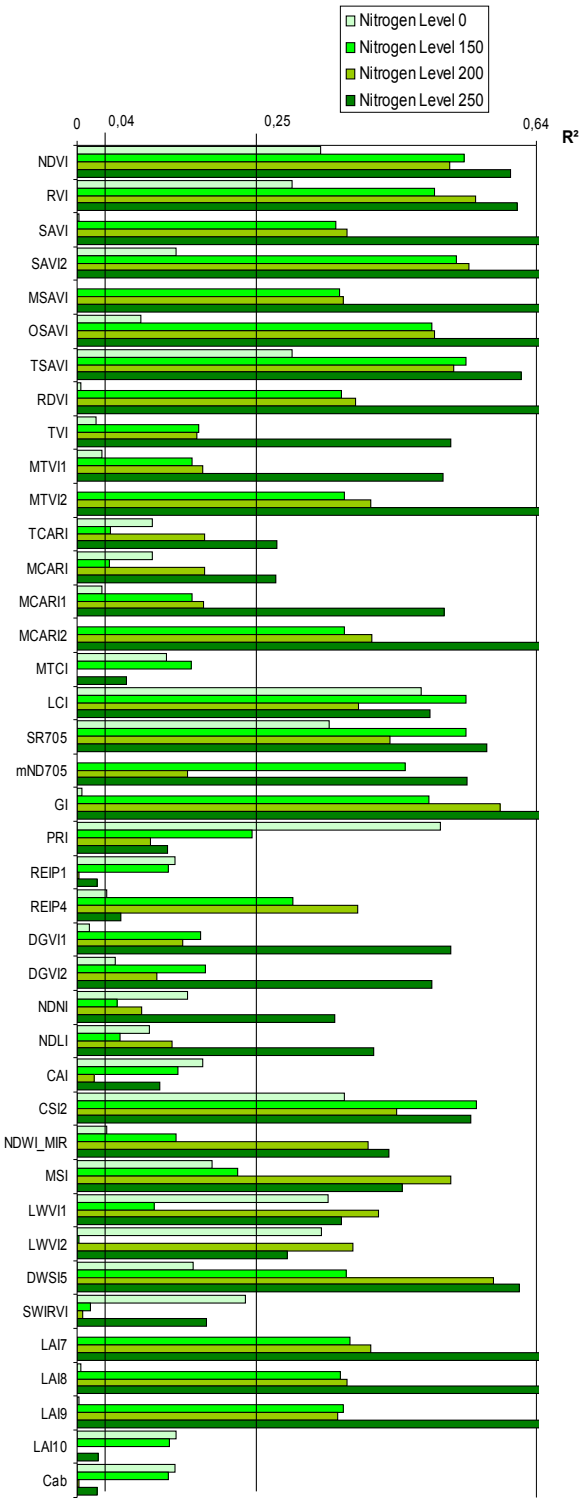

Figure 5.14: Coefficients of Determination for determining LAI by VIs at Plant Scale, Stage 2

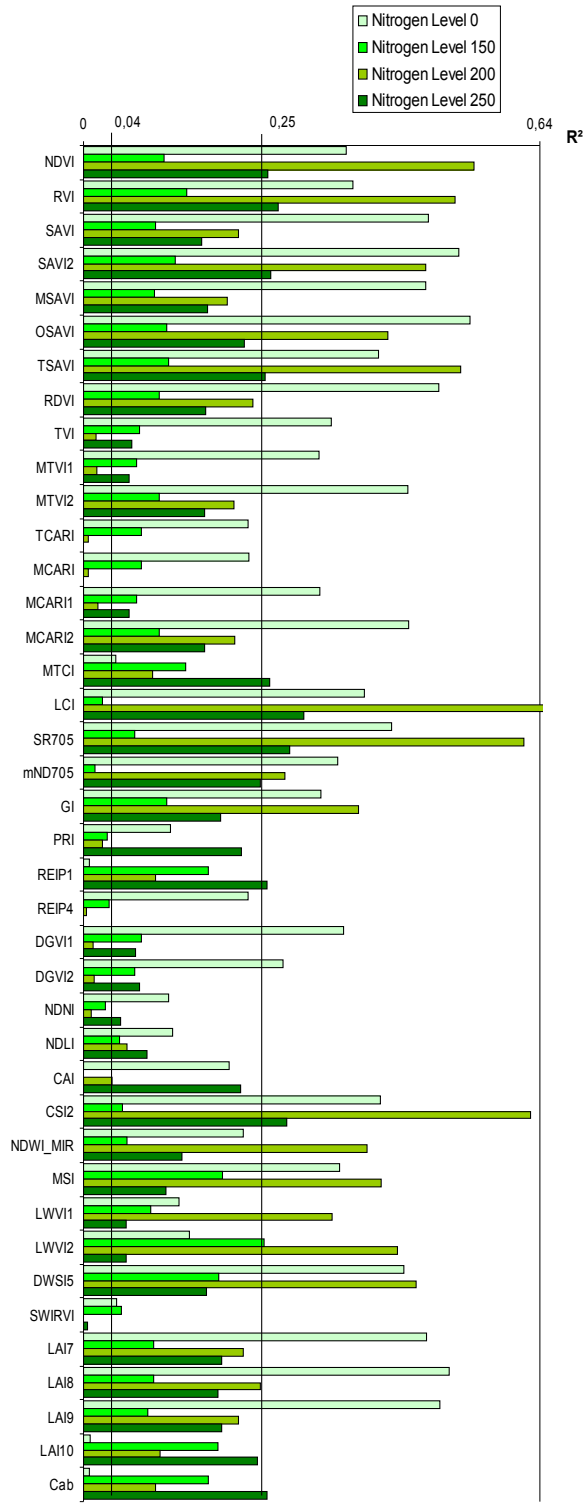

Figure 5.13: Coefficients of Determination for determining C_{ab} by VIs at Plant Scale, Stage 2

Performance assessment of VIs for predicting LAI at different N-levels at stage 2

Strong correlation between VIs and LAI at stage 2 was found for plants grown in plots with nitrogen level 250 with VIs including LAI7 (0,75), LAI8 & LAI9 (0,74), SAVI2, MTVI2 & MCARI2 (0,7), RDVI, MSAVI & OSAVI (0,69) and SAVI (0,68). Moderate correlation was indicated for almost all other VIs, except for SWIRVI, CAI, PRI, MTCI and REIP4 (weak correlation) and LAI10, Cab, REIP1 (no correlation).

Moderate correlation between VIs and LAI was indicated for 23 VIs measured on plants from N-level 200 plots with VIs showing highest values GI (0,59), DWSI5 (0,58), RVI (0,55), SAVI2 (0,55), TSAVI (0,53). Weak correlation was achieved by 11 VIs and no correlation had 4 VIs (Cab, LAI10, SWIRVI, CAI, REIP1, MTCI).

Considering nitrogen level 150 moderate correlations had CSI2 (0,55), TSAVI, LCI, SR705 & NDVI (0,54) and SAVI2 (0,52). Weak correlations had 19 VIs and 4 VIs had no correlation to LAI (SWIRVI and LWVI2).

Nitrogen Level 0 showed the poorest performance for VIs predicting LAI in canopies with 9 VIs having moderate correlation of a medium performance level within this group (PRI (0,5), LCI (0,48), CSI2 (0,37) and SR705 (0,35)). 18 VIs had weak correlation and 13 VIs no correlation

Performance assessment of VIs for predicting C_{ab} at different N-levels at stage 2

On stage 2 the coefficients of determination for estimating C_{ab} by VIs calculated for data collected on plots with Nitrogen Level 200. With $R^2 = 0,65$ the LCI was the only member of group 1, but with 0,63 (CSI2) and 0,62 (SR705) the top inhabitants of group 2 were almost as high. In total, group 2 contained 14, group 3 13 and group 4 12 coefficients of determination.

The second best performance showed the dataset related with Nitrogen Level 0 with 25 coefficients inhabiting group 2. The best were for OSAVI (0,54), SAVI2 (0,53), LAI8 (0,51), LAI9 & RDVI (0,5) and LAI7, SAVI & MSAVI (0,48). Group 3 contained 13 and group 4 with the ones for LAI10, Cab and REIP1 only 3 coefficients with almost no correlation.

Nitrogen Level 250 showed 8 members in group 2, as top scorers LCI (0,31), SR705 & CSI2 (0,29), RVI (0,27) and SAVI2, MTCI & Cab (0,26). With 28 the most coefficients of determination of this level were grouped in group 3. Group 4 contained the ones for SWIRVI, REIP4, MCARI and TCARI.

5.2.3.3 Plant Scale LAI and C_{ab} estimation on Nitrogen Levels at stage 3

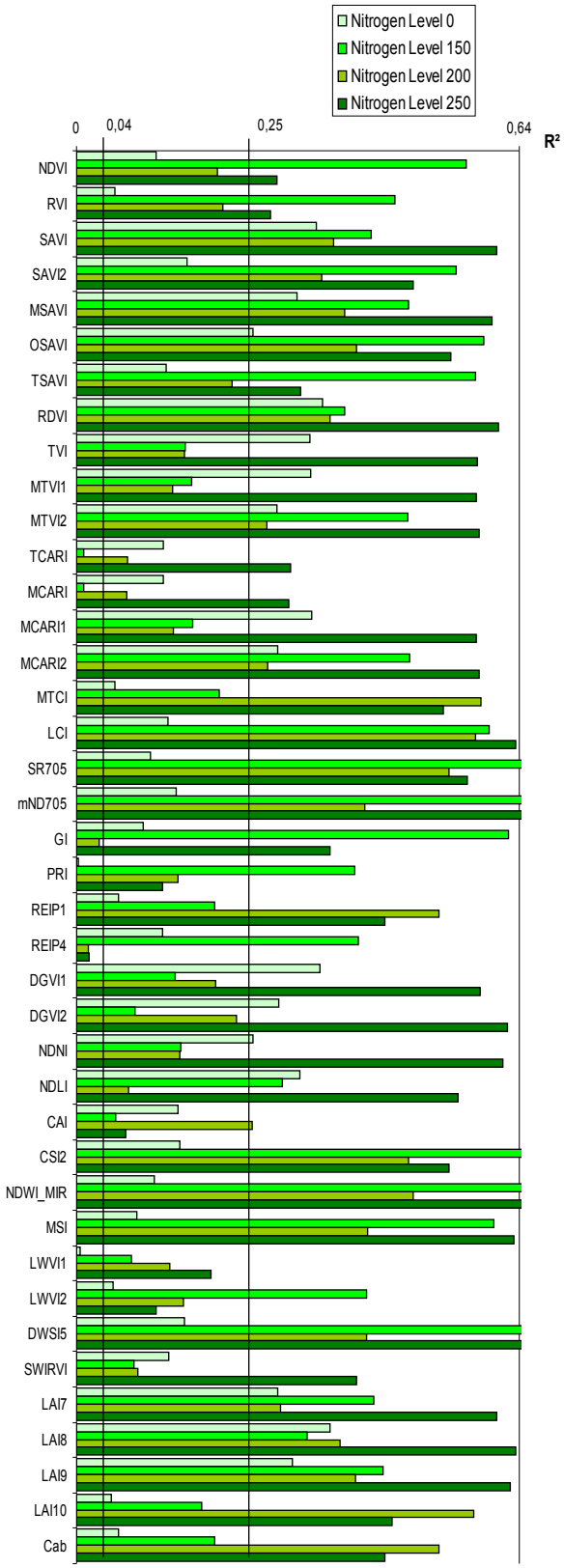

Figure 5.15: Coefficients of Determination for determining LAI by VIs at Plant Scale, Stage 3

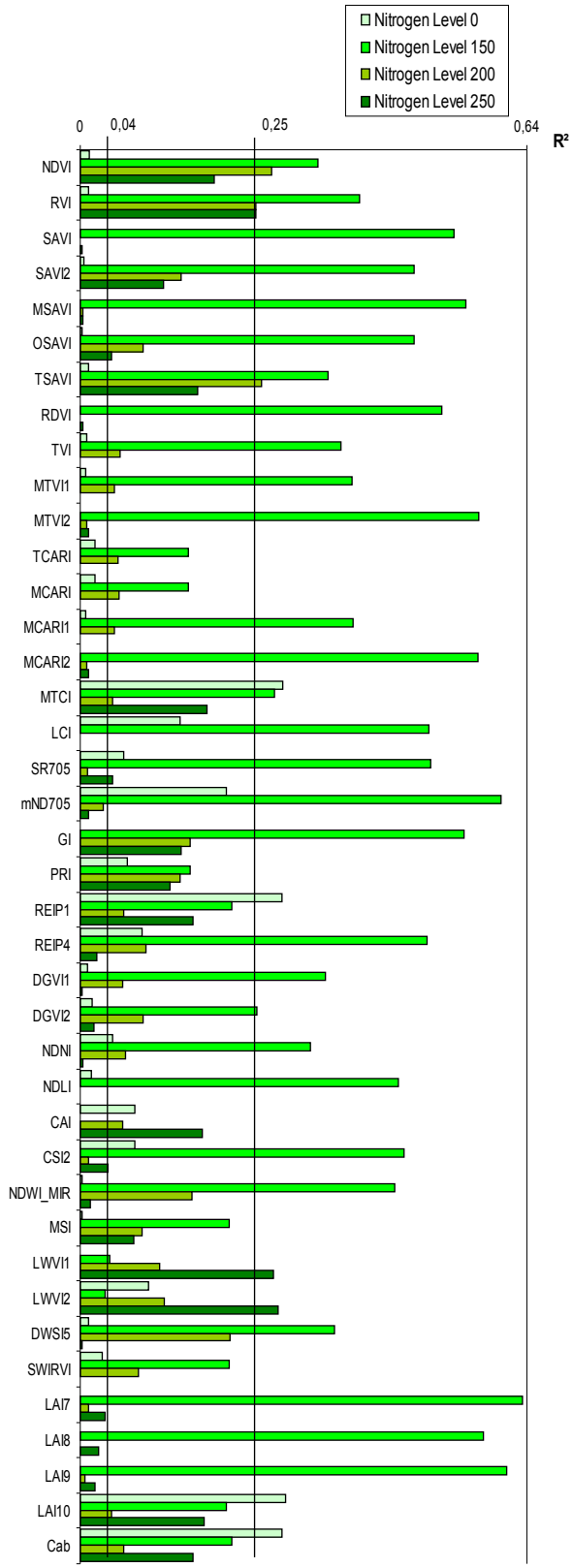

Figure 5.16: Coefficients of Determination for determining C_{ab} by VIs at Plant Scale, Stage 3

Performance assessment of VIs for predicting LAI at different N-levels at stage 3

The best performance (strong correlation) of VIs for estimating LAI by VIs at stage 3 was for the nitrogen level 150 dataset with the VIS including CSI2 & NDWI_MIR (0,77), DWSI5(0,75), SR705 (0,72) and nMD705 (0,66). 20 VIs showed a moderate, 13 VIs weak and 2 VIs (MCARI and TCARI) weak correlation.

Strong correlation, but with lower values as for N-level 150 was given for VIs estimating LAI for plants on Nitrogen Level 250 with mND705 (0,72), DWSI5 (0,7) and NDWI_MIR (0,66). Moderate correlations were shown for almost all other VIs (31). Only PRI, REIP4, CAI and the LWVIs had a weak correlation. There were no VIs with no correlation, that´s why the overall correlation performance is best for this dataset.

At nitrogen level 200 strong correlations were found for MTCI & LCI (0,58), LAI10 (0,57), SR705 (0,54) and Cab (0,52), which were among 22 other VIs within this correlation group. Weak correlation had 16 VIs, and no correlation only GI and REIP4.

Moderate correlation of a relatively lower regression performance was shown for 15 VIs including LAI8 (0,37), RDVI (0,36), SAVI & DGVI1 (0,35) and MCARI1, MTVI1&TVI (0,34) as the best VIs. Weak correlation was given for 24 VIs and no correlation was for one VI (PRI).

Performance assessment of VIs for predicting C_{ab} at different N-levels at stage 3

As for estimating LAI the VIs with the best correlations between VIs and C_{ab} were for nitrogen level 150.

The second best correlations were found for plants on nitrogen level 0 with 4 VIs including MTCI, Cab, REIP1 and LAI10 (all 0,29). Weak correlations were obtained for 9 VIs and 27 VIs had no correlation.

Nitrogen level 250 showed three VIs with moderate correlation at the lowest performance level including the LWVIs (both 0,28) and RVI (0,25). Weak correlation was given by 15 VIs with NDVI (0,19) as best. The remaining 22 VIs had no correlation.

Nitrogen Level 200 had a moderate correlation of VIs with C_{ab}, but with lower values, NDVI (0,27), TSAVI (0,26) and RVI (0,25). Therefore VIs with weak correlation (25 VIs) and VIs with no correlation 15 VIs indicated a slightly better overall performance than the coefficients of N-Level 250.

5.2.3.4 Plant Scale LAI and C_{ab} estimation on Nitrogen Levels at stage 4

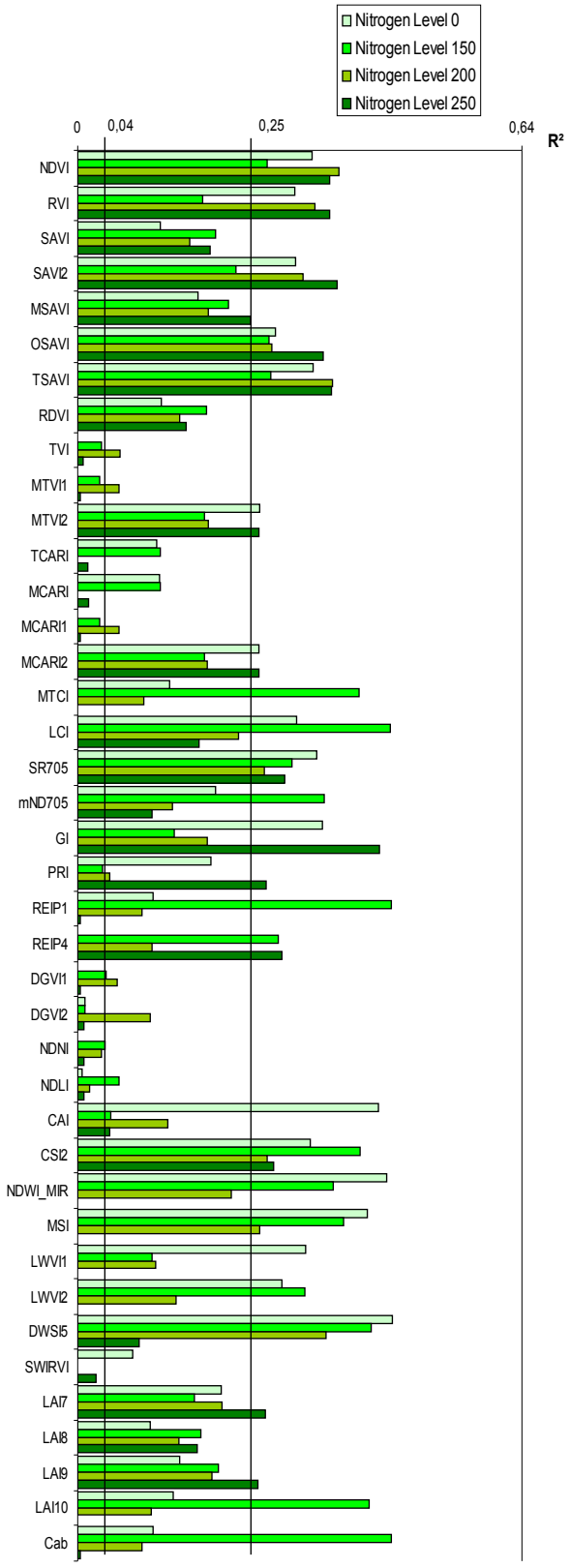

Figure 5.17: Coefficients of Determination for determining LAI by VIs at Plant Scale, Stage 4

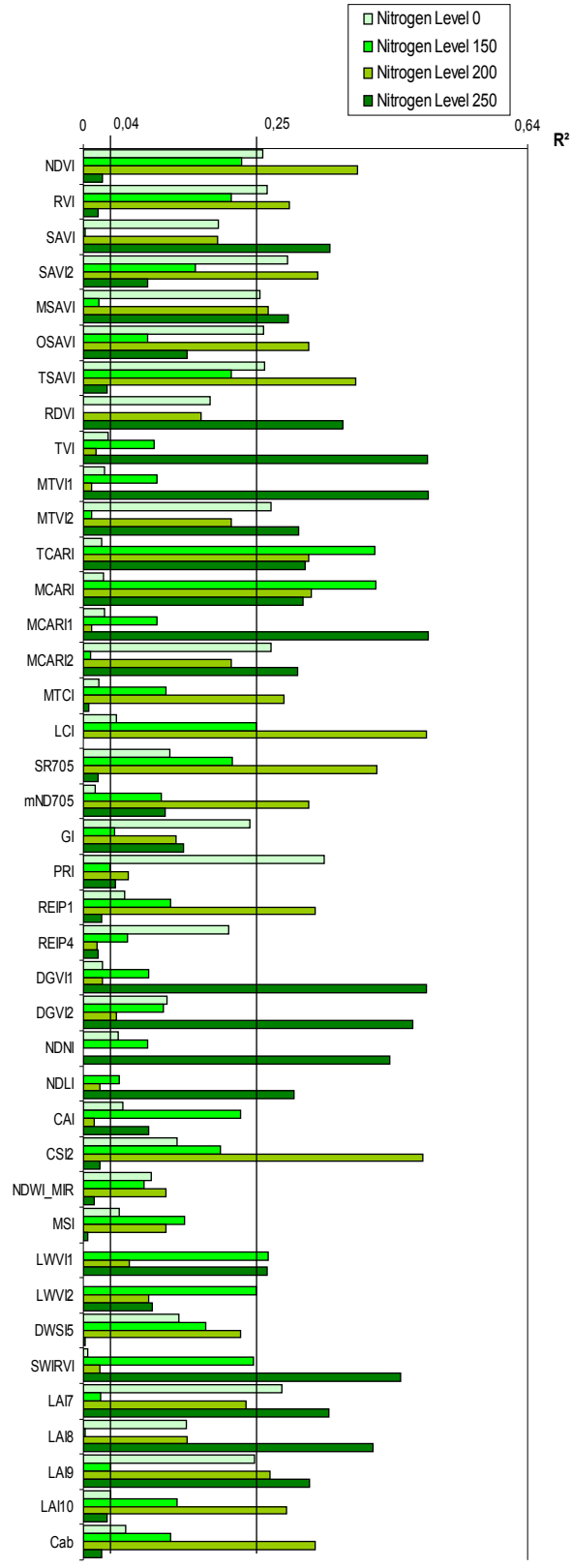

Figure 5.18: Coefficients of Determination for determining C_{ab} by VIs at Plant Scale, Stage 4

Performance assessment of VIs for predicting LAI at different N-levels at stage 4

The estimation of LAI by VIs performed poorest for the last stage. Moderate correlation was only indicated for some VIs in certain nitrogen levels with highest R^2 - values of around 0,45.

Nitrogen level 0 had a moderate correlation of VIs with LAI for 17 VIs including DWSI5 & NDWI_MIR (0,45), CAI (0,43), MSI (0,42), GI (0,35) and SR705 (0,34) as the best performer. Weak correlation was for 15 VIs, while 8 VIs had no correlation.

At nitrogen level 150 15 VIs had moderate correlation with LAI with REIP1, LCI & Cab (0,45), DWSI5 & LAI10 (0,42) and MTCI (0,4) as best performer. Weak correlation was obtained by 19 VIs and no correlation was given by 6 VIs (TVI, MTVI1, MCARI1, DGVI2, NDNI, SWIRVI).

Performance assessment of VIs for predicting C_{ab} at different N-levels at stage 4

The VIs for the estimation of C_{ab} showed the best fit for the last stage for nitrogen level 250 with 19 VIs having a moderate correlation, including TVI, MTVI1, MCARI1 & DGVI1 (all 0,5), DGVI2 (0,47) and SWIRVI (0,46) among the best performer. Weak correlation were found for 9 VIs and 14 VIs had no correlation.

Nitrogen level 200 had VIs that showed the second best correlation to C_{ab}, with LCI & CSI2 (0,49), SR705 (0,42) and NDVI & TSAVI (0,39). Weak correlation was for 15 VIs and 8 VIs had no correlation.

Moderate correlation was given by 10 VIs, including PRI (0,35), SAVI2 & LAI9 (0,29) and MTVI2 & MCARI2 (0,27) . 19 VIs had weak correlation and 11 VIs had no correlation. Thus the VIs applied to nitrogen level 0 performed slightly better than the VIs that were applied to nitrogen level 150.

Nitrogen level 150 showed with 3 coefficients [MCARI & TCARI (0,42), LWVI 0,27)] a moderate correlation, 28 VIs had a weak correlation and 8 VIs no correlation.

5.2.4 Summary and discussion of LAI and C_{ab} estimation at plant scale

At plant scale the dataset including all measurements per stage showed a relatively poor overall performance for predicting both, LAI and C_{ab} by VIs (fig. 5.9). Comparing the figures 5.11, 5.13, 5.15 and 5.17 showing the coefficients of determination for predicting LAI by VIs grouped by nitrogen levels and stages the heterogeneity of the performance of the VIs on the fertilizer trial plots becomes evident. Some VIs show a good performance for one N-level, especially for N-level 250, but a poor one for another one at the same stage.

The exception was stage 2. At this stage most VIs showed their best performance for most N-levels. The plant growth as shown in figure 5.6 gives insight into a potential reasoning for this behaviour. At stage 2 the early growth stadium had passed. The plants were developing their first nodes and further leaves were emerging. The plant growth and leaf development in the different

plots was relatively homogeneous as the different fertilizer application rates were just being taken up by the plants and could not yet have a strong impact. Thus, LAI was relatively best predicted by VIs at this stage compared to the first and the two later stages.

At stage 1 the plants were in the early development phase and only few leaves had emerged, the reflection from the vegetation was still very weak compared to the reflection from the surrounding soil (compare fig. 5.5). Thus, the reflection captured by field spectrometer above small plants represented a more dominant soil reflectance with weak vegetation signal. This spectral reflection situation and the VIs, developed mainly for conditions with a more dominant vegetation coverage may explain their weak performance for predicting LAI at this stage. The exception was N-level 250 with a very good performance of most VIs, because these plants were further developed and their growth was more homogeneous.

At stage 3 plant size and number of leaves were in general further developed over all plots due to advanced growth stage (compare figure 5.7). The plant size and leaf development variation among the plots increased to a different extent due to the impact of different fertilizer application rates. The plots receiving less fertilization showed an increase of the coefficients of determination for stage 3 for most VIs, the plots with the highest fertilizer application rate a slight decrease. The dataset containing all measurements per stage indicates this rise of diversion by a decrease of the R^2-values for most VIs.

At stage 4 plant growth and increase of plant coverage had further developed (compare figure 5.8). The same happened to the range of LAIs within each plot, because the variation of the plant development in each plot increased, too. This high variation was strengthened by not homogeneously distributed fertilizer application and irrigation water within the small plots, resulting in an high within plot variability of plant growth. This may be the reason why the coefficient of determinations for the LAI / VI regressions decreased, compared to stage two and three.

The overall best representation of the performance of the datasets was shown by NDVI and TSAVI. These VIs were not among the very best performing VIs for any dataset, but never showed a poor correlation. The correlation of NDVI and TSAVI with LAI was similar to the average correlation of the other VIs of the same stage and N-level.

Compared with the LAI, the prediction of C_{ab} by VIs showed even higher heterogeneity for most stages, not only for the comparison of different data aggregations, but also within each dataset.

For the prediction of C_{ab} by VIs at plant scale, the first stage represented the time when the variation of plant development and also the variation of chlorophyll within each leaf, plant, plot and over all plots with different fertilizer application rates was the lowest of all four stages. Thus, with homogeneous leaf chlorophyll distribution in each plant and the mainly development of top leaves and not yet developed leaf layer structures, a relatively high correlation between VIs and C_{ab} was

achieved at this stage.

At stage 2 the relationship between VIs and C_{ab} was differing. This may be due to the fact that first leaf layers with different C_{ab} content due to different leaf ages had developed at different locations within each plant, plot, and among the plots with different fertilizer application rates. VIs measured on plants in plots with nitrogen level 0 and 200 showed the highest correlation indices for this stage, N-level 150 and 250 a decrease, compared with stage 1. The overall dataset responded to this diversity with a very low correlation.

In stage 3, the relationship between VIs and C_{ab} increased significantly for plants from plots with N-level 150, but decreased for all other plots. The variation of the regression results of the VIs calculated for the different N-levels had the maximum at this stage, most likely due to development of different leaf layers and a corresponding higher variation of C_{ab} values within the plants.

At stage 4, the variability of the correlations between VIs and C_{ab} for different N-levels decreased again, but the performance shown by the different VIs was very different for each N-level. While one group of VIs showed their best performance for plants within plots of N-level 0 or 150, other ones performed better for level 250 or 200. At this stage each N-level had its own best performing VIs. The overall slightly better correlation than for stage 3 was also evident in the correlation results of the complete dataset (figure 5.10).

Summarizing the plant scale analysis showed that

- the heterogeneity within each dataset, and even more in-between, was too high to use one VI for a stable prediction of LAI or C_{ab}-content. For each dataset some VIs came out as absolute high predictor, but no one could keep this performance over time or over all N-levels at the same stage. This finding may underline the empirical nature of the VIs which seam mainly suitable for a specific environmental and plant growth situation, thus the same VI may potentially not be applied over several temporal stages or different environmental conditions (e.g. different plant cover due to different N-fertilization rates).
- the prediction performance was in general better for LAI than for C_{ab}.
- the prediction performance improved while the data variability decreased for both LAI and C_{ab} when data were split up according to N-levels and temporal stage.

However, these findings must be carefully considered against several facts:

- possible measurement inconsistencies may have occurred, such as that LAI was difficult to measure for plants at an early growth stage, when only few leaves close to the ground were present and LICOR-2000 was difficult to position, thus leading to over- or underestimations of LAI-values for the whole plant.
- possible errors for LAI measurements are also likely at later growth stages, when cotton plants had developed many leaves, thus LAI measurements took partly leaves from neighbouring

plants into consideration that were interweaved with the actual measured plant, such as that LAI was difficult to measure for plants on a late growth stage and may have led to over- or underestimations.

- possible spatial inconsistencies of reflectance and SPAD measurements, such that reflectance was measured from top of the plant therefore taking reflectance mainly from visible leaves into consideration, while SPAD was measured for all leaves located in different layers of the plant and resulting values were averaged for regression with reflectance measurements.

Taking these findings into consideration, future investigations may be improved by taking the following recommendations into consideration:

- In future investigations of single plants, LAI measurements at stage 1 (20.06.), which is about three weeks to one month after the 2-4 leaves stage, should be done by destructive leaf area determination or the LICOR-2000 tool using less detector rings to adjust the instrument to the low coverage. Alternatively and depending on the objective of the research, the measurements may start later, e.g. around stage 2 (28.6.) or stage 3 (16.07.) and last longer, e.g. until harvest (around the beginning to mid September). If for example the LAI and C_{ab} are used as input into crop models for prediction of yield, then measurements at a later growth stage until the time just before harvest are compulsory. Early LAI and C_{ab} measurements could be helpful for early predictions, but then these predictions need to be taken with care considering possible measurement inconsistencies and further changes in plant development deviating from the potential predicted yield. In contrast, if the monitoring of the response of fertilizer and water inputs on LAI and C_{ab} is the focus of the research, then respective measurements should be timed before and after the inputs are taken up by the plant and the effect on plant LAI and C_{ab} can be observed.
- It is generally advised to focus future canopy LAI measurements on measurements of canopies composed of multiple plants, such as that a LAI measurement is performed on several cotton plants within a smaller area taking also the row structure of the cotton plants into account (e.g. measuring in a diagonal from one cotton plant to another cotton plant). Following this measurement strategy the collected data represent the LAI situation of a certain area (e.g. area around 1-1.5 m diagonal) which again can be used for upscaling or outscaling the results to larger areas (e.g. the whole measurement plot) or other areas with similar input situation, respectively.
- Larger fertilizer trial plots would be helpful, because water and fertilizer may be more homogeneously distributed, the number of samples per plot can be increased, border effects to neighbouring plants could be better avoided, thus more and more precise LAI measurements are expected.

- The distribution of C_{ab}-content within different plant layers may have better accentuated a more homogeneous spatial distribution pattern over the different nitrogen levels and with time that can be correlated against respective VIs from spectral reflectance measurements. This strategy was tested on regional scale.

5.3 Multi – temporal LAI and C_{ab} estimation at regional scale

At a regional scale the vegetation indices are no longer calculated based on ASD field spectrometer reflectance data measured from single canopies on the ground, but from Proba-1/CHRIS mode 5 satellite images in order to estimate the spatial distribution of LAI and Cab within fields for a larger region. As described in chapter 4.5.7.2 the VIs were calculated for grid cells. The grid cell size was set according to the double size of one satellite image pixel (17 x 17 m) to 34 x 34 m (2 x 2 raster cells) to minimize border effects.

Due to the limited spectral information of the Proba-1/CHRIS images it was not possible to calculate all 60 VIs as was done with the data gathered with ASD field spectrometer, but 38 VIs were selected and calculated for four temporal stages. For performance assessment of VIs predicting LAI and C_{ab} the coefficients of determination for each VI and LAI as well as C_{ab} is presented in vertical-bar charts sorted by date and data aggregation. The statistics for each VI, date and whole plant are to shown in tables 8.7 to 8.10 in the Appendix.

5.3.1 Regional scale LAI and Chlorophyll estimation

For a comparison of the prediction power of VIs for LAI (fig. 5.19) and C_{ab} / VI (fig. 5.20) the coefficients of determination are shown for the whole plants (not taking the layer structure into consideration) and for all stages in two bar charts together on the same page. The numbers in brackets behind the VIs indicate the respective R^2-values.

Performance assessment of VIs for predicting LAI

For LAI the first collected dataset was at the second stage (28.06.06). At this point in time moderate correlation of VIs to LAI was indicated by 32 VIs. The REIP1 (0,43), Cab1 (0,4) and LAI5&6, MCARI, RVI (0,39) were the best performing VIs. The vegetation indices DGVI1 (0,25), mND705 (0,22), PRI, REIP4 and LAI1 showed a weak correlation. No correlation was shown for CARI (0,014).

At the third stage (16.07.06) almost all VIs showed moderate correlations with R^2 – values around 0,5. Among these VIs the relative best correlation with R^2 more than 0,53 were for the LAI4 (0,5423), NDVI (0,5388), LAI1 (0,5384), mND705 (0,5382), ATSAVI (0,5377) and SAVI2 (0,5367).

At stage 4 (02.08.06) the performance of most VIs was also moderate with R^2 – values

around 0,5, but decreased slightly, compared to stage 3. The best performing VIs were the SR705 (0,5472), LAI1 (0,5468) and mND705 (0,5465). The SAVI-family also showed a moderate correlation with R^2 – values between 0,46 and 0,5.

Performance assessment of VIs for predicting C_{ab}

At the first stage (20.06.06) most VIs showed no relationship to C_{ab} except CARI, REIP1, REIP4, LAI10 and Cab1. This generally poor correlation was most likely due to low plant coverage at this point in time. The CARI showed a weak correlation with R^2 of 0,16. The REIP4 performed best for this stage, and increased with increasing plant development except for stage 2.

At the second stage (28.06.06) the best correlation was achieved with R^2 – values of 0,27 by NDVI and 0,24 by MCARI1. Most of the other VIs had a weak correlation with R^2 – values from 0,06 to 0,16. Only REIP4 and LAI1 showed with R^2 values of 0,02 no correlation.

At the third stage (16.07.06) the VIs DGVI´s (0,43), MCARI1 (0,4), TVI & MTVI1 (0,4) and 19 other VIs showed a moderate correlation. Only the CARI depicted no correlation. The RVI, MCARI, GI, PRI, REIP1 and Cab1&2 showed a weak correlation with R^2-values ranging from 0,1.to 0,24.

The last stage (02.08.06) the good moderate correlation of CSI2 (0,53), mND705 (0,52), NDVI, ATSAVI (0,5) stands out among the other stages. At this point in time the VIs revealed the strongest correlations for almost al VIs. In total 30 VIs showed a moderate correlation, 5 a weak correlation and only 3 VIs (LAI10, Cab1&2) no correlation.

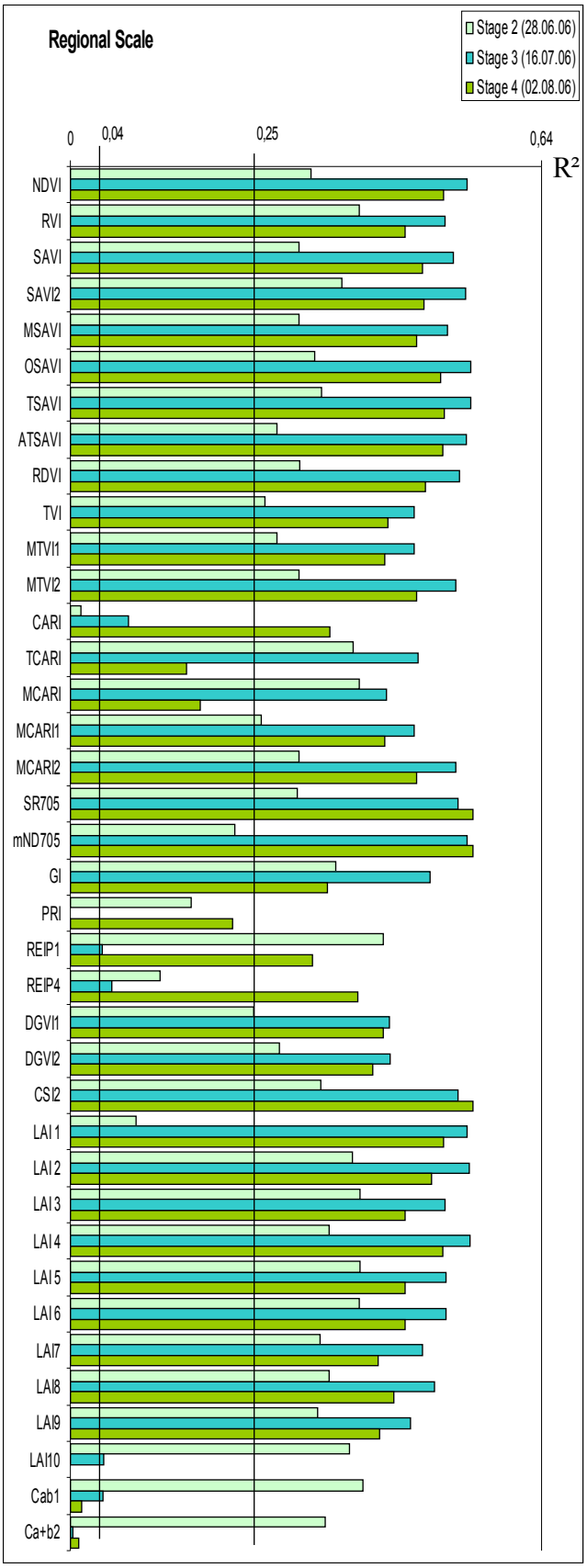

Figure 5.19: Coefficients of Determination for estimating LAI by VIs at Regional Scale, whole plants

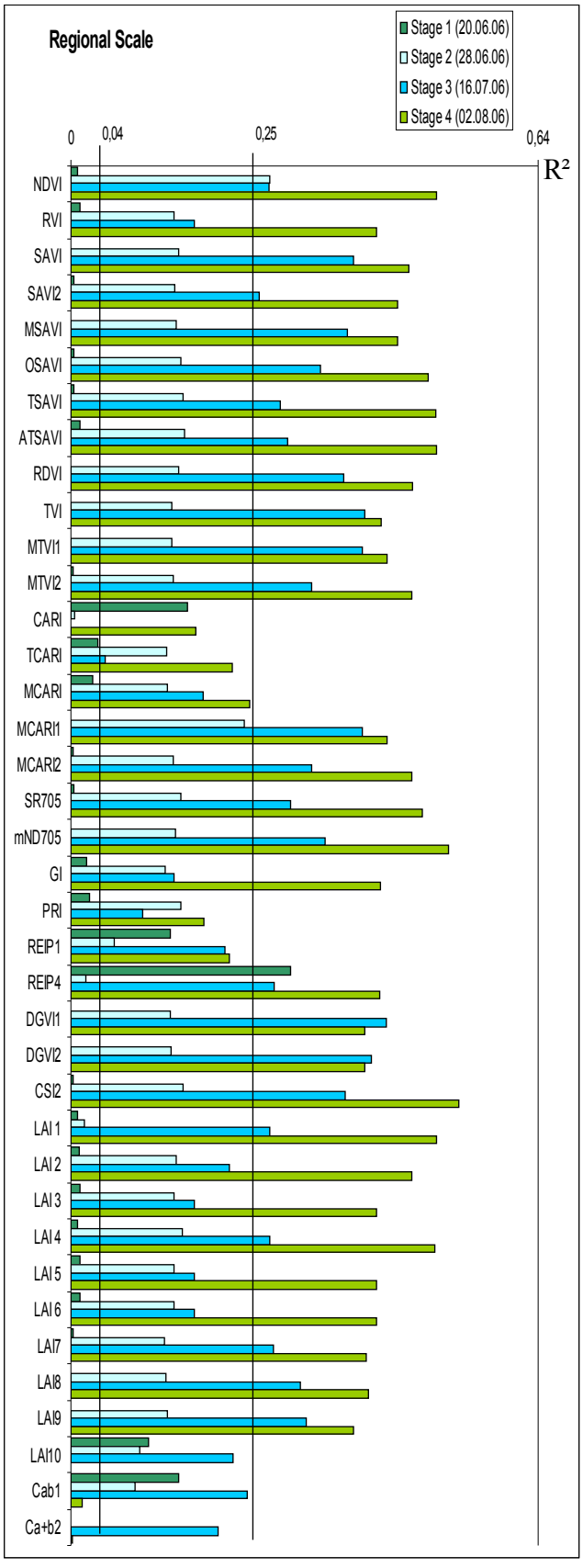

Figure 5.20: Coefficients of Determination for estimating C_{ab} by VIs at Regional Scale, whole plants

5.3.2 Regional Scale LAI and Chlorophyll estimation at a vertical plant profile

To investigate which leaves of the plants have the highest influence on the performance of the VIs for predicting C_{ab} the SPAD based C_{ab} – values were aggregated according to different vertical plant layer compositions, as described in chapter 4.5.7.1. These values were aggregated from top to bottom, at a maximum of five layers. The statistics for LAI and C_{ab} measurements of these respective plant layers or heights are shown in table 5.7. The VIs and corresponding R^2 values presented in this chapter are based on the 2 x 2 raster cell grid.

Table 5.7: Statistics of measured LAI and C_{ab} for different plant stages and dates at regional scale

	Height	Stage	Count	Min	Max	Range	Mean	STDV	CV
Cab 3	Top	1	31	31,80	46,28	14,48	39,17	3,67	9,37
Cab 2-3	Mid-Top	1	31	31,82	43,40	11,58	38,57	3,05	7,9
Cab 1-3	Low-Top	1	33	31,88	41,76	9,88	38,08	2,83	7,42
LAI-Corr	All	2	48	0,44	2,42	1,98	1,11	0,33	30,09
Cab 4	Top	2	6	25,76	35,44	9,68	29,89	3,32	11,12
Cab 3-4	Mid1-Top	2	45	26,16	34,64	8,48	32,21	2,00	6,22
Cab 2-4	Mid2-Top	2	45	27,72	36,64	8,92	33,33	1,62	4,87
Cab 1-4	Low-Top	2	48	27,09	39,02	11,93	33,93	1,93	5,68
LAI - Corr	All	3	41	0,77	3,05	2,28	1,93	0,63	32,36
Cab 5	Top	3	22	24,40	42,88	18,48	30,49	3,99	13,07
Cab 4-5	Mid1-Top	3	36	22,32	35,12	12,80	28,86	2,99	10,36
Cab 3-5	Mid2-Top	3	37	24,08	35,25	11,17	29,68	2,83	9,53
Cab 2-5	Mid3-Top	3	38	24,00	35,70	11,70	30,33	3,01	9,93
Cab 1-5	Low-Top	3	39	23,81	37,05	13,24	31,07	3,24	10,42
LAI	All	4	46	0,72	5,60	4,88	2,47	1,32	53,51
Cab 5	Top	4	43	21,38	35,16	13,78	29,73	3,34	11,24
Cab 4-5	Mid1-Top	4	44	23,40	35,56	12,16	30,66	3,22	10,49
Cab 3-5	Mid2-Top	4	46	24,08	38,03	13,95	31,09	3,30	10,6
Cab 2-5	Mid3-Top	4	46	23,68	39,80	16,12	31,69	3,53	11,13
Cab 1-5	Low-Top	4	46	21,95	42,08	20,13	32,02	4,01	12,52

The data on the LAI-values show that LAI increases with plant development from stage 2 to stage 4 with mean LAIs of 1.11 to 2.47, respectively. Similarly, the total variation indicated by STD and CV of LAI increases with plant development, indicating increasing heterogeneity of LAI with time.
The investigation of the C_{ab} values shows that the mean values increase from top-leaf measurements to measurements when the whole plant profile is considered (Low-Top) for stage 2, 4 and partly for stage 3. For stage 1 this gradient is reversed with highest values for top-leaves and lowest values for the whole plant profile. This indicates that the whole plant C_{ab} content only

estimated from top-leaf values is an under representation for stage 2, 3 and 4, but may be suitable for plants in stage 1. This finding is consistent with the studies of Rücker et al., (2006). Another gradient appeared for the total variation of C_{ab} values in all stages with decreasing STD from top layers to top-mid-layers and increasing STD from top-mid-layers to top-low layers. This shows that the upper plant layers have leaves with more homogeneous C_{ab} contents in leaves than lower plant layers.

The bar charts in figures 5.22 to 5.24 show the coefficients of determination for predicting LAI and C_{ab} by VIs. For the LAI data no other aggregation was performed, thus the description given in chapter 5.3.1 is true for this dataset, too, and no further description given. The bars for the LAI are presented again for a better comparison with the results for the coefficients of determination for estimating C_{ab} by Vis.

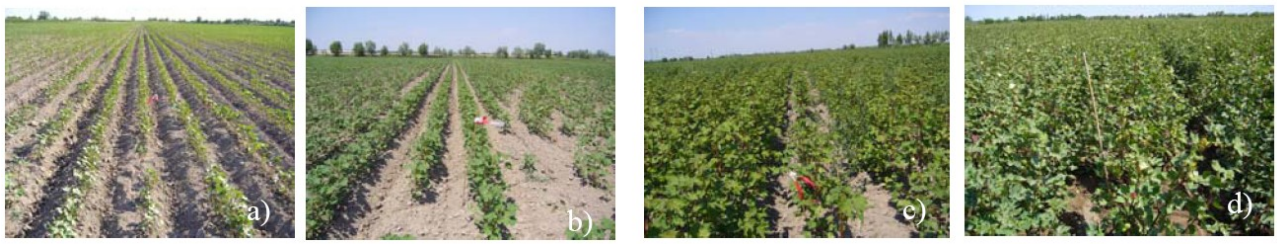

Figure 5.21: Overview photos of validation field 2 at a) 20.06.06 , b) 28.06.06, c)16.07.06, and d) 02.08.06 (at different locations within the field)

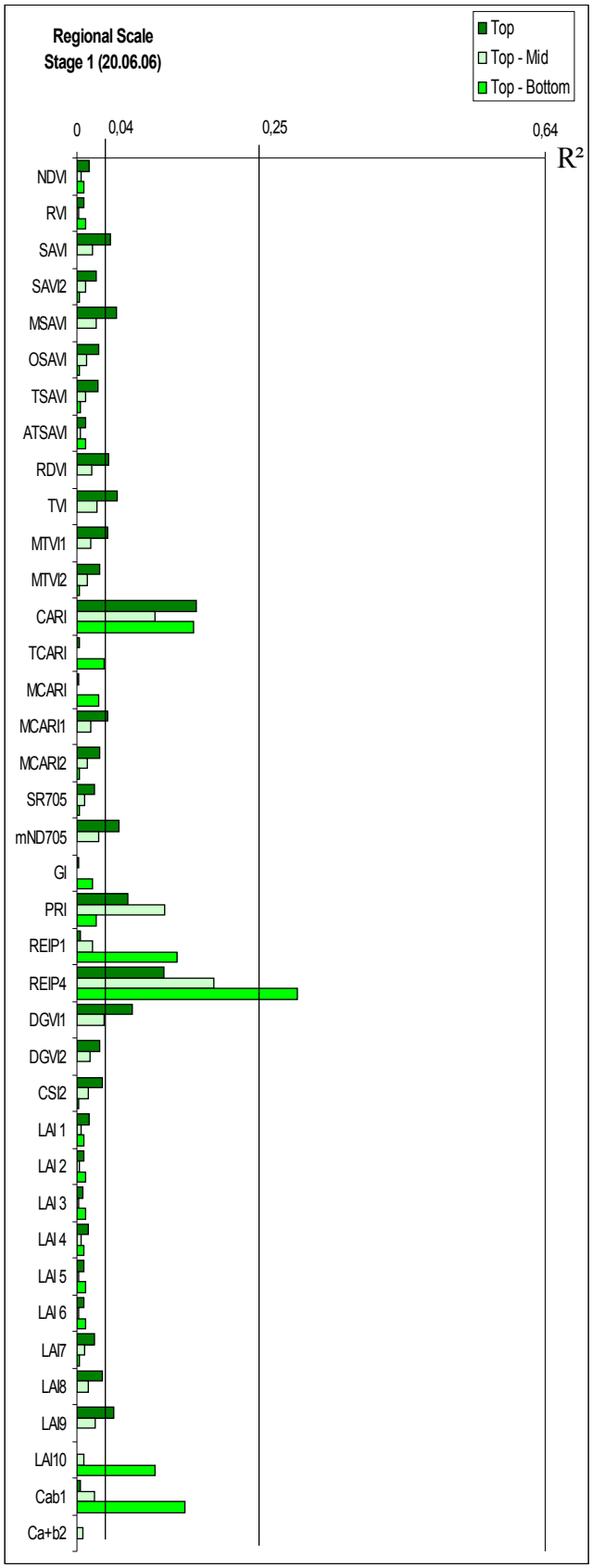

Figure 5.22: Coefficients of Determination for determining C_{ab} by VIs at Regional Scale, Stage 1 (20.06.06) at different plant heights

Performance assessment of VIs for predicting C_{ab} in cotton leaves based on different aggregations of vertical plant layers at stage 1

The VIs for the first stage showed in total no or only a weak correlation with C_{ab}.

The dataset representing the C_{ab}-values of top leaves showed a weak correlation for 8 VIs with CARI (0,16) and REIP4 (0,12) among the best VIs.

The Top - Mid dataset, showed with only three VIs [CARI (0,1), PRI (0,12), REIP4 (0,12)] a weak correlation, while all other VIs had no correlation.

For the top – bottom aggregation REIP4 (0,3) showed, a moderate correlation with $C_{ab,}$ while CARI, REIP1, LAI10 and Cab1 had weak and all others no correlation with $C_{ab.}$

At this stage the plants were very small (compare fig. 5.21a), thus the reflectance from the plant very weak, compared to the reflectance from the soil background. In a relative perspective, the performance of the VIs shows some interesting distribution pattern: some VIs such as the SAVI family, MCARI1 and MCARI2, the TVI, MTVIs and SR705 & MND705 show higher correlation with C_{ab} for the top leaves and almost not correlation for the whole plant. Other VIs such as the REIP´s, LAI10 or Cab1 show just the opposite behaviour. They perform better for the whole plant than only for the top leaves.

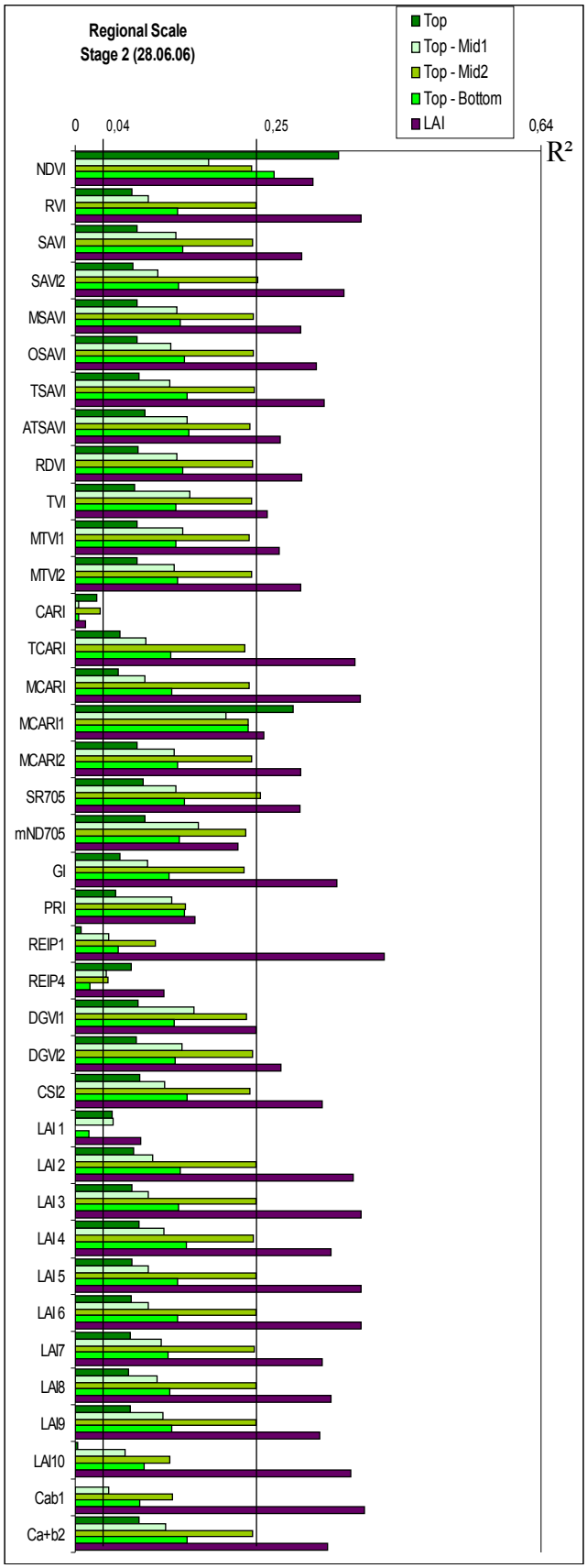

Figure 5.23: Coefficients of Determination for determining LAI and C_{ab} by VIs at Regional Scale, Stage 2 (28.06.06) at different plant heights

Performance assessment of VIs for predicting C_{ab} in cotton leaves based on different aggregations of vertical plant layers at stage 2

At the second stage the dataset with the aggragtaion based on top leaves showed for two VIs (NDVI 0,36, MCARI1 0,3) a moderate correlation with C_{ab}. All the other VIs showed with R^2-values ranging from 0.09 to 0,04 a weak correlation. No correlation was shown for Cab1 (0,01), LAI10 (0,004), REIP1 (0,008) and CARI (0,03).

The dataset containing the VIs for the first two nodes aggregation (Top-Mid1) depicted for all VIs a weak correlation except for one (CARI 0,004). Out of this group, MCARI (0,21), NDVI (0,18) and mND705 (0,17) showed the best correlation.

The absolutely second best, but overall best correlation, was shown for VI correlations with C_{ab} data from the Top-Mid2 dataset, which was created by aggregating the SPAD – values for the upper 3 nodes of the plants, with 31 VIs with R^2-values from 0,25 to 0,23 (best SR705 & mND705 with R^2=0,2543 and SAVI2 with 0,2507). No correlation was given for CARI and Cab2.

The whole plants aggregation (top-bottom) portrayed a rather uniform performance with 34 VIs (best MCARI1 0,24) having a weak correlation and only 3 VIs (LAI1, CARI & REIP4) having no correlation. The NDVI showed with R^2 = 0,27 the absolute best correlation and was the only VI for this dataset with a moderate correlation with C_{ab}.

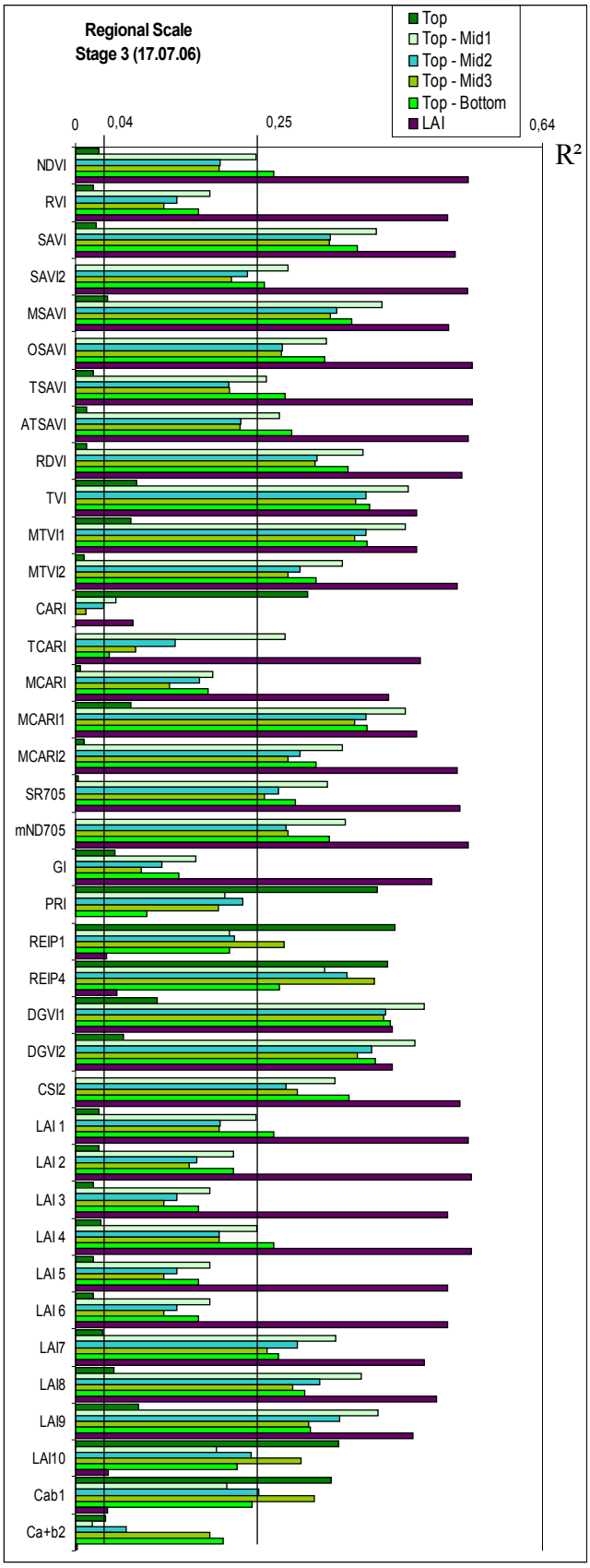

Figure 5.24:Coefficients of Determination for determining LAI and C_{ab} by VIs at Regional Scale, Stage 3 (16.07.06) at different plant heights

Performance assessment of VIs for predicting C_{ab} in cotton leaves based on different aggregations of vertical plant layers at stage 3

The top leaf dataset showed for only 6 coefficients [REIP1 (0,44), REIP4 (0,43), PRI (0,41), LAI10 (0,36) and Cab1 (0,35)] a moderate correlation with $C_{ab.}$ 10 VIs had a weak correlation with C_{ab} with R²-values smaller than 0,1 except for DGVI1 (0,11). 22 VIs depicted no correlation with C_{ab}.

Most VIs showed the best correlation with C_{ab} for the Top-Mid1 dataset. At a nadir view the leaves between these two nodes or plant layers covered or shaded almost all the leaves of the lower nodes or plant layers. All VIs showed R²-values higher than 0,16, except Cab2 and CARI, witch portrayed with 0,02 & 0,06 no correlation. The relationships between VIs and C_{ab} at data aggregation Top-Mid2 and Top-Mid3 showed a similar performance pattern as Top-Mid1, but with an overall lower performance.

The dataset considering all layers together (top-bottom) showed for Cab2, LAI2, CSI2, ATSAVI, TSAVI and NDVI the best R²-values representing moderate correlation with Cab, but had overall similar or slightly higher performance as the datasets top-mid2, top-mid3. The VIs of stage 3 had a better correlation with Cab at different plant layer aggregations, whereas the Vis at stage 1 performed best for mainly the top leaves.

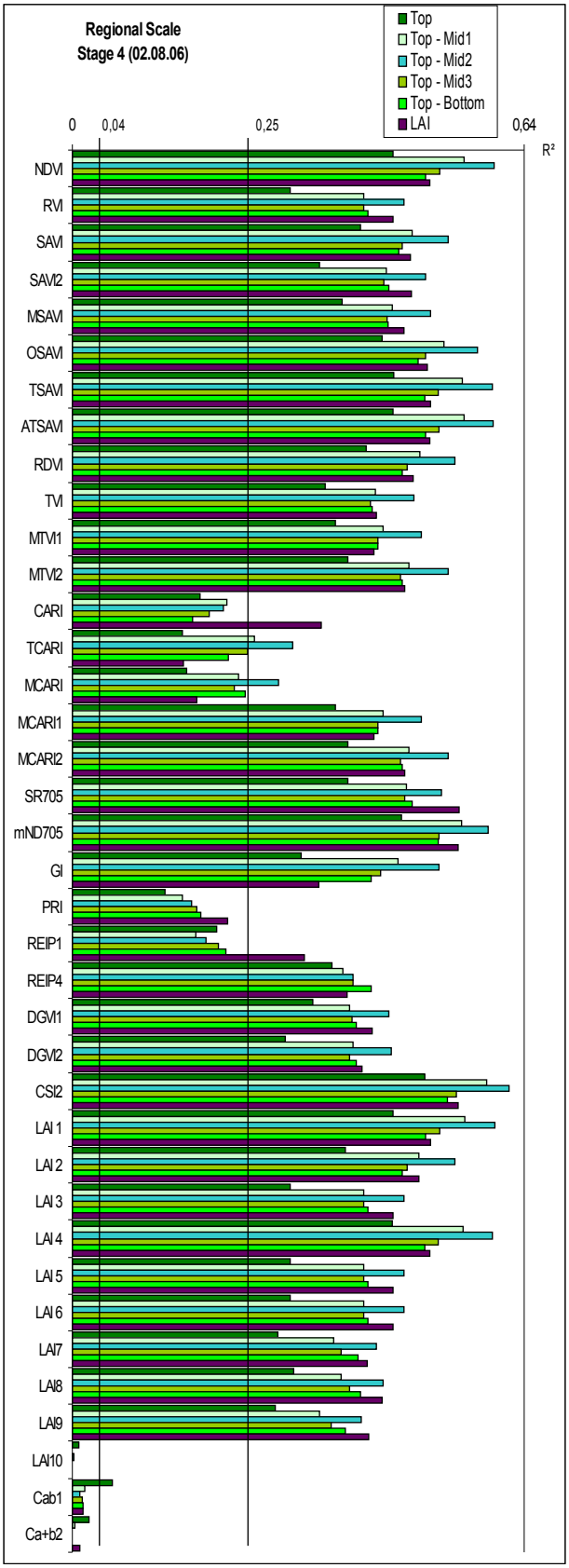

Figure 5.25: Coefficients of Determination for determining LAI and C_{ab} by VIs at Regional Scale, Stage 4 (02.08.06) at different plant heights

Performance assessment of VIs for predicting C_{ab} in cotton leaves based on different aggregations of vertical plant layers at stage 4

The last stage showed the highest plant coverage and a special distribution in the correlations of VIs with C_{ab}. The Top-Mid2 aggregation showed for all VIs the highest level of correlation (moderate correlation), except for CARI, PRI, the REIP´s, LAI10 and the Cab´s, which had weak correlation with $C_{ab.}$ The performance of the datasets Top, Top-Mid1and Top-Mid3 was similar to the one of Top-Mid2, but had lower R^2-values.

The absolute best VIs among the VIs with moderate correlation of the Top-Mid2 dataset were the CSI2 (0,62), NDVI, ATSAVI, TSAVI & LAI4 (0,6) and mND705 (0,59). MCARI1 was with R^2 = 0,5 also part of this group depicting a strong relationship. Almost all other VIs portrayed also a moderate correlation, except CARI (0,21), REIP1 (0,19), PRI (0,17) which had a weak and LAI10 and the Cab´s witch had no correlation.

The dataset aggregated for the whole plant layer structure (top-bottom) performed for some VIs second best (for REIP4 with 0,42 best). The best VIs of this dataset were almost the same as for the Top-Mid2 dataset, with mND705 (0,52), LAI, ATSAVI, NDVI & TSAVI (0,5).

The good correlation between VIs and C_{ab} for the Top-Mid2 dataset shows that at stage 3 the leaves between three upper nodes (from top leaves to mid2 leaves) covered almost all leaves at the lower layers, for which the reflectance of these leaves was not captured by the satellite images.

Overall each dataset showed its own characteristic performance of correlations between VIs and C_{ab} depending on the specific plant layer structure that is typical for the corresponding growing stage. The best correlations were for the data aggregations according to leaves from the plant layers top, top-mid2, top-mid1 for the stages 1-4 and 4, respectively. Furthermore, the performance of correlations increases with time from stage 1 having overall the lowest, to stage 4, with the highest overall correlation performance. Figure 5.21 shows photos of typical plants for each stage.

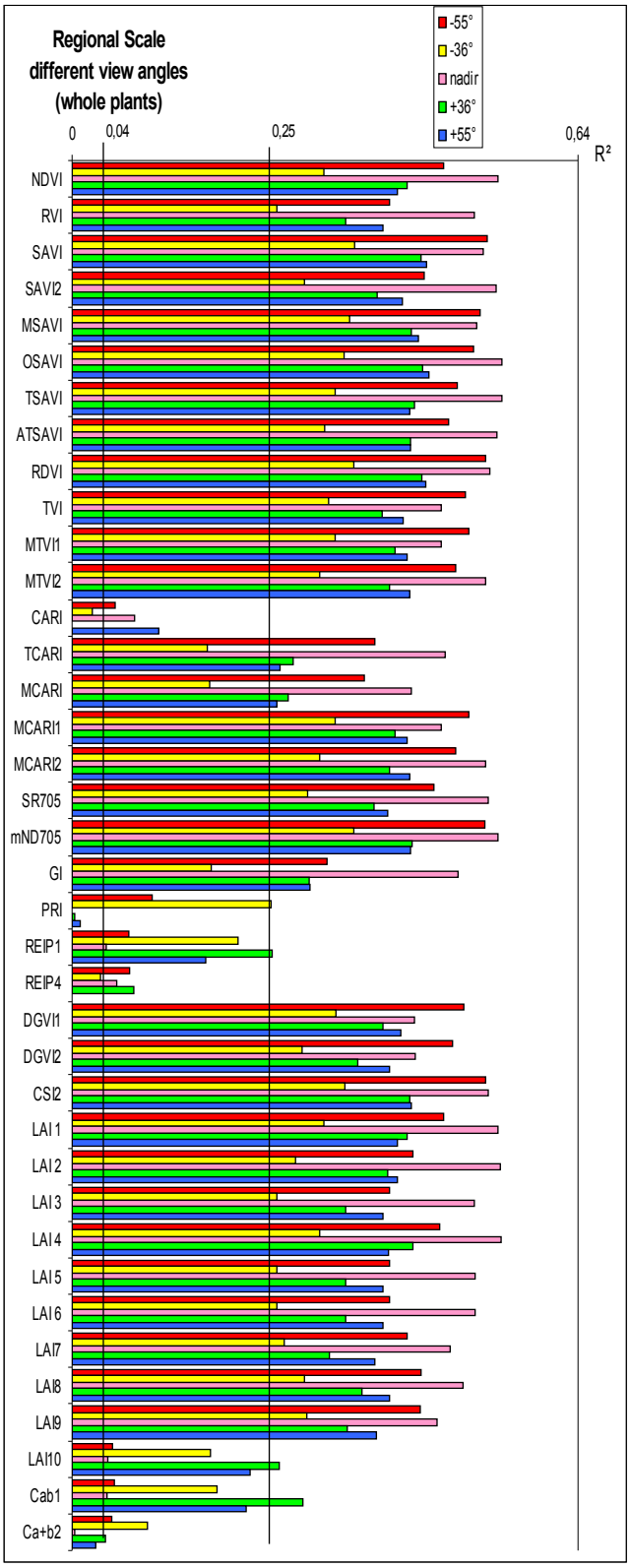

Figure 5.26: Coefficients of Determination for determining LAI by VIs at Stage 3 (16.07.06) at different view angles for whole plants

5.3.3 Regional scale LAI and leaf chlorophyll estimation in cotton leaves at a vertical plant profile with different view angles at stage 3

As one example for investigating the influence of different Proba-1/CHRIS view angles on the regression performance between satellite image based VIs and LAI, the dataset for stage 3 was analysed (figure 5.26).

The nadir view shows the relative best correlation for almost all VIs with moderate relationship levels of R^2 – values up to 0,54 (compare chapter 5.3.1).

The second best fit was shown by the coefficients of determination for estimating LAI by the -55° image. The R^2 – values of the +36° and the +55° images showed almost the same correlation with only slight differences, but at a lower level as for the -55° image. The only exemptions were the VIs REIP1, LAI10 and Cab1 showing the best fit for the +36° image and PRI and Cab2 with the highest coefficients of determination for the -36° image. But these

exemptions showed only third range fits, and were not analysed any further.

For all VIs the -36° image shows the poorest performance. However, this is likely caused by some difficulties while georeferencing this image, resulting in a small distortion, which could not be compensated afterwards and lack of time precluded to rerun the georeferencing process.

The best performance of the VIs based on nadir acquired images is understandable considering that the measurements of LAI in the field were in a straight azimuth orientation of the stem of the plant. However, the different performance of correlations of VIs based on the other view angle images with ground measurements needs further investigation taking sun and Proba-1/CHRIS Sensor angles into account.

Considering the estimation of C_{ab} by VIs form different view angle Proba-1/CHRIS images, C_{ab} of leaves from different aggregations of plant layers were investigated.

For the top layer (figure 5.27), the nadir image showed the absolutely best correlating VIs out of the VIs from all view angles to estimate Cab with six VIs having a moderate correlation including CARI, PRI, REIP1&4, LAI10 and Cab1.

However, considering all VIs from all view angles, VIs based on the image with a view angle of +55° had mostly higher correlations than VIs based on other view angles, including moderate correlations of PRI, REIP1, LAI10 and Cab1 and weak correlations of SAVI, SAVI2, MSAVI, OSAVI, TVI, MTVI1&2, MCARI1, DGVI1&2 and LAI7 to 9. Most of the VIs based on the image with the view angle +36° had a similar correlation pattern than the VIs from the +55° image, but had mainly lower R^2 values.

The CARI calculated by the -36° image showed with $R^2 = 0,45$ the absolutely best correlation for this dataset, but this was the only moderate correlation based on this view angle. LAI10 and Cab1 showed with R^2-values between 0,37 and 0,4 the best correlations based on the -55° and +55° images.

Figure 5.28 shows the coefficients of determination for VIs based on different view angle Proba-1/CHRIS images and C_{ab} calculated for the first two plant layers (top-mid1).

Considering the VIs from all view angles, the nadir image based VIs showed the absolute best and relative highest correlation with Cab with 22 VIs having a moderate correlation performance. The second best correlation was achieved by the +55° and the third best by the +36° based VIs. The VIs based on these two images showed a similar performance as the nadir image, except for RVI, REIP1, LAI2&3, LAI5&6, LAI10 and Cab1 which had better correlation results based on the +55° image.

The -55° image showed the second best performing R^2 – values for DGVI1&2 and TVI.

The -36° image had only for the PRI with $R^2 = 0,27$ the best correlation. For all other VIs this image had the lowest correlation.

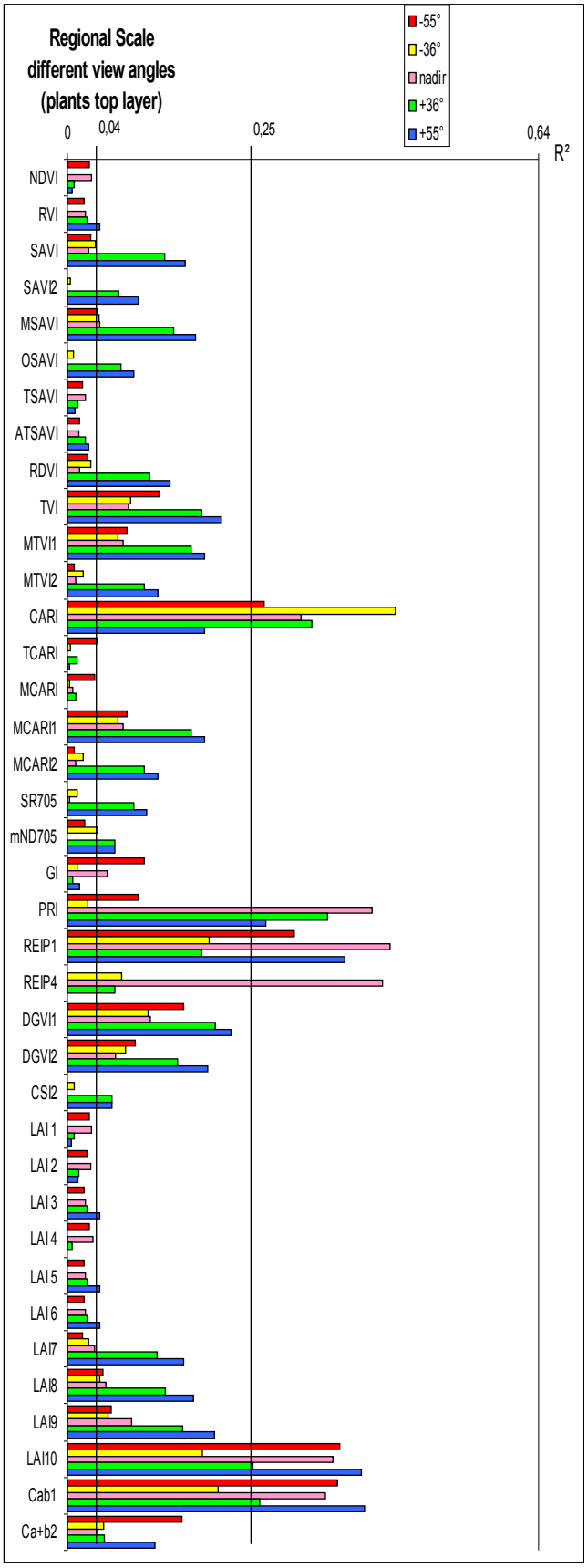

Figure 5.27: Coefficients of Determination for determining C_{ab} by VIs at Stage 3 (16.07.06) at different view angles for the top node

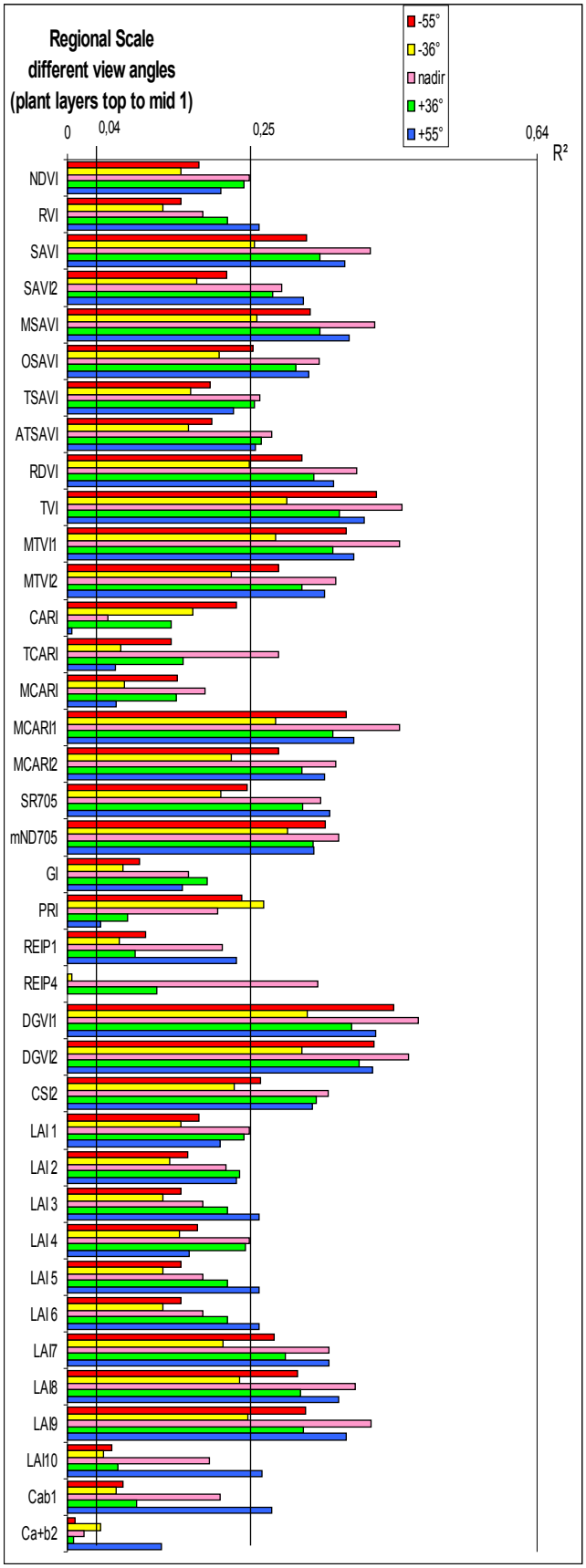

Figure 5.28: Coefficients of Determination for determining C_{ab} by VIs at Stage 3 (16.07.06) at different view angles for first 2 nodes

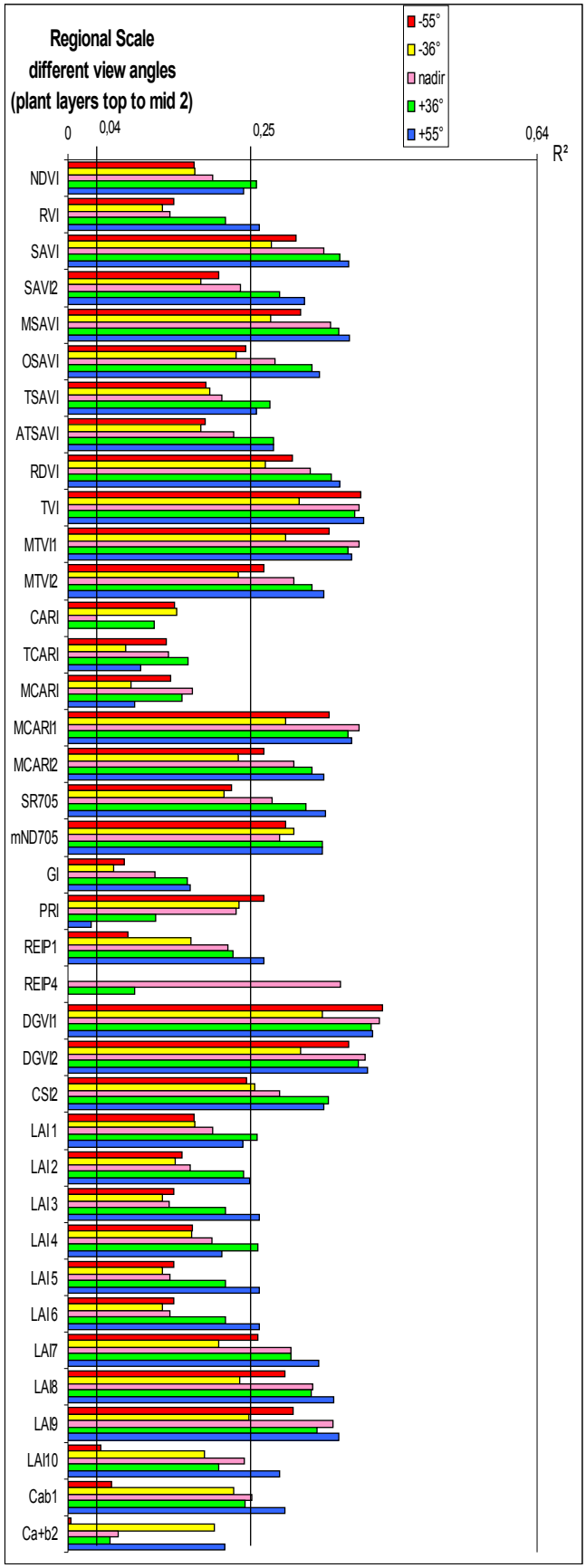

Figure 5.29: Coefficients of Determination for determining C_{ab} by VIs at Stage 3 (16.07.06) at different view angles for first 3 nodes

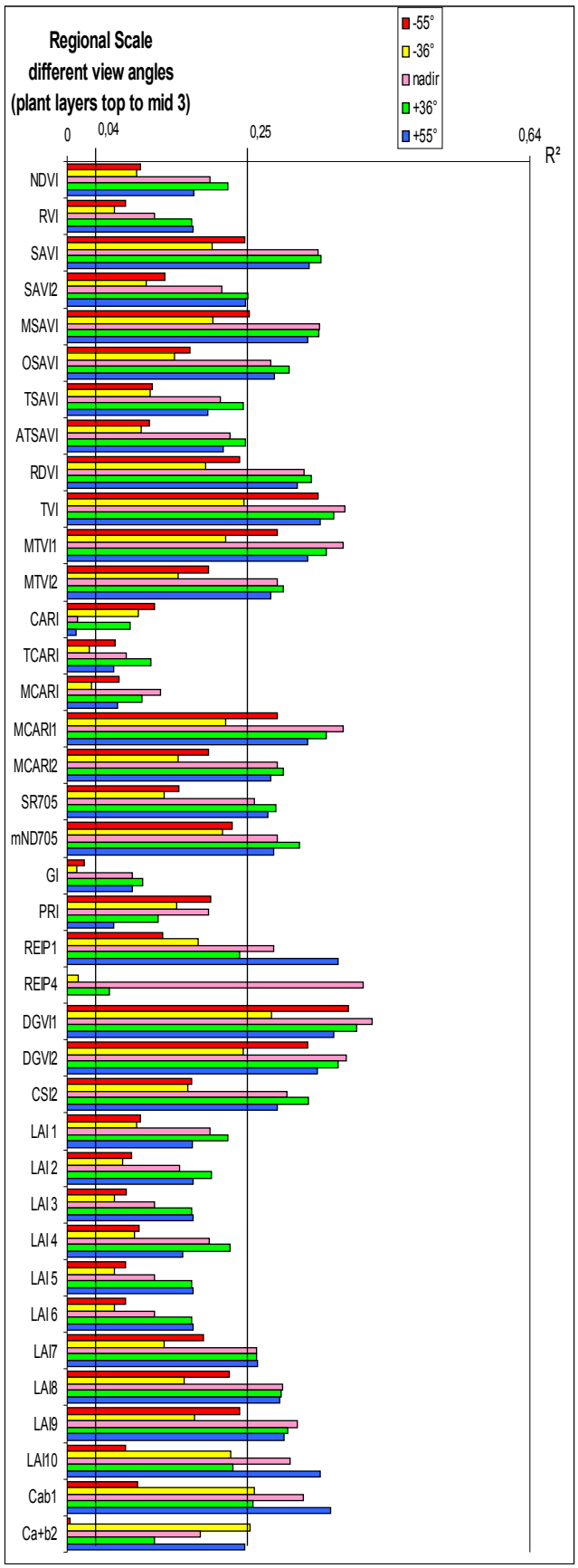

Figure 5.30: Coefficients of Determination for determining C_{ab} by VIs at Stage 3 (16.07.06) at different view angles for first 4 nodes

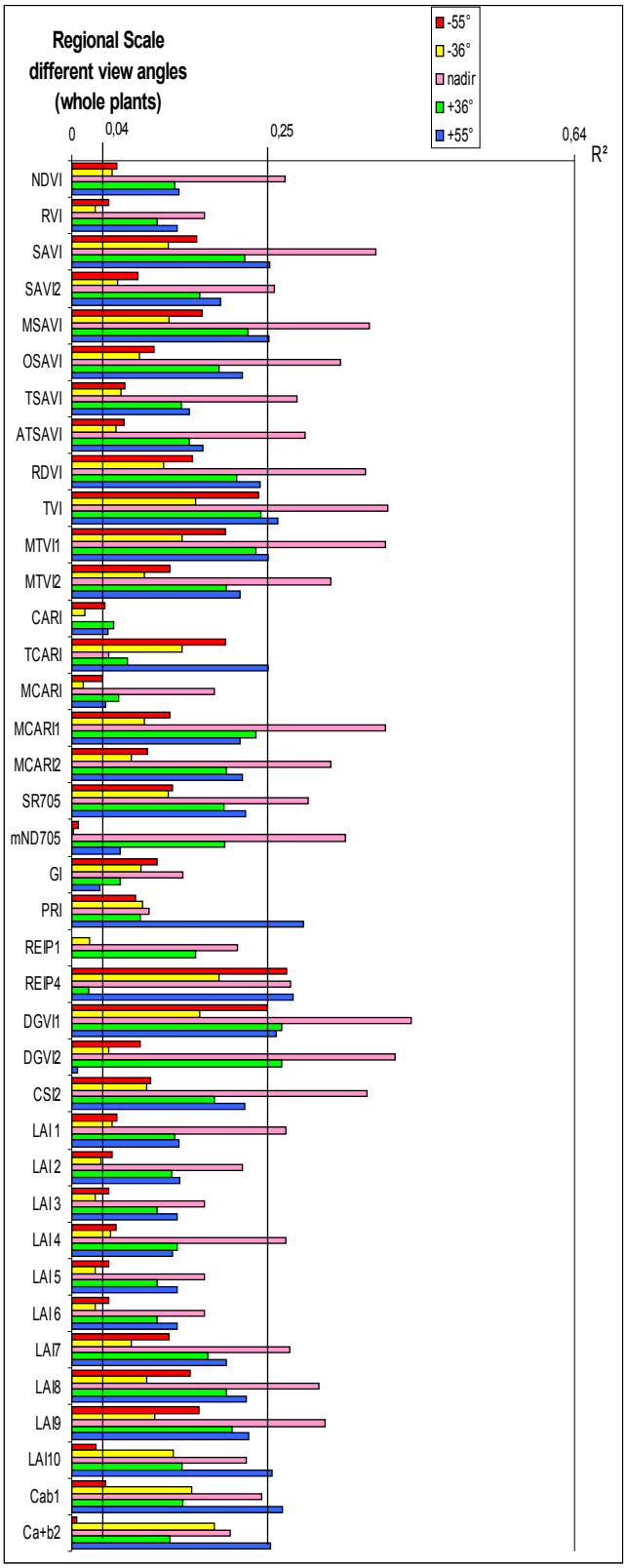

Figure 5.31: Coefficients of Determination for determining Cab by VIs at Stage 3 (16.07.06) at different view angles for the whole plants

Figure 5.29 shows the R²-values for VIs based on different view angle Proba-1/CHRIS images correlated with C_{ab} calculated for the first three plant layers (top-mid2). Overall the highest corellations were based on VIs calculated from the +55° image. The second best correlations were achieved by VIs from the +36° image. But all three performed with rather similar R²-values. The -55° image provided also some VIs of higher correlation, especially for DGVI1. The -36° image showed only for CARI with R² = 0,14 the best correlation.

The R²-values for VIs based on different view angle Proba-1/CHRIS images correlated with C_{ab} calculated for the first four plant layers (top-mid3) are shown in figure 5.30.

The correlations of most of the VIs based on the nadir image had the highest R²-values, followed by the VIs from the +55° and +36° images. The VIs based on images taken under -55° and -36° are both sowing a significantly lower correlation as for the 3 plant layer aggregation.

The VIs based on different view angle Proba-1/CHRIS imgaes correlated with C_{ab} calculated for the C_{ab}-content of the whole plants based on VIs are presented in figure 5.31. The VIs from the nadir image performed by far best for this dataset. As for the other datasets the second and third best fit was achieved by VIs based on the +55° and +36° images. The performance of the -55° and -36° images was poor and the correlation for many VIs weak.

Overall the VIs based on images taken under different view angles showed significantly different performances for estimating LAI and C_{ab}. In

general, the nadir iamge based VIs showed the absolutely best correlation to Lai and C_{ab} for all plant layer aggregations. For LAI the VIs based on the -55° image was second best. For C_{ab} the VIs based on +55° and +36° images showed higher correlation performance with C_{ab} for the upper three plant layers than the VIs based on the nadir image. The VIs based on the -55° and -36° images showed mainly lower correlations with C_{ab} for the different plant layers.

5.3.4 Summary and discussion of LAI and C_{ab} estimation at regional scale

As on plant scale a typical distribution pattern of best correlating VIs with LAI and C_{ab} could be identified on regional scale, too. For these regional datasets LAI measurements started at 28.06.06 (second stage), due to the very low plant coverage at the first stage.

Considering C_{ab} the measured SPAD values of cotton leaves were averaged for different vertical plant layers and correlated with the reflection as acquired by the Proba-1/CHRIS sensor, to identify which plant layers with respective leaves have the maximum influence on the spectral reflection.

At stage 2 the plant coverage within the field was still poor, resulting in a strong influence of the soil reflectance from the furrows on the overall reflectance value gained. The resulting reflectance situation at stage 2 was similar to the one of the first stage at plant scale, with dominating soil spectra while the reflectance from plants was poor (compare fig. 5.21b). Consequently the performance of the VIs to predict LAI was low, as most of the VIs were developed for situations with a reflectance influenced stronger by vegetation.

The estimation of LAI by VIs was best at stage 3. This may explain that the increased plant growth at this stage resulted in a plant canopy almost fully covering the furrows between the rows of the cotton plants. The now strong plant signal in combination with a relatively low variance of plant development within fields resulted in the best correlation of most VIs with LAI for this stage.

The quality of the relationship of LAI and VIs decreased slightly for stage 4. This may be caused by a higher variety of plant development within and between the different fields. But the grade of correlation was still relatively high.

The VIs showing the absolutely best correlation for predicting LAI are given for each stage in table 5.8.

For predicting leaf chlorophyll content by VIs the SPAD-values that were measured at the cotton leaves were aggregated for different vertical plant layers to investigate whether different plant layer compositions have an influence on the performance of the correlation between VIs and leaf chlorophyll of the respective plant layers. For each stage the combination of plant layers showing the best correlation of the coefficients of determination for estimating leaf chlorophyll content was identified in the referring chapter and is shown in table 5.8.

Stage 1 showed a poor performance of VIs except for CARI and REIP4. As on canopy scale, the only reasonable explanation for this low correlation may be the weak plant coverage at this stage. The vertical plant layer aggregation of chlorophyll data showing the best correlation with VIs at stage 2 was the top-mid2 dataset, representing the leaves of the three top plant layers. The circular placement of the leaves around the stem resulted in an almost complete coverage of the lowest plant layer by the higher level ones. As the lower level leaves were mainly shaded by the higher level leaves, the reflection of these lowest level leaves contributed only in a minor percentage to the reflection of the whole plants.

At stage 3 the largest regional dataset was examined, as in addition to the investigation of plant stages also the influence of different acquisition angles was examined using 4 different CHRIS – images that were acquired under different view angles. The different view angles showed for each aggregation of plant layers a different correlation, but were similar to the nadir image. For most plant layers and VIs the nadir image provided the best fit. Overall the best correlation was shown for the top-mid1 plant layer aggregation. Maybe the layer structure of the plants was slightly higher due to the beginning flowering, and the influence of the lower layers was shaded.

At stage 4 almost all VIs showed a very high performance, but the ones for the top-mid 2 plant layer dataset were the best. At this stage the plants started developing first bolls and the coverage was increased by flowers at the top plant layers, while at stage 3 most plants showed a blooming only at the lower plant levels. This overall best correlation of all VIs and also the absolute best VIs for predicting C_{ab} at stage 4 may be used for predicting cotton yield, as the early flower stage was indicated as most appropriate for estimating yield by reflectance as shown elsewhere (Zhao, et al., 2007). The overview on the best fitting correlations with the representative VIs for each stage are given in table 5.8.

Table 5.8: Best performing VIs for estimating LAI or Cab-content for each stage at regional scale

Stage	Dataset	VI	Equation	R^2
2	LAI	REIP1	y = -0,003x + 0,7245	0,43
3	LAI	NDVI	y = 0,1439x + 0,3713	0,54
4	LAI	SR705	y = 0,4573x + 1,8134	0,55
1	Cab (Top-Bottom)	REIP4	y = 1,1026x + 0,6721	0,3
2	Cab (Top)	NDVI	y = 0,016x + 0,0255	0,36
3	Cab (Top-Mid1)	DGVI1	y = 10,391x – 0,0507	0,48
4	Cab (Top-Mid2)	CSI2	y = -28,751x + 1,271	0,62

5.3.5 Selection of the best performing VIs

The correlation of VIs with LAI or C_{ab} - content at regional scale revealed several VIs with higher prediction performance. However, for practical application it would be desirable to select only two VIs, one for LAI and one for C_{ab} prediction, that can be implemented in research during following years and in other areas within Khorezm. Therefore, three criteria for selection of the two best performing VIs to predict LAI and C_{ab} at regional scale, respectively, were set up:

1) best VI prediction performance for a specific stage
2) most stable VI prediction performance over the last 3 stages; (the dataset from stage 2 showed almost no correlation with the data collected on the other days. Thus, the validation of the predictions will be performed for the last three stages of the regional dataset)
3) already tested and proofed VIs with high performance for cotton as found by other authors

The selection of VIs based on criteria 1 was done by selecting the VI with the highest R^2-value for for each dataset and time. These indices were given in the referring chapters and for an overview in table 5.8.

Considering criteria 2 there were a few indices that performed stable over time, as shown in the preceding chapters. But which of these were tested and proofed by other authors for cotton and hyperspectral or at least multispectral satellite data?

For predicting LAI by a VI the NDVI was tested and proofed by Blenk 2005 (p.104) for cotton fields of Uzbekistan based on MODIS satellite data. For the time period from 28.06.04 to 19.08.06 she found the following equation based on a dataset containing 14 samples with R^2 = 0,89:

$$LAI = 3{,}1506 \cdot NDVI - 0{,}4055$$

For predicting LAI or C_{ab}-content by a VI the MCARI1 was tested and proofed by diverse authors and for varying crops. Haboudane et al. (2004) used the MCARI1 to predict the LAI of corn, soybean and wheat, so did He et al. (2006) for mixed grassland ecosystems and Moreno (2004) for diverse crops. Wamunyima (2005) tested the MCARI1 for the estimation of grass biomass production as one of the best correlating VIs and Zarco Tejada et al. (2005(2)) tested the MCARI1 as one of the best VIs to predict the within field variability of C_{ab}-content and the yield of cotton fields located in California, USA.

Therefore, considering all three criteria, NDVI and MCARI1, for LAI and C_{ab} prediction for cotton at regional scale in Khorezm, respectively, was selected in this study. The corresponding equations and performances are shown in table 5.9.

These equations were then used for the regional estimation (and extrapolation) of LAI and C_{ab} over the whole satellite image and the different stages.

Table 5.9: Equations for best correlating VIs for predicting LAI and C_{ab} per given dataset and stage

Stage 2		Stage 3		Stage 4	
Equation	R^2	Equation	R^2	Equation	R^2
LAI = 1,1334*NDVI+0,6211	0,3265	LAI = 3,7433*NDVI-0,5102	0,5388	LAI = 6,6423*NDVI-1,5643	0,5069
C_{ab} = 7,6245*MCARI1+31,953	0,2381	C_{ab} = 25,603*MCARI1+19,224	0,4524	C_{ab} = 24,556*MCARI1+22,749	0,4949
C_{ab}: Top – Mid 2 dataset		C_{ab}: Top – Mid 1 dataset		C_{ab}:Top – Mid 2 dataset	

5.4 LAI and C_{ab} prediction at regional scale

The spatial distributions of LAI and leaf chlorophyll were calculated based on previously selected VIs (NDVI for LAI and MCARI for C_{ab} prediction, respectively) and are shown in the figures 5.33 and 5.34. For orientation within the images 1a and 2a a bright blue zone is highlighted as it streches in the middle of the image from NW to SE just south of the black box demarcating the area of interest. This zone is indicating a mainly sandy area with very little dry vegetation such as small bushes and few patches of sparsely distributed grasses. The sandy field as described in the atmospheric correction section can easily be identified at the western border of this zone in images 1a and 2a. The blue signatures on some fields on the images 2 b are indicating harvested wheat fields where some little grass vegetation grows between the dried stubbles. Thus, these sandy and harvested wheat fields were correctly mapped by low LAI values. The dark blue signatures indicate an LAI of 0 and can be found for the large Shavat primary irrigation channel (winding from SE to NW within the northern part of the images 1a and 2a and in the southern part of image 3a. Some dark red fields in the images 1a and 2a in figure 5.33 seem to be rice or alfalfa fields with very high LAI values.

LAI (figure 5.33)

In the images series 1b, 2b and 3b the increase of LAI with the time can easily be observed in the study fields that were demarcated by field boundaries in black signature. The spatial distribution of LAI within each field can clearly be detected on the 17x17m pixel resolution images. Field 3 shows a triangular-shaped bright area with low LAI in the middle of the field. This part is a levelled former irrigation canal, as shown in figure 5.32. The smaller Field 4 shows higher LAI values. Field 1 shows some bluish pixels at the north-

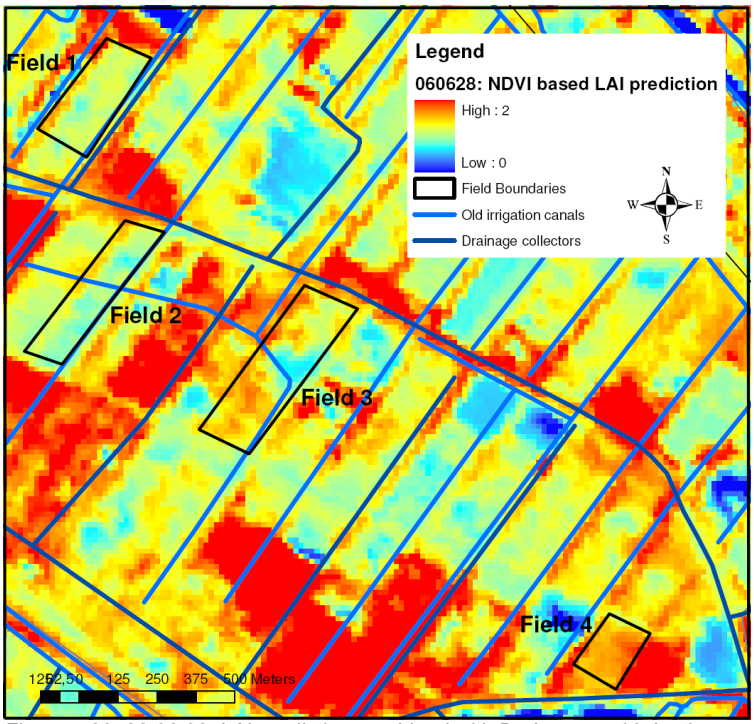

Figure 5.32: 28.06.06: LAI prediction combined with Drainage and Irrigation canal system

eastern border as well as in the middle part indicating lower LAI values. These parts are areas with varying soil quality, maybe due salinisation caused by a relative depression, due to a lack of irrigation water caused by a slightly higher area or due to a lack of fertilizer. Field 1 shows also the lowest LAI values of all four study fields most likely due to the lowest soil quality (soil bonitet of approximately 45), especially in the southern part (2b and 3b). Compared with the measured distribution shown in the figure 5.33 1c, 2c and 3c, the overall spatial patterns and seasonal development of LAI are consistent. However, it becomes also evident that there is considerable spatial variability of LAI with spatial resolution, as indicated by higher variability patterns in the maps showing the measured LAI. A slight decrease of LAI from stage 3 to 4 shown in these measured LAI maps may be caused by the impact of many flowers at stage 3 resulting in an overestimating of LAI, additional to the failure of the plant based LAI measurements.

The validation of these LAI patterns is described in chapter 5.5.

C_{ab} (figure 5.34)

The spatial distribution of the calculated C_{ab}-content at regional scale is displayed in the GIS-maps presented in figure 5.34. The spatial distribution pattern shown by overview images of the 1a, 2a and 3a are similar to the ones for LAI. The detailed scale maps of the b) series are depicting slight differences in the distribution pattern compared with the overview maps for LAI shown in figure 5.33. The spatial distribution of different C_{ab} -concentrations can be easier identified than in the LAI images, though the range of the C_{ab} – values is with 11 μgcm^{-2} for the first image very narrow. The range is increasing with time, but the larger spatial pattern is for the cotton fields still like the existing of the first stage as shown in the last image (3b), which provides with 44 μgcm^{-2} the highest range.

This is maybe due to the higher sensitivity of the MCARI1 on cotton compared with the NDVI. The high range of the NDVI is not only based on cotton, but on all fields covering the area. The NDVI extreme values are for all dates not within the cotton field boundaries, but on other fields around. While the extreme values of the MCARI1 are both located within the cotton fields, at least for the first date. At the second point in time (image 2b) the lowest values are found on other fields, but the highest MCARI1 values are located in Field 3 and 4. At the last date, the extreme values are both not located in the surveyed cotton fields, but the distribution within the field boundaries is still represented at a high resolution. The difference of C_{ab} – values between stage 3 and 4 may be caused by in field inhomogeneities and the fact that not every time the same plant were measured.

Compared with the measured C_{ab} concentration shown by the small rectangles in the fields of the c) – series, the differences are existing, but the represented patterns are showing a good correlation. The quality of this correlation is analysed and discussed for both, LAI and C_{ab} estimation in the validation chapter.

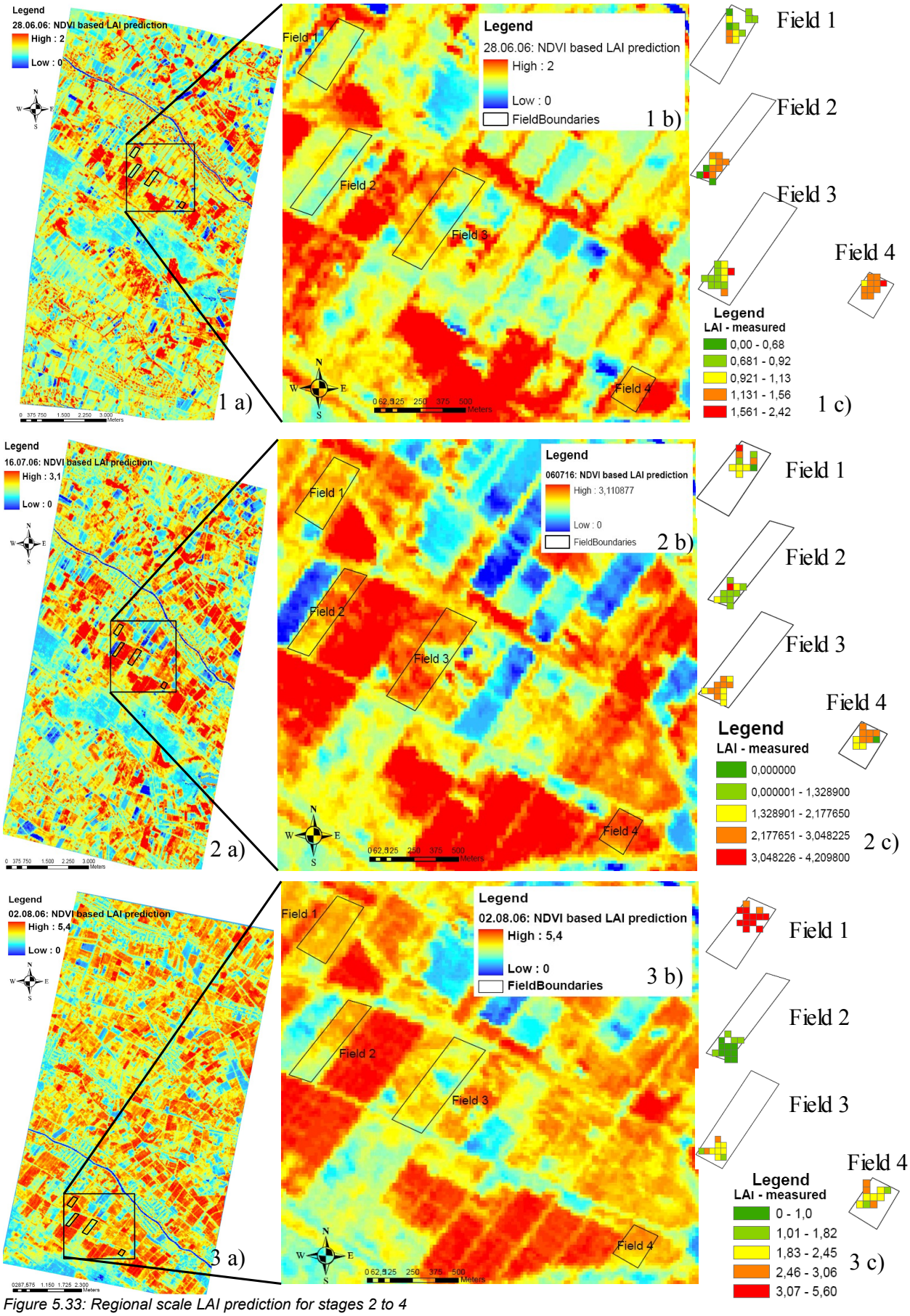

Figure 5.33: Regional scale LAI prediction for stages 2 to 4

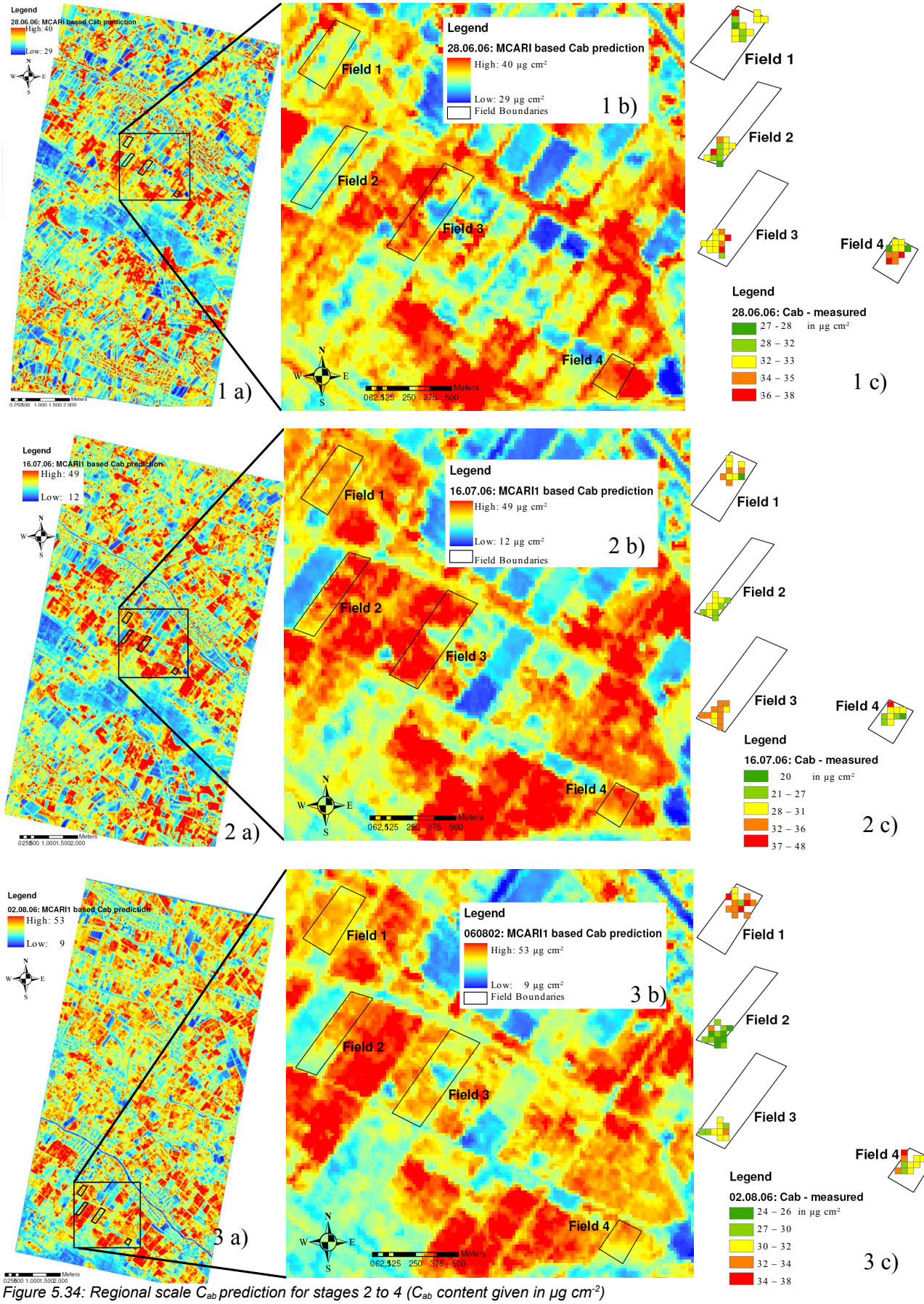

Figure 5.34: Regional scale C_{ab} prediction for stages 2 to 4 (C_{ab} content given in µg cm^{-2})

5.5 Validation of LAI and C_{ab} prediction by VIs at regional scale

To validate a created regression model there are according to Netes et al (1996) three basic ways possible:

1. Collection of new data to check the model and its predictive ability
2. Comparison of results with theoretical expectations, earlier empirical results and simulation results
3. Use of holdout sample to check the model and its predictive ability

The first method is out of question, because the collection of a similar dataset would have required waiting until the cotton will be fully grown again. The third method is not suitable, either because the population of each dataset was too small to split in advance. All samples were needed to create a more profound prediction.

The second way was identified as best suiting for the datasets of this study. For validation a new dataset containing the data of all stages for each field was created, three fields combined to calculate an equation to predict the LAI and C_{ab} -content for the remaining one. These equations, shown in table 5.10 were compared together with equations created for each of the last three dates (table 5.9) to identify one equation showing the best correlation for estimating LAI and one for predicting C_{ab}-content by VIs for the whole regional scale dataset. The power of prediction of the datasets used for validation is shown in scatter plots in figures to XX.

For the LAI datasets table 5.10 shows a increasing performance of prediction for an increasing aggregation. The datasets created by aggregating three fields over three stages showed the highest coefficients of determination (0,66 – 0,49). The LAI shows a continuous development over time. If the plants are growing they develop more leaves and the LAI is increasing. Thus a changing LAI is indicating at all stages on the same behaviour, a increase or decrease of the amount of leaf area. Variations within each dataset are smoothed with an increasing population. Compared with the literature, the high variations of this dataset were most likely caused by the plant based LAI data collection (chapters 4.2.3 & 4.5.5.2) instead of square meter based as done e.g. by Blenk (2005). Due to the high variance within the different fields at each stage the use of one factor of correction per stage was not adequate for all fields, especially field two. Therefore the data aggregations of the different fields are showing altering coefficients of determination. This occurrence has to be kept in mind while evaluating the results of the validation. For validating the prediction of LAI by NDVI the highest level of data aggregation is used as the NDVI was proofed exactly for this kind of datasets by Blenk (2005).

Table 5.10: Coefficients of determination for different datasets at regional scale

Combination of stages	Combi-nation of fields	Predicting LAI by NDVI using the dataset indicated in the first two columns 1)	R^2	Predicting C_{ab} by MCARI1 using the dataset indicated in the first two columns 1)	R^2
All three stages together	1, 2, 3	LAI =4,7557*$NDVI_{1-3}$ – 0,6071	0,5360	C_{ab} = 1,5338*$MCARI1_{1-3}$ + 30,773	0,0040
	1, 3, 4	LAI = 4,3602*$NDVI_{1,3,4}$ – 0,417	0,4963	C_{ab} = -3,2971*$MCARI1_{1,3,4}$ + 33,111	0,0154
	2, 3, 4	LAI =3,2385*$NDVI_{2-4}$ – 0,1074	0,6639	C_{ab} = 0,5034*$MCARI1_{2-4}$ + 30,888	0,0004
	1, 2, 4	LAI = 4,5386*$NDVI_{1,2,4}$ – 0,5107	0,5210	C_{ab} = -0,7681*$MCARI1_{1-3}$ +31,076	0,0008
	3,4	LAI = 3,3486*$NDVI_{3,4}$ – 0,1023	0,6295	C_{ab} = -4,7312*$MCARI1_{3,4}$+34,059	0,0456
	1,2	LAI = 6,9463*$NDVI_{1,2}$ – 1,488	0,6400	C_{ab} = 2,8137*$MCARI1_{1,2}$ + 29,549	0,0115
All stages of each field together	1	LAI = 6,3411*$NDVI_1$ – 0,8711	0,6719	C_{ab} = 0,7*$MCARI1_1$+ 31,752	0,0006
	2	LAI = 1,2138*$NDVI_2$ + 0,5881	0,2181	C_{ab} = -16,787*$MCARI1_2$+ 32,017	0,3147
	3	LAI = 3,4539*$NDVI_3$ -0,1623	0,6712	C_{ab} = -4,8797*$MCARI1_3$ + 34,179	0,0651
	4	LAI = 3,3076*$NDVI_4$ – 0,0865	0,6587	C_{ab} = -22,489*$MCARI1_4$ + 39,555	0,2377
Aggregations of different fields within one stage:					
Stage 4	1, 2, 3	LAI = 8,585*$NDVI_{1-3}$ – 2,4671	0,6790	C_{ab} = 27,266*$MCARI_{1-3}$ + 21,823	0,5795
	1, 3, 4	LAI = 5,0739*$NDVI_{1,3,4}$ – 0,3955	0,1696	C_{ab} = 9,5276*$MCARI1_{1,3,4}$ + 29,003	0,0717
	2, 3, 4	LAI = 3,6479*$NDVI_{2-4}$ – 0,2775	0,5661	C_{ab} = 20,312*$MCARI1_{2-4}$ + 23,555	0,4468
	1, 2, 4	LAI = 7,1602*$NDVI_{1,2,4}$ – 1,8327	0,5494	C_{ab} = 27,666*$MCARI1_{1,2,4}$ + 21,883	0,5449
Stage 3	1, 2, 3	LAI = 3,785*$NDVI_{1-3}$ – 0,5628	0,5586	C_{ab} = 28,812*$MCARI_{1-3}$ + 18,302	0,6028
	1, 3, 4	LAI =3,0415*$NDVI_{1,3,4}$ – 0,0239	0,3248	C_{ab} = 25,681*$MCARI1_{1,3,4}$ + 19,114	0,4050
	2, 3, 4	LAI = 3,6403*$NDVI_{2-4}$ – 0,4224	0,5477	C_{ab} = 24,968*$MCARI1_{2-4}$ + 19,442	0,4922
	1, 2, 4	LAI =3,9581*$NDVI_{1,2,4}$ – 0,6857	0,5499	C_{ab} =15,367*$MCARI1_{1,2,4}$ +22,48	0,0978
Stage 2	1, 2, 3	LAI =0,3722*$NDVI_{1-3}$ – 0,8035	0,0448	C_{ab} = 7,9096*$MCARI_{1-3}$ + 31,916	0,2113
	1, 3, 4	LAI =1,4252*$NDVI_{1,3,4}$ – 0,9043	0,3348	C_{ab} = 8,4631*$MCARI1_{1,3,4}$ + 31,756	0,1957
	2, 3, 4	LAI = 1,5978*$NDVI_{2-4}$ – 0,4755	0,3725	C_{ab} = 7,5266*$MCARI1_{2-4}$ + 31,956	0,3036
	1, 2, 4	LAI = 1,6917*$NDVI_{1,2,4}$ – 0,5238	0,5109	C_{ab} = 7,1368*$MCARI1_{1,2,4}$ + 32,046	0,1874

Note: 1) Subscript figures in the equations indicate the respective field numbers.

For the C_{ab} datasets table 5.10 is showing a completely different behaviour of the coefficients of determination. The highly aggregated datasets over the whole measurement cycle (stage 2 - 4) are showing a very poor correlation, while the aggregation of three fields at the same stage are almost all high performing with a maximum R^2-value of 0,6. In contrast to LAI the cotton C_{ab}-content is not developing in a linear manner. The within - plant distribution of leaf C_{ab}-content of cotton is varying over time (chapter 2.1). As shown in the preceding chapters regarding the plant layer datasets, the leaf chlorophyll content of the different plant layers is changing over time within each plant. This change makes an data aggregation of different stages inadequate to create a stable prediction of C_{ab}-content by VIs. Furthermore the MCARI1 was proofed by Zarco-Tejada et al. (2005 (2)) as very sensitive to identify within field variability of C_{ab}. To predict and monitor this within - field variability of the cotton fields is the main objective of this thesis. Therefore its only consequent to use the datasets this prediction is created with at its best. Thus the validation was fulfilled with the lowest aggregated datasets which means for each stage separately. The equation calculated for three fields of the same stage is validated with the remaining field of each. This process is repeated for all three stages. The resulting equation for each stage can be used to predict the C_{ab} – content of

cotton plants at this growing stage by MCARI1 calculated based on Proba-1/CHRIS hyperspectral satellite nadir images.

Validation of LAI prediction by NDVI

Creation of equation to calculate LAI Validation of this equation on remaining field

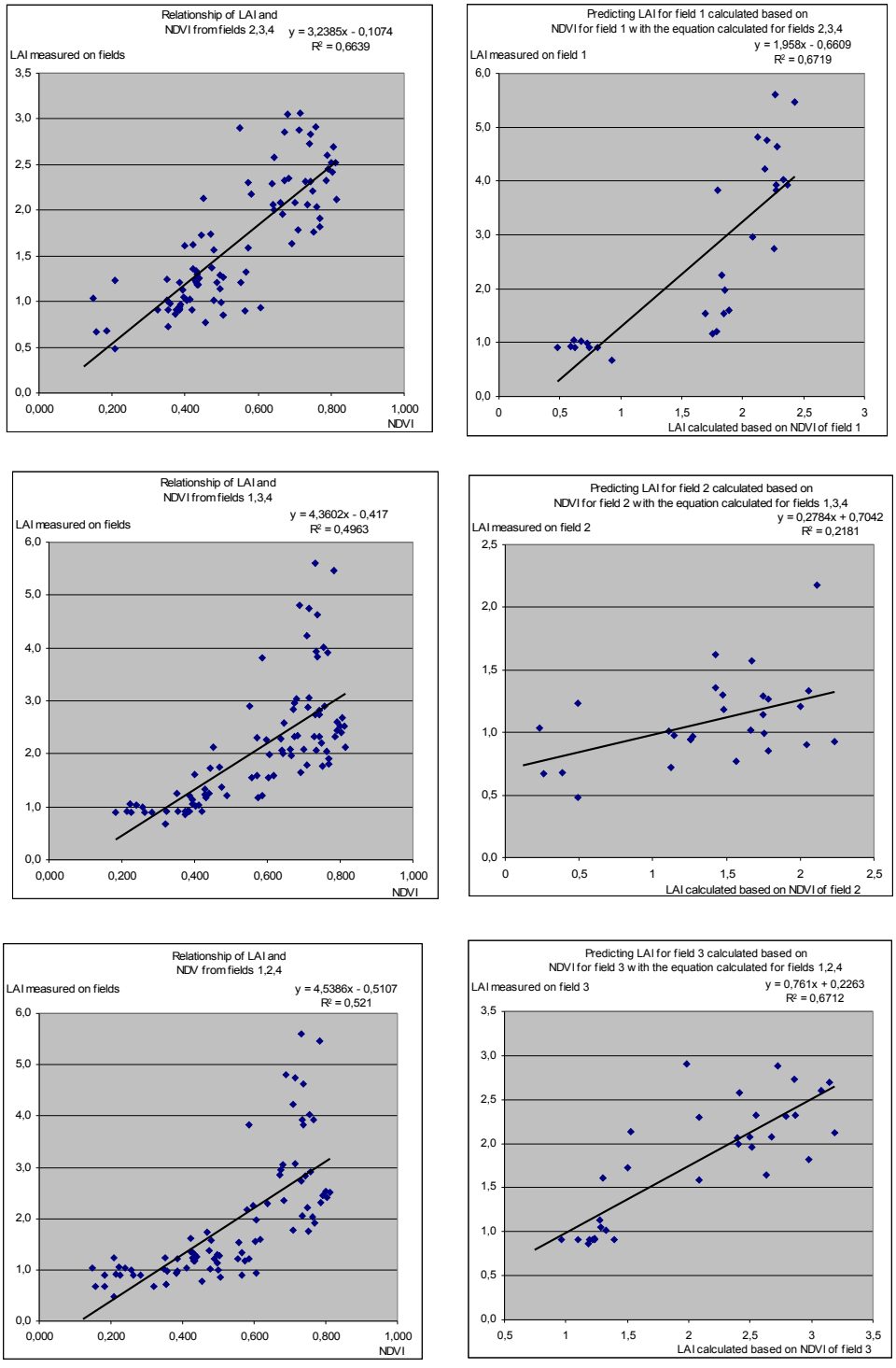

Figure 5.35: Validation of NDVI based prediction of LAI (part 1)

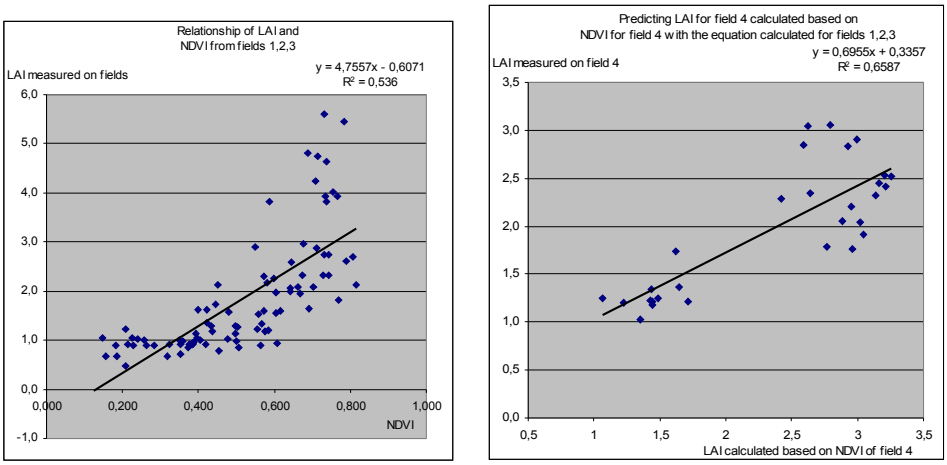

Figure 5.36: Validation pf NDVI based prediction of LAI (part 2)

Table 5.11: Results of LAI validation per field over all stages at regional scale

Field	Equation	R^2
1	$LAI_{gem} = 1,958*LAI_{NDVI} + 0,6609$	0,6719
2	$LAI_{gem} = 0,2784*LAI_{NDVI} + 0,7042$	0,2181
3	$LAI_{gem} = 0,761*LAI_{NDVI} + 0,2263$	0,6712
4	$LAI_{gem} = 0,6955*LAI_{NDVI} + 0,3357$	0,6587

The equations calculated for the different datasets to transfer NDVI to LAI (table 5.10) are quite similar. The factor of gradient is ranging from 4,7557 to 3,2385 and the offset factor from -0,1074 to -0,6071. The factors of the equation found by Blenk 2005 are completely within these range. The coefficients of determination given in table 5.11 are indicating the correlation of measured LAI and LAI calculated by NDVI using the referring equation shown in table 5.10. As result of the validation process the highest of these R^2-values are indicating the best performing equation. With R^2 = 0,6719 the validation made on field 1 seems to be the best, but the R^2 of the validation represented by field 3 is with R^2=0,6712 almost as high. To decide which one will be the result the coefficients of determination of the referring equations shown in table 5.10 are taken into account. With an R^2 of 0,6639 the power of prediction of the equation validated with field 1 is significantly higher than the R^2 of 0,521 of the equation used for the validation with field 3. Therefore the resulting equation to transfer NDVI into LAI for the datasets of this thesis is :

$$LAI_{t_1} = 3,2385 * NDVI_{t_1} - 0,1074$$

with t_1 = from same dataset

Validation of C_{ab} prediction by MCARI1 at stage 4

Creation of equation to calculate C_{ab}

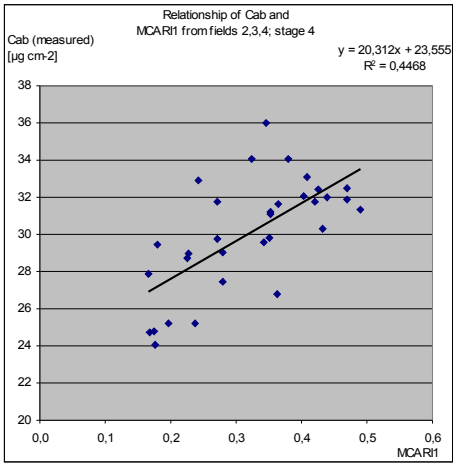

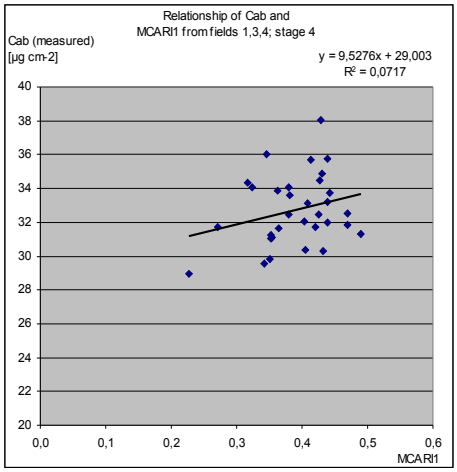

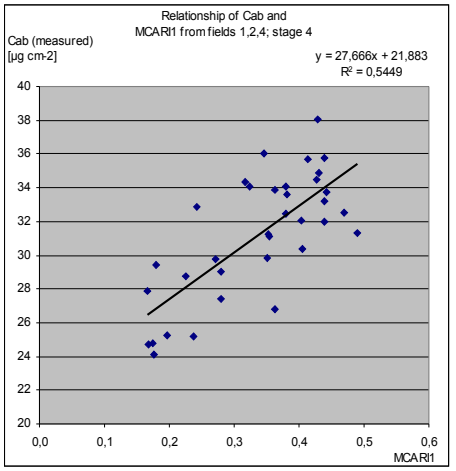

Validation of this equation on remaining field

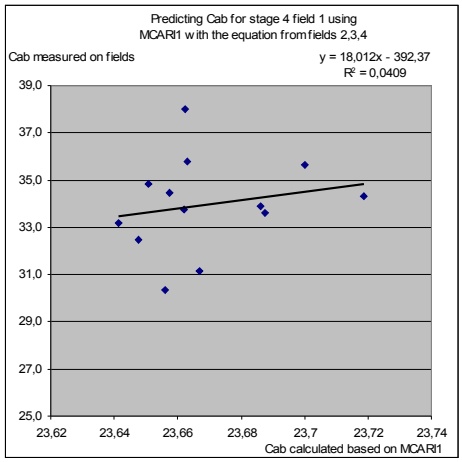

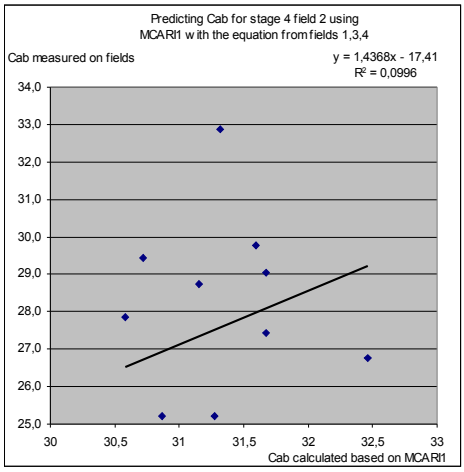

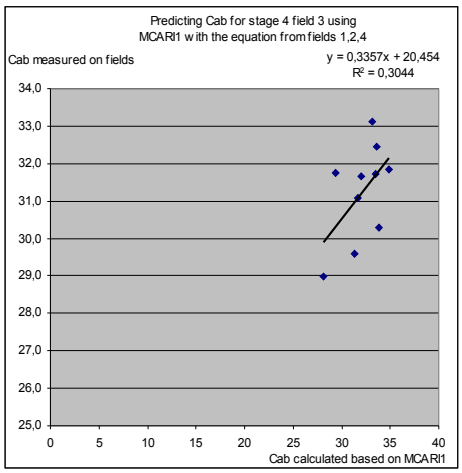

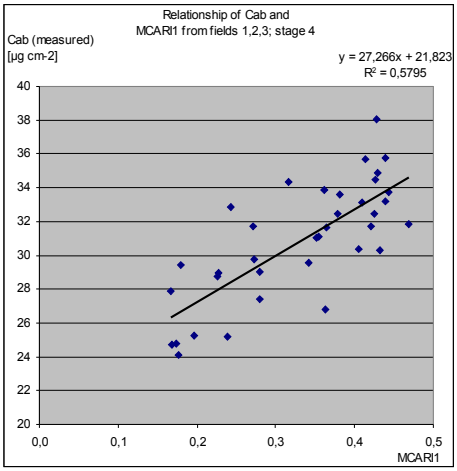

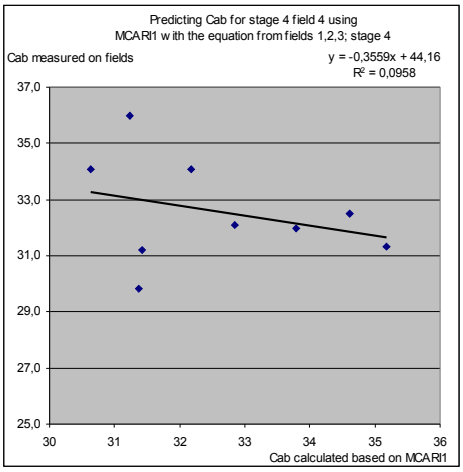

Validation of C_{ab} prediction by MCARI1 at stage 3

Creation of equation to calculate C_{ab} Validation of this equation on remaining field

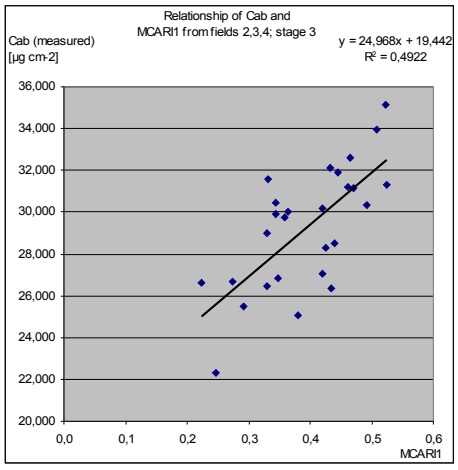

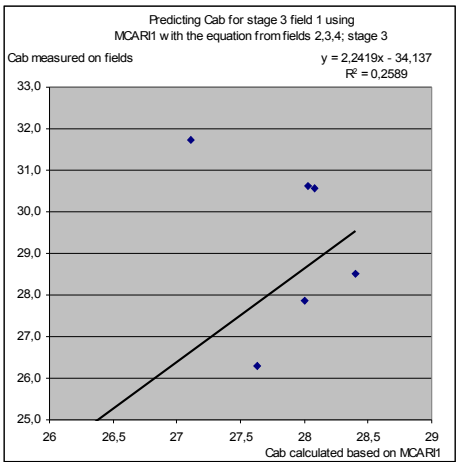

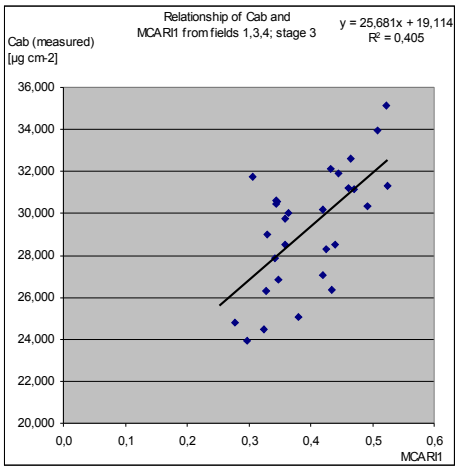

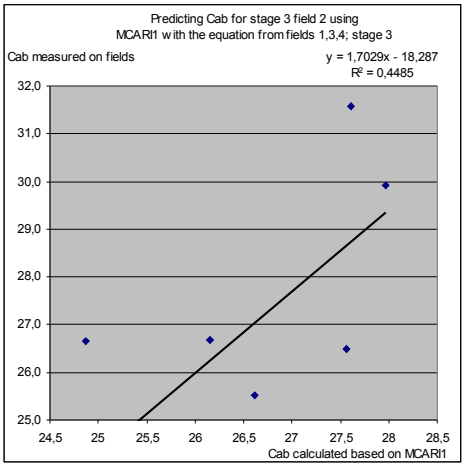

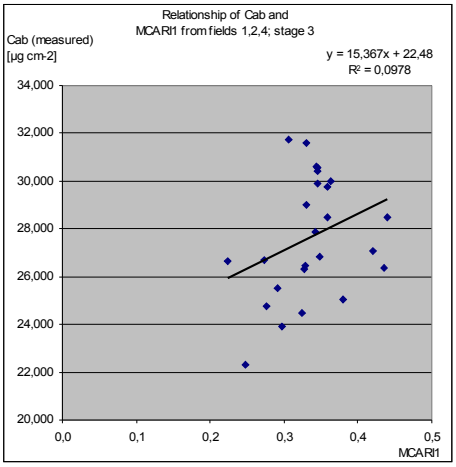

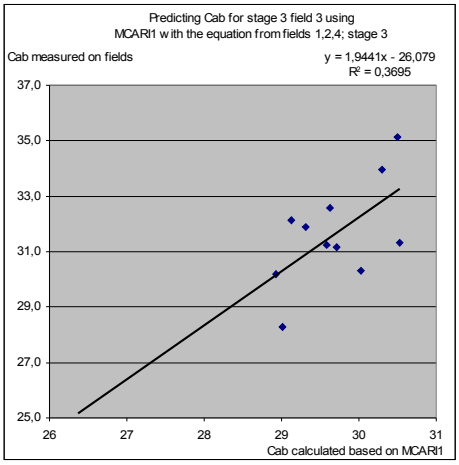

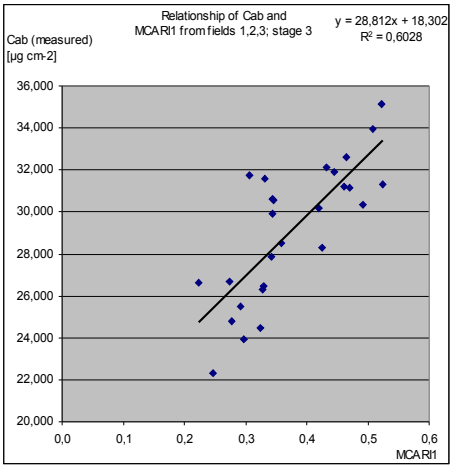

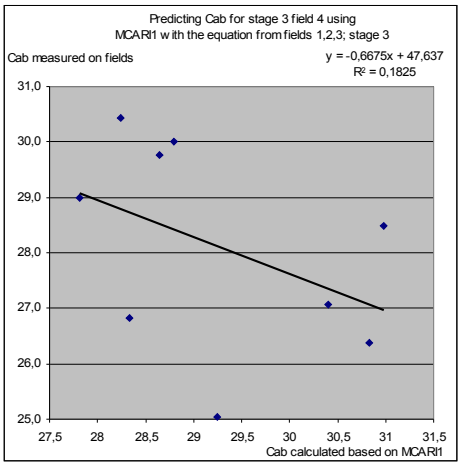

Validation of C_{ab} prediction by MCARI1 at stage 2

Creation of equation to calculate C_{ab} Validation of this equation on remaining field

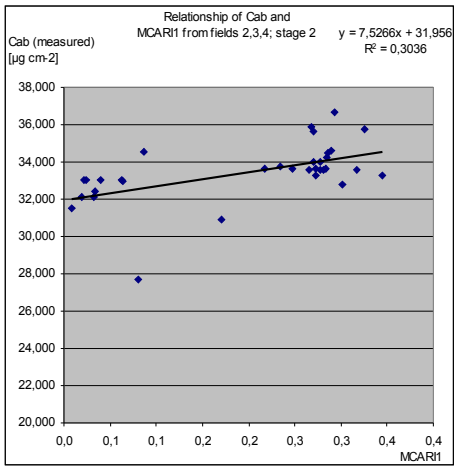

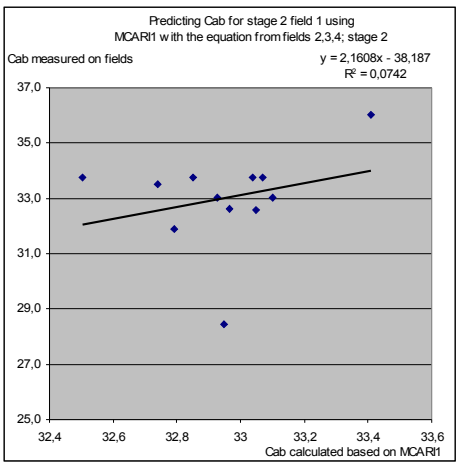

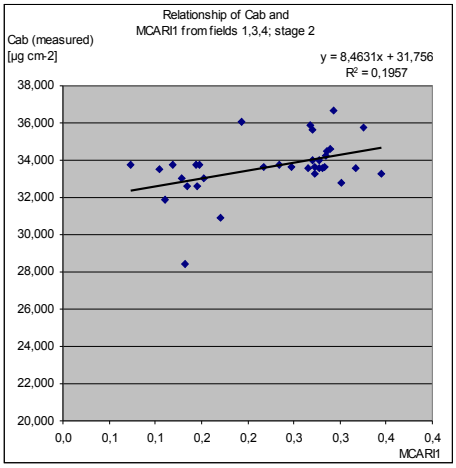
Relationship of Cab and
MCARI1 from fields 1,3,4; stage 2
Cab (measured)
[µg cm-2]
y = 8,4631x + 31,756
R² = 0,1957
38,000
36,000
34,000
32,000
30,000
28,000
26,000
24,000
22,000
20,000
0,0 0,1 0,1 0,2 0,2 0,3 0,3 0,4 0,4
MCARI1

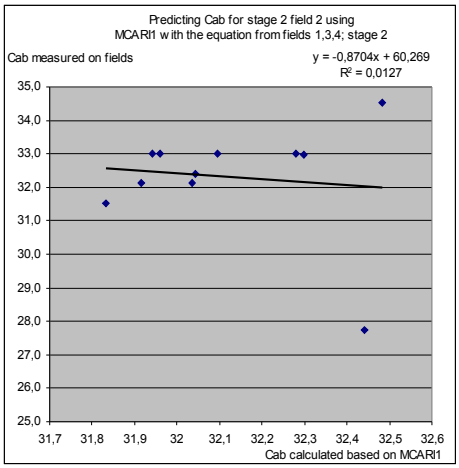
Predicting Cab for stage 2 field 2 using
MCARI1 with the equation from fields 1,3,4; stage 2
Cab measured on fields
y = -0,8704x + 60,269
R² = 0,0127
35,0
34,0
33,0
32,0
31,0
30,0
29,0
28,0
27,0
26,0
25,0
31,7 31,8 31,9 32 32,1 32,2 32,3 32,4 32,5 32,6
Cab calculated based on MCARI1

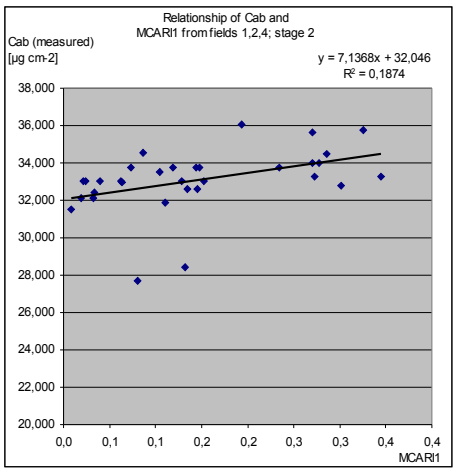
Relationship of Cab and
MCARI1 from fields 1,2,4; stage 2
Cab (measured)
[µg cm-2]
y = 7,1368x + 32,046
R² = 0,1874
38,000
36,000
34,000
32,000
30,000
28,000
26,000
24,000
22,000
20,000
0,0 0,1 0,1 0,2 0,2 0,3 0,3 0,4 0,4
MCARI1

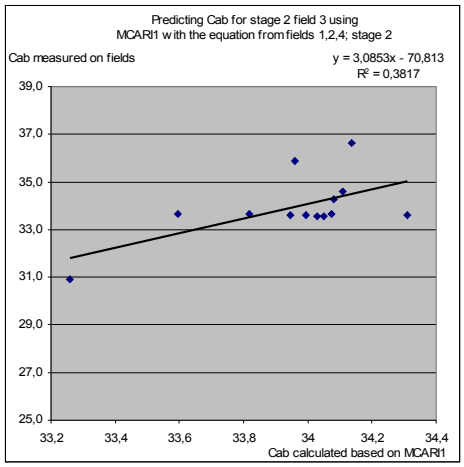
Predicting Cab for stage 2 field 3 using
MCARI1 with the equation from fields 1,2,4; stage 2
Cab measured on fields
y = 3,0853x - 70,813
R² = 0,3817
39,0
37,0
35,0
33,0
31,0
29,0
27,0
25,0
33,2 33,4 33,6 33,8 34 34,2 34,4
Cab calculated based on MCARI1

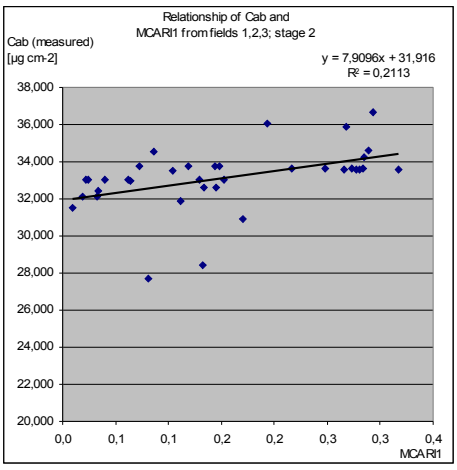
Relationship of Cab and
MCARI1 from fields 1,2,3; stage 2
Cab (measured)
[µg cm-2]
y = 7,9096x + 31,916
R² = 0,2113
38,000
36,000
34,000
32,000
30,000
28,000
26,000
24,000
22,000
20,000
0,0 0,1 0,1 0,2 0,2 0,3 0,3 0,4
MCARI1

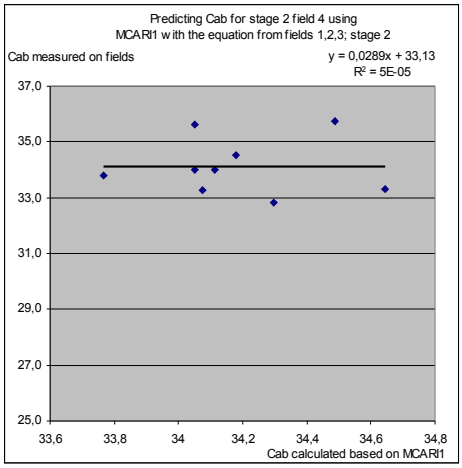
Predicting Cab for stage 2 field 4 using
MCARI1 with the equation from fields 1,2,3; stage 2
Cab measured on fields
y = 0,0289x + 33,13
R² = 5E-05
37,0
35,0
33,0
31,0
29,0
27,0
25,0
33,6 33,8 34 34,2 34,4 34,6 34,8
Cab calculated based on MCARI1

Table 5.12: Results of C_{ab} validation per field and stage at regional scale

Stage	Field	Equation	R^2
4	1	C_{ab} = 18,012*MCARI1 – 392,37	0,0409
	2	C_{ab} = 1,4368*MCARI1 – 17,41	0,0996
	3	C_{ab} = 0,3357*MCARI1 + 20,454	0,3044
	4	C_{ab} = -0,3559*MCARI1 + 44,16	0,0958
3	1	C_{ab} = 2,2419*MCARI1 – 34,137	0,2589
	2	C_{ab} = 1,7029*MCARI1 – 18,287	0,4485
	3	C_{ab} = 1,9441*MCARI1 -26,079	0,3695
	4	C_{ab} = -0,6675*MCARI1 + 47,637	0,1825
2	1	C_{ab} = 2,1608*MCARI1 – 38,187	0,0742
	2	C_{ab} = -0,8704*MCARI1 + 60,269	0,0127
	3	C_{ab} = 3,0853*MCARI1 - 70,813	0,3817
	4	C_{ab} = 0,0289*MCARI1 + 33,13	0,00005

The results of the validation of equations to transform MCARI1 into C_{ab}-content are not as definitely as for LAI. One reason is for sure the small population of the datasets used for validation. Another reason may be the inaccuracy of +/- 3 units of the Minolta SPAD-502. If this inaccuracy is taken into account most coefficients of determination will increase significantly. Sripada et al. (2005) and Scharf & Lory (2002) are suggesting the use of relative instead of absolute values to achieve a more reliable indicator of N-status calculated from data derived from aerial imagery. Maybe this step would be able to increase the performance of the datasets, but this has to be topic of another thesis. The coefficients of determination are indicating for each stage the best performing equation. This is the one with the highest R^2-values as shown in table 5.12. The corresponding equations are shown in table 5.10. The equations to transfer MCARI1 into C_{ab}-content for cotton for each date are:

28.06.06: $C_{ab_{t_1}} = 7{,}1368 \cdot MCARI1_{t_1} + 32{,}046$

16.07.06: $C_{ab_{t_1}} = 25{,}681 \cdot MCARI1_{t_1} + 19{,}114$

02.08.06: $C_{ab_{t_1}} = 27{,}666 \cdot MCARI1_{t_1} + 21{,}883$

With t_1 = from same dataset

6. Conclusions and Outlook

For improving crop growth and supporting targeted fertilizer application in Uzbekistan, To estimate LAI and C_{ab} (indicator for crop growth and leaf nitrogen content, respectively) were estimated in cotton leaves of the Khorezm-127 variety by spectral vegetation indices in a site the need of N-fertilizer application on cotton fields in Uzbekistan the Khorezm region by remote sensing, this study investigated at three different spatial scales (leaf, plant and region), and at four temporal stages during the growing season in 2006. The respective data were collected by a Minolta SPAD-502 (SPAD) chlorophyll meter, a LICOR 2000 LAI – meter and an ASD field spectrometer as well as by hyperspectral Proba-1/CHRIS images of different view angles

At leaf scale laboratory determined C_{ab} - concentration was used to calibrate the SPAD by linking the laboratory results to the SPAD measured at the same leaf. Thereby a regression equation was developed and used to predict from SPAD values cotton leaf chlorophyll content at plant and regional scale.

At plant scale the SPAD, LAI and reflectance was measured on Fertilizer Trial Plots with four different levels of nitrogen application during four temporal stages. The collected data were aggregated according to plant and fertilizer application rates. The overall dataset showed very weak correlations for almost all VIs. The datasets aggregated by fertilizer application rate (N-Level) showed a high variability within each plot, but some VIs correlated well with LAI or C_{ab} at some stages and Nitrogen Levels. However, no VI showed a good correlation for all fertilizer stages.

At regional scale LAI and SPAD were measured on cotton plants on four farmer managed fields during three temporal stages when Proba-1/CHRIS multiangular hyperspectral satellite images covering all four fields were acquired. The LAI values were aggregated for all fields and all stages and showed with an increasing data aggregation an as well increasing correlation with VIs, especially with the NDVI calculated based on the nadir images. The SPAD values were aggregated according to vertical plant layers, and the ability of VIs from satellite images to predict the C_{ab} content of different combinations of plant layers was tested. As for LAI the nadir image showed the best correlations for estimating C_{ab} by VIs. As a result one plant layer combination was identified for each stage which proofed the best correlation for predicting C_{ab} by VIs. Some VIs showed a stable correlation performance for these datasets, but as best the MCARI1 was identified and validated. For validation a regression equation was created that predicts C_{ab} by MCARI1 for three fields and for each stage and afterwards the equation was used to predict the C_{ab} content of the fourth field of the same stage. The prediction was then validated with the respective measurements on the ground. The same procedure was done for LAI and the NDVI, but with a dataset combining all measurements of the seasons together.

As a result one equation was created to predict LAI by NDVI at any of the three stages. To

calculate the C_{ab} content by MCARI1, equations for each stage another equation were developed, as the distribution of Cab within the cotton plant is changing over time in a non-linear way.

The results of plant and regional scale were incommensurable due to the different plant growth and the large heterogeneity of LAI and C_{ab} within the fertilizer trial plots. To create a more homogeneous sample population the plots and thus the number of samples per plot were too small. For further investigations larger plots are recommended with may lead together with homogeneous water and fertilizer management to more homogeneous plant development within each plot. Further improvements are to aggregate the SPAD values by N-Level and plant layer. For this the best suitable plant layers as found at regional scale in this study may be used.

For improved atmospheric corrections the reflectance measurements of a bare soil field should be repeated during each satellite overpass, if possible. To validate the results of the atmospheric correction process reflection data of few big fields, if possible cotton fields, should be measured at a standardized measurement height of around 2m above ground at each satellite overpass.

The LAI and SPAD values collected on the fields should not be acquired following an X-shaped path, but a dense regular grid to ease the interpolation of the measured values. LAI should be measured per square meter and not per plant, C_{ab} averaged at plant layers, as it was done for this study.

For integrating this research further into agricultural practice, the next step will be to identify critical chlorophyll values, in order to identify possible nutrient deficiencies. The Cab distribution map combined with a very detailed soil bonitet map may be helpful for improving the fertilizer application recommendations for the specific season and field.

To cover whole region the findings may be upscaled to the 300 by 300m pixel of MERIS satellite data. In combination with a successful landuse classification and similar studies for other crops, fertiliser recommendations may be given per crop and field for whole regions at different stages during the season. The VIs used for this study have some big advantages, as they are relatively easy to calculate, thus they are directly applicable, but the comparison with the results of radiation transfer models would be very interesting to evaluate the quality of the VIs identified as best correlating in this thesis.

7.References:

ADMAS, S., Arend, I., Köhler, K., Rollenfitsch, F. (2005): **Abschlussbericht zu den spektralen Laboruntersuchungen des Austrocknungsexperiments** im Rahmen des Interdisziplinären Forschungspraktikum Fernerkundung / Geobotanik Sommer 2005.

BAEZ-GONZALEZ, A.D., Chen, P.Y., Tiscareno-Lopez, M., Srinivasan, R., 2002: **Using satellite and field data with crop growth modeling to monitor and estimate corn yield in Mexico**. In: Crop Science, 42, pp. 1943-1949.

BARET, F., Foutry, T., 1997: **Radiometric estimates of nitrogen status in crops**. In: Lemaire, G. (Ed.), Diagnosis of the Nitrogen Status in Crops. Springer Verlag, New York, pp. 201-277.

BARET, F., Guyot, G., Major, D.J. (1989): **TSAVI: a vegetation index which minimizes soil brightness effects on LAI and APAR estimation**. In: IGARSS 1989, 12th Canadian symposium on Remote Sensing 10-14.07.1989, pp. 1355-1358.

BARET, F., Guyot, G. (1991): **Potentials and limits of vegetation indices for LAI and APAR assessment**. In: Remote Sensing Environment, 35, pp. 161-173, ELSEVIER.

BASTIAANSSEN, W.G.M., Ali, S., 2003: **A new crop yield forecasting model based on satellite measurements applied across the Indus Basin, Pakistan**. In: Agric. Ecosyst. And Environ. , 94, pp. 181-191.

BEAN, D. (2000): **Classifying Vegetation Using Remote Sensing**. In: http://www.geog.ubc.ca/courses/geog516/talks_2000/classifyingvegetation.htm. (visited 26.10.06, verified 29.03.07)

BEGIEBING, S., Bach, H., Waldmann, D., Mauser, W. (2004): **Analyses of Spaceborne Hyperspectral and Directional CHRIS Data to Deliver Crop Status for Precision Agriculture.** VISTA Geowissenschaftliche Fernerkundung GmbH, Gabelsbergerstrasse. 51, D-80333 Munich, Germany, www.vista-geo.de

BEGIEBING, S. & BACH, H. (2005); **Analyses of hypersprectral and directional CHRIS data for agricultural monitoting using a canopy reflectance model,** In: 3rd Chris Proba Workshop, ESA-ESRIN Frasgati, 21.-23.3.2005.

BROGE, N.H., Leblanc, E. (2000): **Comparing prediction power and stability of broadband and**

hyperspectral vegetation indices for estimation of green leaf area index and canopy chlorophyll density. In: Remote Sensing of Environment, 76, pp. 156-172. ELSEVIER.

BROGE, N.H., Mortensen, J.V. (2002): **Deriving green crop area index and canopy chlorophyll density od winter wheat from spectral reflectance data.** in: Remote Sensing of Environment, 81, pp. 45-57. ELSEVIER.

BROGE, N.H. (2003); **Prediction of Green Canopy Area Index and Canopy Chlorophyll Density of homogeneous canopies from measurements of spectral reflectance in the visible and near-infrared domain,** PhD thesis, DIAS reports, Tjele, http://www.agrsci.dk, ISSN pp. 1397-9884.

CLEVERS, J.G.P.W., (1989): **Application of a weighted infrared – red vegetation index for estimating leaf area index by correcting for soil moisture**. Remote Sensing of Environment, 29(1), pp. 25-37.

CONRAD, C., Ruecker, G.R., Colditz, R.R., Strunz, G., Dech, S., 2004a: **Crop monitoring using multi-temporal MODIS remote sensing data in Khorezm**. In: Humbolt-workshop "The use of GIS and simulation models for research and decision support in Central Asia", Tashkent, Uzbekistan, 9-11 July 2004.

CONRAD, C., Ruecker, G.R., Schweitzer, C., Dech, S., Haefeez, M., 2004b: **Modelling seasonal actual evapotranspiration with remote sensing and GIS in Khorezm region, Uzbekistan**. In: Proc. Of the 11th SPIE international Symposium on Remote Sensing, Maspalomas, Gran Canaria, Spain, 13-16 September 2004.

CUTTER, M.A. (2006): **HDFclean V2**. Av. at http://earth.esa.int/object/index.cfm?fobjectid=4409 (Assessed 1 March 2007; verified 06 March 2007).

CUTTER, M.A., L. S. Johns (2005): **CHRIS Data Format,** Sira, Issue 4.2, Doc:271.DO.13.

DALEZIOS, N.R., Domenikiotis,C., Loukas, A., Tzortzios, S.T., Kalaitzidis, C., 2001. **Cotton yield estimation based on NOAA/AVHRR produced NDVI**. In: Phys. Chem. Earth (B), 26, pp. 247-251.

DASH, J., Curran, P.J. (2004): E**valuation of the MERIS terrestrial chlorophyll index (MTCI)**. In: Advances in Space Research, COSPAR publication, www.sciencedirect.com, ELSEVIER.

DAUGHTRY, C.S.T., Walthall, C.L., Kim, M.S., Brown de Colstoun, E., McMurtrey, J.E. III (2000): **Estimating corn leaf chlorophyll concentration from leaf and canopy reflectance**. In: Remote Sensing of Environment, 74, pp. 229-239, ELSEVIER.

DAWSON, T.P., Curran, P.J. (1998); **A new technique for interpolating the reflectance red edge position**. In: International Journal of Remote Sensing, Vol.19, No.11, pp. 2133-2139.

DEMIRCAN, A. (1995): **Die Nutzung fernerkundlicher bestimmter Pflanzenparameter zur flächenhaften Modellierung von Ertragsbildung und Verdunstung**. Geobuchverlag, Reihe B, Bd.20, München.

DIEPENBROCK, W., Fischbeck, G., Heyland, K.-U. Knauer, N. (1999): **Spezieller Pflanzenbau**. München, Wien.

DORAISWAMY, P.C., Hatfield, J.L., Jackson, T.J., Ahhmedov, B., Prueger, J., Stern, A., 2003: **Crop conditions and yield simulations using Landsat and MODIS**. In: Remote Sensing of Environment, 92, pp. 548-559.

DORIGO, W., Bachmann, M., Heldens, W. (2007): **AS Toolbox & Processing of field spectra, User´s manual.** German Aerospace Center (DLR), http://www.ares.caf.dlr.de .

DORIGO, W., Zurita-Milla, R., de Wit, A.J.W., Brazile, J., Singh, R., Schaepman, M.E. (2006): **A review on reflective remote sensing and data assimilation techniques for enhanced agroecosystem modeling**. In: Int. Journal of Applied Earth Observation and Geoinformation 2006, ELSEVIER.

EASTWOOD, J.A., Yates, M.G., Thomson, A.G., Fuller, R.M. (1997): **The reliability of vegetation indices for monitoring saltmarsh vegetation cover.** In: International Journal of Remote Sensing, 1997, Vol.18, No.18, pp. 3901-3907, ELSEVIER.

ELVIDGE, C.D., Chen, Z.(1995): **Comparison of Broad-Band and Narrow-Band Red and Near-Infrared Vegetation indices**. In: Remote Sensing of Environment, 54, pp. 38-48, ELSEVIER.

ESA homepage: http://www.esa.int/esaEO/SEMZ4SOFHTE_index_0.html

FAO (1998): **World reference base for soil resources**, FAO, Rome, ISSS-AISS-IBG, ISRIC

FAO (2003): **Fertilizer use by crop in Uzbekistan**, First Version, published by FAO (Food and Agriculture Organisation of the United Nations), Rome, 2003.

FAOSTAT data (2006a): **Trade / Crops & Livestock primary & processed**, last accessed 11/06.

FAOSTAT data (2006b): **Production / Crops Primary**, last accessed 11/06.

FOURTY, T., Baret, F., Jacquemoud, S., Schmuck, G., Verdebout, J. (1996): **Leaf optical properties with explicit description of its biochemical composition: direct and inverse problems**. In: Remote Sensing of Environment, 56(2), pp. 104-117, ELSEVIER.

FRANKE, G. (1994):**Nutzpflanzen der Tropen und Subtropen**. Bd. 2: Spezieller Pflanzenbau, Stuttgart.

GARDNER, B.R., Blad, B.L. (1986): **Evaluation of spectral reflectance models to estimate corn ceaf area while minimizing the influence of soil background effects**. In: Remote Sensing of Environment, 20, pp. 183-193, ELSEVIER.

GIANNICO, C. (2007): **Remote sinsing of vegetation in the calabrian region**. In: Acta Astronautica, 60, pp. 119-131. (www.elsevier.com/locate/actaastro)

GOWARD, S.N., Williams, D.L., (1997): **Landsat and Earth system science: development of terrestrial monitoring**. In: Photogrametric Eng. Remote Sensing, 63, pp. 887-900.

GRIMES, D.W., El-Zik, K.M. (1990): **Cotton**. In: Stewart, B.A. & Nielsen, D.R. (Editors): Irrigation of agricultral crops, Agronomy, No.30, Madison, pp. 741-773.

GROTEN, S.M.E. 1993: **NDVI-crop monitoring and early yield assessment of Burkina Faso**. In: International Journal of Remote Sensing, 14, pp. 1495-1515.

HABOUDANE, D., Miller, J.R., Tremblay, N., Zarco-Tejada, P.J., Dextraze, L. (2002): **Integrated narrow-band vegetation indices for prediction of crop chlorophyll content for application to precision agriculture**. In: Remote Sensing of Environment, 81, pp. 416-426, ELSEVIER.

HABOUDANE, D., Miller, J.R., Pattey, E., Zarco-Tejada, P.J., Strachan I.B. (2004): **Hyperspectral vegetation indices and novel algorithms for predicting green LAI of crop canopies. Modelling and validation in the context of precision agriculture**. In: Remote Sensing

of Environment, p.1-16, online version 2004, http://www.elsevier.com/locate/rse

HALL, D. O., Rao, K.K. (1987): **Photosynthesis (4th edition)**. Great Britain: Edward Arnold.

Hamilton, L.C. (1990): **Modern data analysis: a first course in applied statistics**. Wadsworth, ... California.

HATCHELL, D. (Editor) (1999): **Analytical Spectral Devices, Inc. (ASD) Technical Guide**. 3rdedition.

HAWTHORNE, B. (2006): **Hawth´s Tool for ArcGIS 9.1 version 3.26** . downloadable at ..http://www.spatialecology.com/htools/download.php. (visited 27.10.06, verified 08.03.07)

HE, Y., Guo, X., Wilmshurst, J. (2006): Studying mixed grassland ecosystems I: suitable hyperspectral vegetation indices. In: Can. J. Remote Sensing, Vol.32, No.2, pp. 98-107.

HUETE, A.R. (1988): **A soil – adjusted vegetation index (SAVI)**. In Remote Sensing of Environment, 25, 3, pp. 295 – 309, ELSEVIER.

JIANG, Z., Huete, A.R., Chen, J., Chen, Y., Li, J., Yan, G., Zhang, X. (2006): **Analysis of NDVI and scaled difference vegetation index retrievals of vegetation fraction**. In: Remote Sensing of Environment, 101, pp. 366-378, ELSEVIER.

JONCKHEER, I., Fleck, S., Nackaerts, K., Muys, B., Coppin, P., Weiss,M., Baret, F. (2004): **Review of methods for in situ leaf area index determination, Part I: Theories, sensors and hemispherical photography.** In: Agricultural and Forest Methology, 121, pp. 19-35.

JORDAN, C.F., (1969): **Derivation of leaf area index from quality of light on the forest floor**. In: Ecology, 50, pp. 663-666.

KIENZLER, K. (2007): **Potential for increasing nitrogen use efficiency in cotton and winter wheat for irriganted agriculture in Khorezm, Uzbekistan**. PhD thesis, University of Bonn, Germany, forthcoming 2007.

KIM, M.S. (1994): **The use of narrow spectral bands for improving remote sensing estimation of fractionally absorbed photosynthetically active radiation**. Master Thesis, Department of Geography, University of Maryland, College Park, MD.

KNEUBÜHLER, M., Kötz, B., Richter, R., Schaepman, M., Itten, K.(2005): **Geometric and Radiometric**

Pre-Processing of CHRIS/Proba over Mountainous Terrain. 3rd CHRIS / Proba Workshop Frascati, RSL.

KONICA Minolta (1989): **Chlorophyll meter SPAD-502 instruction manual**.

LI-COR MANUAL: **LAI-2000 Plant Canopy Analyzer**. In: http://www.licor.com/env/PDF_Files/LAI2000.pdf

LIU, W.T., Kogan, F.N., (1996): **Monitoring regional drought using the Vegetation Condition Index**. In: International Journal of Remote Sensing, 17, 14, pp. 2761-2782.

LILLESAETER, O. (1982): **Spectral reflectance of partly transmitting leaves: Laboratory measurements and mathematical modeling**. Remote Sensing Environment, 12, pp. 247-254, ELSEVIER.

LEBLON, B. (2006): Soil and vegetation optical properties. In: Volume 4, applications in Remote Sensing, University of New Brunswick, Fredericton, Canada, http://www.r-s-c-c.org/rscc/Volume4/Leblon/leblon.htm .

MAJOR, D.J., Baret, F. and Guyot, G. (1990): **A ratio vegetation index adjusted for soil brightness**. In: International Journal of Remote Sensing, 11, pp. 727 – 740.

MARTIUS, C., Lamers, J., Ibraghimov, N., Vlek, P. (2004): **Towards a sudtainable use of natural resources in the aral sea basin**. Centre for Developing Research (ZEF), Bonn.

MAUNEY, J.R. (1984): **Anatomy and Morphology of Cultivated Cottons**. In: Kohel, R.J., Lewis, C.F. (Editors): Cotton. Agronomy, No.24, Madison, pp. 59-80.

MORAN, M.S., Inoue, Y., Barnes, E.M. (1997): **Opportunities and limitations from image-based remote senisng in precision crop management**. In: Remote Sensing of Environment, 61, pp. 319-346, ELSEVIER.

MOULIN, S., Bondeau, A., Delécolle, R., 1998: **Combining agricultural crop models and 613 satellite observations: from field to regional scales**. International Journal of Remote Sensing, 19, pp. 1021-1036.

MUTANGA, O., Skidmore, A.K., Prins, H.H.T. (2004): **Predicting in situ pasture quality in the**

. Kruger National Park, South Africa, Using continuum-removed absorption features. In: Remote Sensing of Environment, 89 (3), pp. 393-408, ELSEVIER.

NETES, J., Kutner, M.H., Nachtsheim, L.J., Wasserman, W. (1996): **Applied linear statistical models**. Boston, Masachusetts.

PIDWIRNY (1999): **Vital water graphics**. Website of the UNEP. In: http://www.unep.org/vitalwater/25.htm Last accessed: 17.03.07

QI, J., Chebouni, A., Huete, A.R., Kerr, Y.H., Sorooshian, S. (1994): **A modified soil adjusted vegetation index**. In: Remote Sensing of Environment, 48, 2, pp. 119-126, ELSEVIER.

QUARMBY, N.A., Milnes, M., Hindle, T.L., Silleos, N., 1993: **The use of multi-temporal NDVI measurements from AVHRR data for crop yield estimation and prediction**. In: International Journal of Remote Sensing, 14, pp. 199-210.

RASULOV, A.M. (1989): **Soils for the USSR Cotton Belt,** Cotton Compendium (in Uzbek) Tashkent.

RICHARDS, J. A. (1995): **Remote Sensing Digital Image Analysis,** 2nd edition. Springer Verlag. Berlin Heidelberg New York.

RICHARDSON, A.J., Wiegand, C.L. (1977): **Distinguishing vegetation from soil background ... information (by gray mapping of Landsat MSS data)**. Photogrammetric Eng. Remote Sensing, 43, pp. 1541-1552.

RICHTER, R. (2006); **Atmospheric / Topographic Correction for Satellite Imagery**. ATCOR-2/3 User Guide, Version 6.3 BETA, Eigenverlag, Oberpfaffenhofen.

RONDEAUX, G., Steven, M., Baret, F. (1996): **Optimization of Soil-Adjusted Vegetation Indices**. In: Remote Sensing of Environment, 55, pp. 95-107, ELSEVIER.

ROUJEAN, J.-L., Breon, F.-M.(1995): **Estimating PAR Absorbed by Vegetation from Bidirectional Reflectance Measurements**, In: Remote Sensing of Environment, 51, pp. 375 – 384, ELSEVIER.

RÜCKER, G., CONRAD, C. (2003): **Exploring Leaf Area Index Development and Land Cover Classification in the Lower Amu-Darya Basin in Uzbekistan on Multi-Temporal and Multi-Spatial Remote Sensing Data**. ZEF Work Papers for Sustainable Development in

Central Asia, No.5.

RÜCKER, G., Strunz, G., Lamers, J., Ibragimov, N., Kienzler, K. (2005): **Remote sensing based estimation of chlorophyll and nitrogen concentration in fields of cotton in Khorezm**. Midterm Report 2005.

RÜCKER, G., Dorigo, W.A., Lamers, J., Ibragimov, N., Kienzler, K., Strunz, G., Mueller, A., Vlek P.L.G. (2006): **Regional estimation of leaf chlorophyll in cotton in Uzbekistan by upscaling a vegetation Index from plant scale to Proba-1/CHRIS Hyperspectral Satellite Data**. Proba-1/CHRIS Workshop 2006.

SCHARF, P.C., Lory. J.A (2002): **Calibrating corn color from aerial photographs to predict sidedress nitrogen need**. In: Agron. J., 94, pp. 397-404.

SIMS, D.A., Gamon, J.A. (2002): **Relationships between leaf pigment content and spectral reflectance across a wide range of species, leaf structures and developmental stages**. In: Remote Sensing of Environment, 81, pp. 337-354, ELSEVIER.

SMITH, M., Allen, R., Monteith, J.L., Pereira, L.A, Perrier, A., Segeren, A., 1991: **Report on the expert consultation for the revision of FAO methodology of crop water requirements**. In: FAO / AGL, Rome.

SRIPADA, R.P.,. Heiniger, R.W., White,J.G., Weisz, R. (2005): **Aerial color infrared photography for determining late-season nitrogen requirements in corn.** In: Agron. J., 319, 97, pp. 1443-1451.

TESTON, F. (2004): **Overview of Proba Mission**. 2nd ESA CHRIS/Proba Workshop 2004, ESA Special Publication SP-578, CD-Rom.

THIAM, A., Eastman, J.R. (2001): **Vegetation Indices**. In: idrisi32 Guide to GIS and Image Processing Volume 2, Clark University, Worchester, Massachusets.

VLEK, P.L.G., Frohberg, K., Debiel, T. (2003): **Field Research and Development of a restructuring concept (2004-2006)**. In: Economic and Ecological Restructuring of Land- and Water Use in the Region Khorezm (Uzbekistan) Project Phase II, Bonn.

WADDLE, B.A. (1984): **Crop Growing Practices**. In: Kohel, R.J. & Lewis, C.F. (Editors): Cotton, Agronomy, No.24, Madison, pp. 234-263.

WAMUNYIMA, S. (2005): **Estimating Fresh Grass Biomass at Landscape Level Using Hyperspectral Remote Sensing**. Thesis Msc GISc, International Institute for Geo-Information Science and Earth Observation, Enschede, the Netherlands.

WATSON, D.J. (1947): **Comparative physiological studies in the growth of field crops**. In: Ann. Bot. 11, pp. 41-76.

WEISS, M., Baret, F., Leroy, M., Hautecoeur, O., Prevot, L., Bruguier, N. (2000): **Validation of neural network techniques for the estimation of canopy biophysical variables from vegetation data** in: Vegetation – 2000, Lago Maggiore, Italy. (http://vegetation.cnes.fr/)

WEISS, M., Baret, F., Smith, G.J., Jonckheere, I., Coppin, P. (2004): **Rieview of methods for in situ leaf area index (LAI) dermintaion, Part II: Estimation of LAI, errors and sampling**. In: Agricultural and Forest Methology, 121, pp. 37-53.

WELLES, J.M., Norman, J.M. (1991): **Instrument for Indirect Measurement of Canopy Architecture**. In: Agronomy Journal, 83, No.5, pp. 37-53.

WITT, H. (1998): **Die spektralen und räumlichen Eigenschaften von Fernerlundungssensoren bei der Ableitung von Vegetationsparametern**. Dissertation, Freie Universität Berlin, Fachbereich Geowissenschaften.

ZARCO – TEJADA , P.J., Berjon, A., Lopez – Lozano, R., Miller, J.R., Martin, P., Cachorro, V., Gonzalez, M.R., de Frutos, A. (2005 (1)): **Assessing vineyard condition with hyperspectral indices: Leaf and canopy reflectance simulation in a row-structured discontinuous canopy.** In: remote Sensing of Environment, 99, pp. 271 – 287, ELSEVIER

ZARCO – TEJADA, P.J., Ustin, S.L., Whiting, M.L. (2005 (2)): **Temporal and Spatial Relationsships between Within-Field Yield Variability in Cotton and High-Spatial Hyperspectral Remote Sensing Imagery**. In: Agronomy Journal, 97, No. 3, pp. 641-653.

ZEF BONN (2003): **Economic and Ecological Restructuring of Land- and Water Use in the Region Khorezm, Uzbekistan**. Project Phase II Field Research and Development of a Restructuring Concept (2004-2006). Eigenverlag. Bonn.

8.Appendix

Table 8.1: Input data for atmospheric correction process ATCOR for all Proba-1/CHRIS images

Date	View angle nominal [degree]	Observation zenith angle [degree]	Observation azimuth angle [degree]	Solar zenith angle [degree]	Visibility [Km]
20.06.06	-55	53,08	195,45	21	23
20.06.06	-36	33,81	197,2	21	23
20.06.06	0	4,7	218,24	21	23
20.06.06	36	28,46	7,74	21	23
20.06.06	55	50,3	10,4	21	23
28.06.06	-55	52,26	184	22	21
28.06.06	-36	33,69	176,34	22	21
28.06.06	0	10,89	139,12	22	21
28.06.06	36	29,02	27,81	22	21
28.06.06	55	49,57	20,24	22	21
07.07.06	-55	51,52	191,83	23	41
07.07.06	-36	32,34	190,62	23	26
07.07.06	0	3,91	170,34	23	21
07.07.06	36	26,73	15,46	23	26
07.07.06	55	48,16	13,86	23	41
16.07.06	-55	51,9	199,01	24	41
16.07.06	-36	32,96	203,2	24	41
16.07.06	0	8,01	224,29	24	21
16.07.06	36	27,44	359,54	24	41
16.07.06	55	48,31	6,77	24	41
02.08.06	-55	53,71	195,34	27	41
02.08.06	-36	34,05	197,03	27	41
02.08.06	0	4,46	218,43	27	21
02.08.06	36	28,56	7,99	27	41
02.08.06	55	50,05	10,51	27	n.a.

Table 8.2: Statistics for Leaf Scale computed for VIs and C_{ab}

Total: 20 Leaves	Min	Max	Range	Mean	StdV	CV	R^2
NDVI	0,64	0,85	0,21	0,73	0,06	7,94	0,4366
RVI	4,52	12,5	7,98	6,8	1,95	28,72	0,4828
SAVI	0,51	0,65	0,14	0,57	0,04	6,49	0,4148
SAVI2	3,41	6,69	3,28	4,54	0,82	17,99	0,4741
MSAVI	0,51	0,7	0,19	0,59	0,05	8,3	0,4402
OSAVI	0,58	0,75	0,18	0,66	0,05	7,16	0,4368
TSAVI	0,59	0,83	0,24	0,7	0,07	9,47	0,4382
ATSAVI	-0,24	-0,14	0,11	-0,2	0,03	-14,74	0,4339
RDVI	0,48	0,61	0,13	0,54	0,03	6,45	0,4127
TVI	22,7	29,24	6,55	26,37	1,78	6,77	0,3201
MTVI1	0,57	0,75	0,18	0,67	0,05	6,97	0,3433
MTVI2	0,51	0,79	0,27	0,63	0,07	10,45	0,5179
CARI	0,25	0,42	0,17	0,33	0,05	14,48	0,9160
TCARI	0,13	0,25	0,11	0,19	0,03	15,35	0,4134
MCARI	0,04	0,08	0,04	0,06	0,01	15,33	0,4116
MCARI1	0,57	0,75	0,18	0,67	0,05	6,97	0,3425
MCARI2	0,51	0,78	0,27	0,63	0,07	10,44	0,5169
MTCI	1,39	2,58	1,19	1,85	0,3	16,12	0,3697
LCI	0,3	0,44	0,14	0,36	0,03	8,48	0,0251
SR705	2,63	4,27	1,64	3,34	0,38	11,31	0,0308
mND705	0,62	0,79	0,18	0,68	0,04	6,44	0,1395
GI	0,34	0,71	0,37	0,55	0,09	15,94	0,5877
PRI	-0,07	-0,01	0,05	-0,04	0,01	-30,86	0,3183
REIP	0,72	0,72	0	0,72	0	0,15	0,4330
REIP	0,7	0,72	0,01	0,71	0,01	0,75	0,2854
DGVI1	0,35	0,43	0,08	0,4	0,02	6,25	0,2699
DGVI2	0,01	0,01	0	0,01	0	8,01	0,0668
NDNI	0,14	0,19	0,05	0,18	0,01	7,31	0,0024
NDLI	0,05	0,07	0,02	0,05	0	9,06	0,0247
CAI	-0,01	0	0,01	-0,01	0	-36,06	0,5046
CAI2	-0,37	-0,18	0,19	-0,28	0,05	-15,99	0,2917
CSI2	0,23	0,38	0,15	0,3	0,03	11,18	0,0439
NDWI_MIR	0,53	0,66	0,14	0,58	0,03	5,16	0,0232
MSI	0,45	0,6	0,15	0,55	0,04	6,82	0,5301
LWVI1	0,01	0,03	0,02	0,02	0	22,73	0,6384
LWVI2	0,03	0,08	0,04	0,05	0,01	18	0,5483
DWSI5	1,57	1,94	0,37	1,69	0,09	5,06	0,0784
SWIRVI	1,66	2,54	0,88	2,09	0,23	10,99	0,3519
SWIRLI	0,11	0,41	0,3	0,25	0,09	34,47	0,1797
SWIRSI	-1,03	-0,32	0,71	-0,68	0,19	-27,52	0,4303
LAI 1	2,48	3,73	1,25	3,02	0,34	11,22	0,4366
LAI 2	2,99	4,69	1,7	3,62	0,45	12,32	0,4616
LAI 3	1,57	3,61	2,04	2,15	0,5	23,17	0,4828
LAI 4	2,22	2,96	0,74	2,6	0,22	8,45	0,3968
LAI 5	0,83	4,62	3,79	1,91	0,93	48,59	0,4828
LAI 6	0,98	3,58	2,59	1,72	0,63	36,85	0,4828
LAI 7	1,46	3,93	2,48	2,27	0,56	24,88	0,5260
LAI 8	1,62	3,63	2,02	2,42	0,5	20,43	0,4305
LAI 9	5,79	13,3	7,51	8,5	1,8	21,13	0,4561
LAI 10	2,47	4,97	2,5	3,63	0,65	17,8	0,3918
Ca+b	3,65	3,86	0,21	3,76	0,05	1,44	0,4331
Ca+b	9,55	26,82	17,28	16,24	4,44	27,34	0,1440

Table 8.3: Statistics for plant scale dataset for VIs and LAI / C_{ab} Stage 1 (20.06.06)

Total: 134	Min	Max	Range	Mean	STDV	CV	R² Cab	R² LAI
NDVI	0,28	0,77	0,48	0,58	0,08	14,48	0,00005	0,00120
RVI	1,79	7,51	5,72	3,93	1,05	26,75	0,00007	0,00001
SAVI	0,17	0,6	0,43	0,42	0,07	17,42	0,00003	0,00020
SAVI2	1,4	4,73	3,33	2,86	0,6	21,02	0,00001	0,00020
MSAVI	0,15	0,62	0,47	0,41	0,08	20,25	0,00005	0,00010
OSAVI	0,22	0,67	0,45	0,5	0,08	15,25	0,00000	0,00040
TSAVI	0,11	0,73	0,62	0,51	0,1	20,03	0,00006	0,00110
ATSAVI	-0,42	-0,18	0,24	-0,28	0,04	-15,24	0,00002	0,00090
RDVI	0,16	0,57	0,4	0,4	0,07	17,26	0,00002	0,00050
TVI	4,85	28,82	23,97	17,2	4,41	25,64	0,00200	0,00005
MTVI1	0,11	0,73	0,62	0,44	0,11	26,22	0,00220	0,00010
MTVI2	0,1	0,64	0,54	0,4	0,1	24,64	0,00220	0,00000
CARI	0,01	0,39	0,38	0,19	0,07	38,75	0,00020	0,00130
TCARI	0,04	0,25	0,21	0,14	0,04	29,75	0,09620	0,00700
MCARI	0,01	0,08	0,07	0,05	0,01	29,83	0,09570	0,00700
MCARI1	0,11	0,73	0,62	0,44	0,11	26,27	0,00220	0,00010
MCARI2	0,1	0,64	0,54	0,39	0,1	24,69	0,00210	0,00000
MTCI	1,14	2,31	1,16	1,72	0,26	15,13	0,35180	0,04990
LCI	0,15	0,4	0,25	0,29	0,04	14,64	0,09250	0,02210
SR705	1,47	3,54	2,07	2,42	0,37	15,2	0,04010	0,01080
mND705	0,3	0,7	0,4	0,55	0,06	11,12	0,11700	0,02270
GI	0,52	1,16	0,64	0,8	0,1	13,19	0,02020	0,01310
PRI	-0,12	-0,03	0,08	-0,06	0,02	-24,4	0,10930	0,00960
REIP	0,71	0,72	0,01	0,72	0	0,17	0,33340	0,04590
REIP	0,7	0,72	0,02	0,72	0,01	0,8	0,11610	0,00050
DGVI1	0,09	0,45	0,36	0,27	0,06	24,06	0,00040	0,00020
DGVI2	0	0,01	0,01	0,01	0	25,11	0,00010	0,00120
NDNI	0,05	0,2	0,15	0,13	0,03	21,79	0,00010	0,00030
NDLI	0,02	0,06	0,05	0,04	0,01	21,77	0,02280	0,02280
CAI	-0,01	0,01	0,02	-0,01	0	-31,76	0,00760	0,03460
CAI2	-0,35	-0,04	0,31	-0,17	0,06	-36,46	0,00005	0,00280
CSI2	0,28	0,68	0,4	0,42	0,06	15,31	0,03460	0,01180
NDWI_MIR	0,21	0,68	0,46	0,49	0,08	16,94	0,01530	0,00250
MSI	0,45	0,79	0,34	0,57	0,06	10,22	0,00750	0,00001
LWVI1	0,02	0,03	0,01	0,02	0	12,18	0,00270	0,02720
LWVI2	0,03	0,08	0,05	0,06	0,01	22,61	0,01970	0,00050
DWSI5	1,09	1,95	0,86	1,52	0,15	9,71	0,00020	0,00070
SWIRVI	0,57	2,17	1,6	1,39	0,35	25,47	0,00920	0,00050
SWIRLI	-0,29	0,33	0,62	0,03	0,13	420,08	0,02680	0,00030
SWIRSI	-0,72	0,58	1,3	-0,08	0,27	-331,16	0,00360	0,00080
LAI 1	0,41	3,22	2,81	2,12	0,49	23,01	0,00005	0,00120
LAI 2	1,7	3,86	2,16	2,71	0,4	14,81	0,00001	0,00050
LAI 3	0,87	2,33	1,46	1,42	0,27	18,72	0,00003	0,00020
LAI 4	0,83	2,75	1,91	1,97	0,34	17,24	0,00004	0,00100
LAI 5	-0,47	2,25	2,72	0,54	0,5	92,33	0,00000	0,00040
LAI 6	0,09	1,95	1,86	0,79	0,34	43,41	0,00000	0,00040
LAI 7	0,32	2,32	1,99	1,01	0,38	37,63	0,00330	0,02060
LAI 8	0,25	2,79	2,54	1,08	0,46	42,55	0,00010	0,02460
LAI 9	1,25	9,35	8,1	4,02	1,48	36,84	0,00020	0,00030
LAI 10	1,85	4,61	2,76	3,34	0,63	18,96	0,34630	0,04980
Ca+b	3,56	3,83	0,27	3,73	0,06	1,59	0,33340	0,04590
Ca+b	2,43	34,77	32,33	19,45	6,57	33,78	0,14320	0,01890

Table 8.4: Statistics for plant scale dataset for VIs and LAI / C_{ab} Stage 2 (28.06.06)

Total: 140	Min	Max	Range	Mean	StdV	CV	R² Cab	R² LAI
NDVI	0,46	0,84	0,37	0,68	0,08	11,39	0,0426	0,2232
RVI	2,73	11,36	8,64	5,59	1,78	31,89	0,0236	0,2483
SAVI	0,28	0,64	0,36	0,5	0,06	12,82	0,0395	0,1831
SAVI2	1,99	5,81	3,82	3,76	0,82	21,75	0,0329	0,2573
MSAVI	0,25	0,68	0,43	0,5	0,08	15,44	0,0374	0,1913
OSAVI	0,36	0,73	0,36	0,59	0,07	11,42	0,0472	0,2279
TSAVI	0,35	0,82	0,47	0,63	0,09	14,35	0,0461	0,2272
ATSAVI	-0,33	-0,15	0,18	-0,23	0,04	-16,94	0,0443	0,2292
RDVI	0,27	0,6	0,34	0,47	0,06	12,73	0,0383	0,1835
TVI	9,19	31,73	22,54	21,24	4,07	19,14	0,0192	0,0923
MTVI1	0,23	0,81	0,58	0,54	0,1	19,35	0,0183	0,0907
MTVI2	0,21	0,73	0,52	0,51	0,09	18,49	0,0324	0,1879
CARI	-0,02	0,39	0,41	0,2	0,09	43,72	0,0063	0,0009
TCARI	0,08	0,25	0,17	0,17	0,03	20,22	0,0095	0,0247
MCARI	0,03	0,08	0,06	0,05	0,01	20,24	0,0097	0,0247
MCARI1	0,23	0,81	0,58	0,54	0,1	19,37	0,0184	0,0911
MCARI2	0,21	0,73	0,52	0,51	0,09	18,52	0,0326	0,1882
MTCI	1,3	2,19	0,88	1,72	0,15	8,96	0,0105	0,1414
LCI	0,23	0,44	0,22	0,33	0,04	11,1	0,0447	0,2943
SR705	1,92	4,21	2,29	2,87	0,42	14,63	0,0329	0,2763
mND705	0,43	0,69	0,25	0,6	0,04	6,38	0,0303	0,2145
GI	0,43	0,98	0,55	0,66	0,1	15,73	0,0260	0,1870
PRI	-0,12	-0,03	0,09	-0,06	0,02	-25,33	0,0126	0,0205
REIP	0,71	0,72	0	0,72	0	0,09	0,0095	0,1307
REIP	0,7	0,72	0,01	0,72	0	0,36	0,0177	0,0565
DGVI1	0,15	0,48	0,33	0,33	0,06	18,23	0,0211	0,0962
DGVI2	0	0,01	0,01	0,01	0	19,4	0,0138	0,0747
NDNI	0,08	0,21	0,13	0,16	0,02	15,42	0,0007	0,0477
NDLI	0,02	0,06	0,04	0,04	0,01	14,9	0,0228	0,0228
CAI	-0,01	0	0,01	-0,01	0	-24	0,0061	0,0358
CAI2	-0,36	-0,08	0,28	-0,23	0,05	-21,61	0,0002	0,0939
CSI2	0,24	0,52	0,28	0,36	0,05	14,24	0,0456	0,2538
NDWI_MIR	0,29	0,69	0,39	0,56	0,06	9,76	0,0199	0,1917
MSI	0,42	0,73	0,31	0,52	0,04	8,4	0,0575	0,2699
LWVI1	0,02	0,04	0,02	0,03	0	15,39	0,0520	0,2426
LWVI2	0,02	0,09	0,07	0,06	0,01	18,9	0,0788	0,2397
DWSI5	1,2	2,11	0,91	1,7	0,15	8,96	0,0396	0,3003
SWIRVI	0,76	2,55	1,78	1,66	0,31	18,45	0,0008	0,0147
SWIRLI	-0,21	0,45	0,66	0,14	0,11	77,4	0,0027	0,0244
SWIRSI	-0,99	0,39	1,38	-0,28	0,24	-87,26	0,0002	0,0102
LAI 1	1,46	3,65	2,19	2,7	0,45	16,65	0,0426	0,2232
LAI 2	2,21	4,54	2,34	3,27	0,5	15,37	0,0337	0,2372
LAI 3	1,11	3,32	2,2	1,84	0,45	24,69	0,0236	0,2483
LAI 4	1,51	2,95	1,44	2,38	0,31	13,14	0,0443	0,2150
LAI 5	-0,02	4,08	4,1	1,33	0,85	63,48	0,0236	0,2483
LAI 6	0,4	3,21	2,81	1,33	0,58	43,59	0,0236	0,2483
LAI 7	0,49	3,21	2,73	1,52	0,53	34,88	0,0206	0,0206
LAI 8	0,46	3,46	3	1,67	0,6	36,1	0,0246	0,0246
LAI 9	1,94	12,04	10,1	5,96	1,99	33,33	0,0249	0,1999
LAI 10	2,24	4,33	2,09	3,27	0,36	11,04	0,0071	0,1288
Ca+b	3,62	3,81	0,2	3,73	0,03	0,9	0,0095	0,1306
Ca+b	6,96	29,79	22,84	18,06	4,99	27,62	0,0003	0,0139

Table 8.5: Statistics for plant scale dataset for VIs and LAI / C_{ab} Stage 3 (16.07.06)

Total: 128	Min	Max	Range	Mean	StdV	CV	R² Cab	R² LAI
NDVI	0,54	0,91	0,368	0,750	0,060	8,03	0,0388	0,11410
RVI	3,37	21,24	17,867	7,568	2,589	34,21	0,0112	0,08160
SAVI	0,39	0,7	0,309	0,567	0,060	10,54	0,0731	0,17060
SAVI2	2,56	8,83	6,261	4,723	0,945	20,01	0,0337	0,14950
MSAVI	0,38	0,79	0,410	0,584	0,075	12,88	0,0696	0,17360
OSAVI	0,47	0,81	0,342	0,661	0,057	8,56	0,0671	0,17070
TSAVI	0,47	0,9	0,431	0,718	0,070	9,76	0,0443	0,12190
ATSAVI	-0,29	-0,11	0,188	-0,188	0,030	-16,08	0,0492	0,13900
RDVI	0,37	0,67	0,298	0,536	0,056	10,51	0,0721	0,16950
TVI	15,17	35,52	20,350	24,503	4,121	16,82	0,0487	0,11150
MTVI1	0,39	0,91	0,516	0,623	0,105	16,87	0,0444	0,10410
MTVI2	0,37	0,87	0,502	0,602	0,089	14,83	0,0478	0,13870
CARI	-0,2	0,34	0,539	0,127	0,105	82,36	0,0045	0,00180
TCARI	0,11	0,27	0,156	0,184	0,032	17,43	0,0028	0,00080
MCARI	0,04	0,09	0,052	0,061	0,011	17,43	0,0027	0,00080
MCARI1	0,39	0,91	0,516	0,622	0,105	16,87	0,0446	0,10450
MCARI2	0,37	0,87	0,502	0,602	0,089	14,83	0,0480	0,13920
MTCI	1,31	2,42	1,104	1,741	0,243	13,96	0,2430	0,20710
LCI	0,24	0,47	0,225	0,366	0,040	10,99	0,1890	0,24310
SR705	2,13	4,74	2,603	3,224	0,460	14,27	0,1038	0,19980
mND705	0,49	0,71	0,215	0,614	0,043	7,01	0,1822	0,18780
GI	0,28	0,83	0,547	0,587	0,095	16,28	0,0045	0,03140
PRI	-0,15	-0,04	0,107	-0,080	0,018	-22,53	0,0264	0,00060
REIP	0,72	0,72	0,005	0,717	0,001	0,14	0,2548	0,19610
REIP	0,7	0,72	0,014	0,717	0,003	0,49	0,1896	0,05740
DGVI1	0,23	0,54	0,310	0,378	0,062	16,43	0,0578	0,12720
DGVI2	0,01	0,01	0,007	0,008	0,001	17,71	0,0447	0,11090
NDNI	0,12	0,22	0,104	0,164	0,021	12,63	0,0431	0,09950
NDLI	0,03	0,05	0,024	0,043	0,004	10,05	0,0228	0,02280
CAI	-0,01	0	0,006	-0,005	0,001	-23,27	0,0145	0,02090
CAI2	-0,38	-0,16	0,220	-0,271	0,043	-15,78	0,0273	0,10620
CSI2	0,21	0,47	0,258	0,316	0,044	13,99	0,1399	0,19900
NDWI_MIR	0,49	0,74	0,257	0,626	0,043	6,9	0,0901	0,18440
MSI	0,34	0,57	0,231	0,459	0,038	8,16	0,1038	0,21140
LWVI1	0,02	0,05	0,026	0,031	0,005	14,47	0,1200	0,11500
LWVI2	0,05	0,11	0,066	0,074	0,011	15,56	0,0596	0,09060
DWSI5	1,48	2,4	0,918	1,899	0,150	7,89	0,0667	0,17670
SWIRVI	1,18	2,47	1,288	1,786	0,275	15,4	0,0117	0,04290
SWIRLI	-0,01	0,42	0,432	0,193	0,096	49,84	0,0101	0,04370
SWIRSI	-0,94	0,12	1,055	-0,374	0,222	-59,46	0,0123	0,04180
LAI 1	1,92	4,07	2,146	3,134	0,352	11,23	0,0388	0,11410
LAI 2	2,51	5,4	2,884	3,786	0,482	12,74	0,0273	0,10850
LAI 3	1,28	5,84	4,561	2,348	0,661	28,15	0,0112	0,08160
LAI 4	1,83	2,96	1,133	2,663	0,214	8,04	0,0513	0,10630
LAI 5	0,28	8,77	8,487	2,274	1,230	54,08	0,0112	0,08160
LAI 6	0,61	6,42	5,807	1,972	0,841	42,66	0,0112	0,08160
LAI 7	0,86	5,36	4,500	2,121	0,691	32,56	0,0206	0,02060
LAI 8	0,84	5,04	4,194	2,414	0,774	32,07	0,0246	0,02460
LAI 9	3,29	19,03	15,738	8,452	2,629	31,1	0,05	0,17900
LAI 10	2,31	4,87	2,560	3,313	0,562	16,97	0,24	0,20130
Ca+b	3,63	3,85	0,225	3,730	0,051	1,38	0,25	0,19620
Ca+b	8,21	37,45	29,246	18,290	4,926	26,94	0,04	0,03640

Table 8.6: Statistics for plant scale dataset for VIs and LAI / C_{ab} Stage 4 (02.08.06)

Total: 144	Min	Max	Range	Mean	StdV	CV	R² Cab	R² LAI
NDVI	0,53	0,96	0,430	0,770	0,078	10,13	0,0048	0,11410
RVI	3,23	45,72	42,492	9,433	6,469	68,57	0,0026	0,00320
SAVI	0,41	0,75	0,339	0,614	0,059	9,56	0,0010	0,04290
SAVI2	2,57	11,4	8,831	5,377	1,503	27,96	0,0030	0,01270
MSAVI	0,4	0,86	0,455	0,643	0,077	11,97	0,0023	0,03850
OSAVI	0,47	0,85	0,375	0,696	0,063	9,1	0,0034	0,02040
TSAVI	0,46	0,95	0,494	0,743	0,088	11,82	0,0049	0,00540
ATSAVI	-0,3	-0,08	0,218	-0,175	0,038	-21,81	0,0043	0,00790
RDVI	0,39	0,73	0,341	0,582	0,057	9,76	0,0006	0,04500
TVI	17,3	42,57	25,271	27,472	4,256	15,49	0,0005	0,04890
MTVI1	0,44	1,09	0,649	0,701	0,109	15,58	0,0006	0,05100
MTVI2	0,38	0,94	0,569	0,658	0,099	15,12	0,0088	0,03090
CARI	-0,82	0,39	1,212	0,010	0,180	1877	0,0217	0,01460
TCARI	0,03	0,31	0,274	0,191	0,042	22,03	0,0253	0,00160
MCARI	0,01	0,1	0,093	0,063	0,014	22,22	0,0244	0,00160
MCARI1	0,44	1,09	0,649	0,700	0,109	15,57	0,0006	0,05100
MCARI2	0,37	0,95	0,572	0,658	0,099	15,13	0,0088	0,03080
MTCI	1,18	2,76	1,577	1,813	0,314	17,29	0,1192	0,06420
LCI	0,27	0,51	0,237	0,385	0,051	13,36	0,0462	0,04450
SR705	2,13	5,62	3,491	3,356	0,667	19,87	0,0133	0,02340
mND705	0,43	0,73	0,300	0,611	0,057	9,35	0,0451	0,02730
GI	0,21	0,93	0,720	0,601	0,140	23,32	0,0300	0,00330
PRI	-0,18	-0,04	0,146	-0,075	0,025	-33,57	0,0610	0,00920
REIP	0,71	0,72	0,007	0,718	0,001	0,19	0,1436	0,07650
REIP	0,7	0,72	0,019	0,717	0,003	0,48	0,0837	0,03560
DGVI1	0,28	0,65	0,377	0,429	0,064	14,96	0,0000	0,05090
DGVI2	0,01	0,01	0,009	0,009	0,002	16,94	0,0005	0,03500
NDNI	0,13	0,22	0,097	0,167	0,020	12,17	0,0023	0,03280
NDLI	0,04	0,06	0,026	0,049	0,005	10,67	0,0228	0,02280
CAI	-0,01	0	0,008	-0,005	0,002	-32,29	0,0046	0,04310
CAI2	-0,38	-0,15	0,229	-0,287	0,053	-18,33	0,0042	0,01580
CSI2	0,18	0,47	0,292	0,309	0,057	18,51	0,0108	0,02610
NDWI_MIR	0,53	0,8	0,275	0,681	0,045	6,65	0,0082	0,12770
MSI	0,28	0,5	0,225	0,399	0,043	10,81	0,0156	0,15800
LWVI1	0,03	0,07	0,041	0,041	0,008	18,36	0,0301	0,10810
LWVI2	0,08	0,18	0,108	0,118	0,019	16,05	0,0285	0,13510
DWSI5	1,67	3,21	1,549	2,135	0,251	11,75	0,0000	0,09850
SWIRVI	1,03	2,5	1,467	1,768	0,275	15,58	0,0081	0,00380
SWIRLI	-0,08	0,45	0,531	0,182	0,098	53,92	0,0087	0,00760
SWIRSI	-0,94	0,21	1,153	-0,365	0,222	-60,72	0,0075	0,00220
LAI 1	1,83	4,34	2,510	3,248	0,455	14,02	0,0048	0,00430
LAI 2	2,45	6,09	3,635	3,984	0,693	17,4	0,0049	0,00470
LAI 3	1,24	12,09	10,848	2,824	1,651	58,47	0,0026	0,00320
LAI 4	0,27	2,96	2,692	2,633	0,375	14,25	0,0014	0,00003
LAI 5	0,21	20,4	20,184	3,160	3,073	97,24	0,0026	0,00320
LAI 6	0,56	14,37	13,810	2,578	2,102	81,54	0,0026	0,00320
LAI 7	0,88	7,04	6,165	2,642	1,076	40,73	0,0206	0,02060
LAI 8	0,95	7,34	6,388	3,202	1,128	35,24	0,0246	0,02460
LAI 9	3,69	25,84	22,150	10,953	3,854	35,19	0,0005	0,03150
LAI 10	2,04	6,3	4,266	3,612	0,794	21,99	0,1285	0,07140
Ca+b	3,59	3,93	0,341	3,753	0,067	1,79	0,1436	0,07650
Ca+b	5,63	78,01	72,376	19,279	9,942	51,57	0,0116	0,00030

Table 8.7: Statistics for regional scale dataset for VIs and C_{ab} Stage 1 (20.06.06)

Stage 1	Min	Max	Range	Mean	STDV	CV	R^2 C_{ab}
NDVI	0,07	0,41	0,34	0,2	0,09	44,29	0,0091
RVI	1,16	2,43	1,27	1,53	0,3	19,52	0,0121
SAVI	0,05	0,28	0,22	0,14	0,06	41,77	0,0010
SAVI2	1	1,89	0,89	1,28	0,21	16,51	0,0036
MSAVI	0,05	0,25	0,21	0,12	0,05	42,48	0,0002
OSAVI	0,06	0,34	0,28	0,17	0,07	42,93	0,0039
TSAVI	-0,13	0,3	0,42	0,03	0,11	335,55	0,0045
ATSAVI	-0,54	-0,36	0,18	-0,47	0,05	-10,04	0,0118
RDVI	0,05	0,26	0,21	0,13	0,06	41,94	0,0012
TVI	-0,29	9,21	9,5	3,59	2,56	71,25	0,0001
MTVI1	-0,04	0,23	0,26	0,07	0,07	102,99	0,0013
MTVI2	-0,03	0,2	0,23	0,06	0,06	104,63	0,0031
CARI	0,12	0,19	0,07	0,17	0,02	9,54	0,1601
TCARI	-0,03	0,05	0,08	0	0,02	1030,2	0,0370
MCARI	-0,01	0,02	0,03	0	0,01	1000,7	0,0295
MCARI1	-0,04	0,23	0,26	0,07	0,07	102,99	0,0013
MCARI2	-0,03	0,2	0,23	0,06	0,06	104,63	0,0031
SR705	1,13	1,96	0,83	1,41	0,21	15,01	0,0036
mND705	0,1	0,4	0,31	0,23	0,09	37,79	0,0000
GI	1,05	1,33	0,29	1,24	0,07	5,71	0,0214
PRI	-0,11	-0,08	0,03	-0,09	0,01	-8,35	0,0261
REIP	0,72	0,73	0,01	0,72	0	0,3	0,1363
REIP	0,71	0,73	0,02	0,71	0,01	0,79	0,3012
DGVI1	0,03	0,16	0,13	0,08	0,03	40,49	0,0003
DGVI2	0	0,02	0,01	0,01	0	46,88	0,0001
CSI2	0,52	0,88	0,37	0,73	0,1	14,38	0,0029
LAI 1	-0,83	1,15	1,97	-0,09	0,51	-600,5	0,0092
LAI 2	1,32	2,05	0,73	1,54	0,17	11,33	0,0115
LAI 3	0,71	1,04	0,32	0,81	0,08	9,46	0,0122
LAI 4	0,07	1,31	1,24	0,53	0,32	60,48	0,0094
LAI 5	-0,77	-0,17	0,6	-0,59	0,14	-23,93	0,0121
LAI 6	-0,11	0,3	0,41	0,01	0,1	937,35	0,0121
LAI 7	0,2	0,47	0,27	0,28	0,06	22,56	0,0034
LAI 8	0,12	0,45	0,33	0,21	0,07	34,6	0,0010
LAI 9	0,81	1,98	1,17	1,16	0,27	23,38	0,0000
LAI 10	5,49	29,65	24,16	10,35	4,86	46,92	0,1064
Ca+b	3,89	4,34	0,45	4,05	0,11	2,7	0,1478
Ca+b	1	101,86	100,86	19,58	28,46	145,33	0,0015

Table 8.8: Statistics for regional scale dataset for VIs and LAI / C_{ab} Stage 2 (28.06.06)

Stage 2	Min	Max	Range	Mean	STDV	CV	R^2 LAI	R^2 C_{ab}
NDVI	0,12	0,49	0,37	0,3	0,11	37,13	0,0919	0,2044
RVI	1,28	2,91	1,63	1,94	0,48	24,65	0,1190	0,2177
SAVI	0,09	0,36	0,27	0,23	0,08	36,75	0,0831	0,2024
SAVI2	1,11	2,3	1,19	1,62	0,35	21,82	0,1101	0,2171
MSAVI	0,08	0,35	0,26	0,21	0,08	38,15	0,0847	0,2043
OSAVI	0,11	0,43	0,32	0,27	0,1	36,93	0,0882	0,2042
TSAVI	-0,06	0,41	0,46	0,18	0,14	79,85	0,0905	0,2060
ATSAVI	-0,52	-0,32	0,19	-0,42	0,06	-14,25	0,0880	0,2002
RDVI	0,09	0,34	0,26	0,22	0,08	36,75	0,0828	0,2031
TVI	1,5	14,08	12,59	8,17	4,03	49,35	0,0727	0,2015
MTVI1	0,01	0,35	0,34	0,18	0,11	58,08	0,0748	0,1966
MTVI2	0,01	0,3	0,29	0,15	0,09	60,14	0,0850	0,2019
CARI	0,15	0,22	0,07	0,19	0,01	7,47	0,0168	0,0004
TCARI	-0,02	0,08	0,09	0,03	0,03	90,69	0,0350	0,2035
MCARI	-0,01	0,03	0,03	0,01	0,01	90,64	0,0956	0,1794
MCARI1	0,01	0,35	0,34	0,18	0,11	58,08	0,0748	0,1966
MCARI2	0,01	0,3	0,29	0,15	0,09	60,14	0,0850	0,2019
SR705	1,23	2,26	1,03	1,7	0,32	19,04	0,0939	0,2244
mND705	0,17	0,47	0,3	0,34	0,1	30,46	0,0571	0,1950
GI	0,97	1,29	0,32	1,15	0,09	8,15	0,1005	0,1879
PRI	-0,1	-0,07	0,03	-0,08	0,01	-9,65	0,0487	0,1171
REIP	0,72	0,73	0,01	0,72	0	0,17	0,2331	0,0588
REIP	0,71	0,72	0,01	0,71	0	0,41	0,0257	0,0301
DGVI1	0,06	0,24	0,18	0,16	0,06	36,52	0,0693	0,1984
DGVI2	0,01	0,03	0,02	0,01	0,01	45,58	0,0892	0,2142
CSI2	0,44	0,81	0,37	0,61	0,12	19,4	0,0722	0,2021
LAI 1	-0,53	1,6	2,13	0,51	0,65	127,57	0,0916	0,2044
LAI 2	1,39	2,3	0,9	1,78	0,27	15,14	0,1130	0,2159
LAI 3	0,74	1,16	0,42	0,91	0,12	13,41	0,1191	0,2179
LAI 4	0,25	1,61	1,36	0,91	0,41	45,69	0,0943	0,2060
LAI 5	-0,71	0,06	0,78	-0,4	0,23	-57,3	0,1191	0,2177
LAI 6	-0,07	0,46	0,53	0,14	0,16	107,81	0,1185	0,2173
LAI 7	0,23	0,67	0,44	0,41	0,13	32,04	0,1049	0,2113
LAI 8	0,15	0,71	0,56	0,38	0,17	44,22	0,1118	0,2181
LAI 9	0,94	2,91	1,97	1,77	0,59	33,42	0,1048	0,2153
LAI 10	4,7	13,72	9,03	6,95	1,53	22,06	0,1034	0,0934
Ca+b	3,84	4,15	0,31	3,95	0,06	1,48	0,1199	0,0963

Table 8.9: Statistics for regional scale dataset for VIs and LAI / C_{ab} Stage 3 (16.07.06)

Stage 3	Min	Max	Range	Mean	STDV	CV	R^2 LAI	R^2 C_{ab}
NDVI	0,43	0,82	0,38	0,64	0,12	18,73	0,5388	0,2718
RVI	2,53	9,93	7,39	5,32	2,27	42,61	0,5094	0,1692
SAVI	0,28	0,55	0,27	0,41	0,08	18,65	0,5200	0,3866
SAVI2	1,94	5,23	3,3	3,26	0,95	29,24	0,5367	0,2584
MSAVI	0,25	0,57	0,31	0,4	0,09	22,13	0,5118	0,3784
OSAVI	0,35	0,68	0,33	0,52	0,1	18,39	0,5436	0,3416
TSAVI	0,32	0,79	0,47	0,57	0,14	25,3	0,5439	0,2866
ATSAVI	-0,35	-0,16	0,19	-0,25	0,06	-22,74	0,5377	0,2967
RDVI	0,27	0,52	0,26	0,39	0,07	18,56	0,5288	0,3734
TVI	9,19	20,83	11,64	14,6	3,26	22,36	0,4673	0,4025
MTVI1	0,22	0,52	0,3	0,36	0,08	23,16	0,4673	0,3995
MTVI2	0,21	0,58	0,37	0,37	0,11	28,55	0,5228	0,3298
CARI	0,02	0,13	0,1	0,09	0,03	29,06	0,0789	0,0002
TCARI	0,05	0,1	0,05	0,08	0,02	19,87	0,4721	0,0468
MCARI	0,02	0,03	0,02	0,03	0,01	19,79	0,4294	0,1812
MCARI1	0,22	0,52	0,3	0,36	0,08	23,16	0,4673	0,3995
MCARI2	0,21	0,58	0,37	0,37	0,11	28,55	0,5228	0,3298
SR705	1,97	4,82	2,86	3,14	0,79	25,2	0,5264	0,3010
mND705	0,37	0,66	0,3	0,52	0,08	16,19	0,5382	0,3478
GI	0,56	1,07	0,51	0,85	0,16	18,84	0,4884	0,1417
PRI	-0,16	-0,1	0,06	-0,12	0,01	-12,3	0,0010	0,0985
REIP	0,72	0,72	0	0,72	0	0,14	0,0426	0,2109
REIP	0,7	0,72	0,02	0,71	0,01	0,79	0,0563	0,2789
DGVI1	0,16	0,34	0,17	0,24	0,05	19,97	0,4336	0,4317
DGVI2	0,02	0,04	0,02	0,03	0,01	22,14	0,4342	0,4114
CSI2	0,21	0,51	0,3	0,34	0,09	25,34	0,5265	0,3753
LAI 1	1,29	3,51	2,23	2,48	0,7	28,17	0,5384	0,2721
LAI 2	2,11	4,32	2,21	3,12	0,7	22,32	0,5420	0,2167
LAI 3	1,06	2,95	1,89	1,77	0,58	32,61	0,5094	0,1691
LAI 4	1,4	2,9	1,51	2,22	0,48	21,75	0,5423	0,2723
LAI 5	-0,12	3,4	3,51	1,2	1,08	89,35	0,5095	0,1692
LAI 6	0,34	2,74	2,4	1,24	0,74	59,36	0,5096	0,1693
LAI 7	0,47	1,85	1,38	0,94	0,38	39,85	0,4777	0,2776
LAI 8	0,45	2,09	1,64	1,07	0,46	42,71	0,4948	0,3139
LAI 9	1,96	7,49	5,53	3,92	1,51	38,55	0,4623	0,3223
LAI 10	3,75	6,4	2,65	5,15	0,79	15,23	0,0449	0,2221
Ca+b	3,77	3,93	0,16	3,86	0,05	1,2	0,0439	0,2416
Ca+b	30,22	51,68	21,46	37,13	3,76	10,12	0,0031	0,2021

Table 8.10: Statistics for regional scale dataset for VIs and LAI / C_{ab} Stage 4 (02.08.06)

Stage 4	Min	Max	Range	Mean	STDV	CV	R^2 LAI	R^2 C_{ab}
NDVI	0,35	0,8	0,45	0,61	0,14	23,46	0,5069	0,5006
RVI	2,1	8,92	6,82	4,98	2,04	41,01	0,4548	0,4188
SAVI	0,24	0,53	0,3	0,4	0,09	21,71	0,4786	0,4624
SAVI2	1,67	4,89	3,22	3,16	0,94	29,78	0,4807	0,4479
MSAVI	0,22	0,55	0,33	0,39	0,1	24,42	0,4696	0,4477
OSAVI	0,3	0,66	0,37	0,5	0,11	22,36	0,5026	0,4892
TSAVI	0,22	0,77	0,54	0,54	0,17	31,91	0,5074	0,4997
ATSAVI	-0,39	-0,17	0,22	-0,26	0,07	-26,66	0,5062	0,5007
RDVI	0,23	0,51	0,28	0,38	0,08	21,8	0,4827	0,4678
TVI	6,77	19,46	12,69	13,72	3,61	26,34	0,4307	0,4248
MTVI1	0,17	0,49	0,32	0,34	0,09	27,16	0,4266	0,4333
MTVI2	0,14	0,54	0,39	0,35	0,11	32,54	0,4705	0,4667
CARI	0,01	0,13	0,12	0,06	0,03	44,17	0,3525	0,1708
TCARI	0,02	0,1	0,08	0,07	0,02	26,9	0,1577	0,2216
MCARI	0,01	0,03	0,03	0,02	0,01	27	0,1321	0,1321
MCARI1	0,17	0,49	0,32	0,34	0,09	27,16	0,4266	0,4333
MCARI2	0,14	0,54	0,39	0,35	0,11	32,54	0,4705	0,4667
SR705	1,65	4,44	2,79	2,98	0,84	28,3	0,5472	0,4810
mND705	0,29	0,64	0,35	0,49	0,1	21,28	0,5465	0,5176
GI	0,64	1,24	0,6	0,93	0,16	17,57	0,3488	0,4241
PRI	-0,15	-0,09	0,06	-0,12	0,02	-12,89	0,2201	0,1826
REIP	0,72	0,73	0,01	0,72	0	0,26	0,3289	0,2175
REIP	0,7	0,73	0,02	0,71	0,01	0,88	0,3897	0,4233
DGVI1	0,14	0,32	0,18	0,23	0,05	22,63	0,4245	0,4025
DGVI2	0,01	0,03	0,02	0,02	0,01	28,47	0,4103	0,4023
CSI2	0,23	0,61	0,38	0,37	0,12	32,18	0,5468	0,5310
LAI 1	0,79	3,4	2,6	2,33	0,84	35,99	0,5070	0,5009
LAI 2	1,87	4,14	2,26	3,02	0,72	23,78	0,4908	0,4668
LAI 3	0,95	2,69	1,74	1,69	0,52	30,91	0,4548	0,4188
LAI 4	1,08	2,85	1,77	2,13	0,58	27,23	0,5062	0,4988
LAI 5	-0,32	2,92	3,24	1,05	0,97	92,78	0,4548	0,4187
LAI 6	0,2	2,41	2,22	1,13	0,66	58,67	0,4548	0,4188
LAI 7	0,38	1,59	1,21	0,87	0,32	36,98	0,4181	0,4044
LAI 8	0,36	1,93	1,57	1,05	0,44	41,56	0,4393	0,4077
LAI 9	1,67	6,87	5,2	3,87	1,4	36,17	0,4198	0,3870
LAI 10	3,89	15,66	11,76	6,06	2,46	40,66	0,0008	0,0006
Ca+b	3,78	4,2	0,42	3,9	0,09	2,38	0,0150	0,0157
Ca+b	29,99	56,34	26,35	39,05	6,59	16,87	0,0110	0,0017